SNAP-21 PROGRAM, PHASE II

DEEP SEA RADIOISOTOPE-FUELED THERMOELECTRIC GENERATOR POWER SUPPLY SYSTEM

QUARTERLY REPORT NO. 4

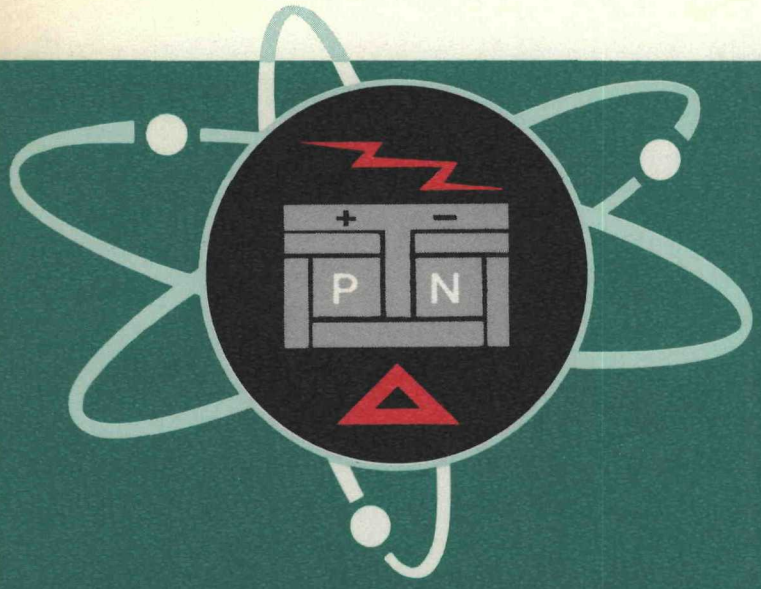

3M Isotope Power Products
MINNESOTA MINING & MANUFACTURING CO.
2501 HUDSON ROAD, ST. PAUL, MINN. 55119 PH. 631-2500

DISCLAIMER

SNAP-21 PROGRAM, PHASE II

DEEP SEA RADIOISOTOPE-FUELED THERMOELECTRIC GENERATOR POWER SUPPLY SYSTEM

QUARTERLY REPORT NO. 4

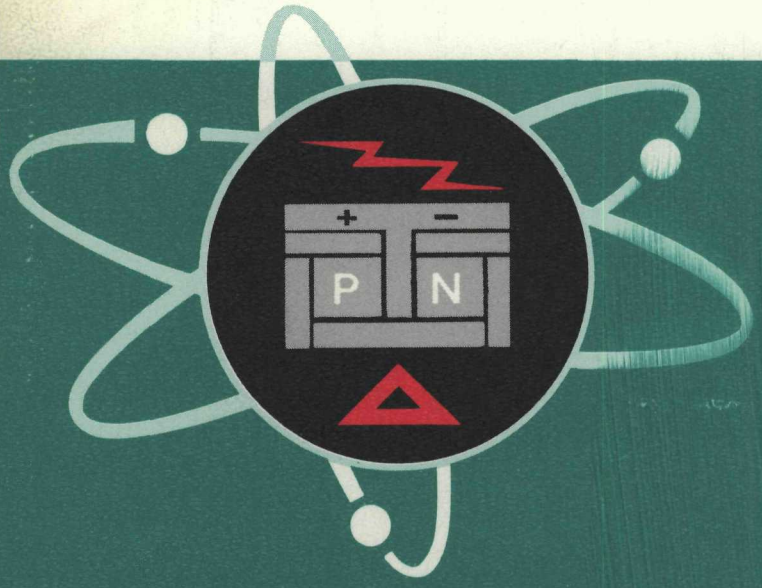

3M Isotope Power Products
MINNESOTA MINING & MANUFACTURING CO.
2501 HUDSON ROAD, ST. PAUL, MINN. 55119 PH. 631-2500

Report No. MMM 3691-20

AEC RESEARCH AND DEVELOPMENT REPORT

This report has been prepared under contract AT(30-1)3691
with the U.S. Atomic Energy Commission

SNAP-21 PROGRAM, PHASE II

DEEP SEA RADIOISOTOPE-FUELED THERMOELECTRIC GENERATOR POWER SUPPLY SYSTEM

QUARTERLY REPORT NO. 4

JULY 1967

Period Covered
April 1, 1967 to June 31, 1967

Prepared by
F.K. Fox

Approved by
J. Brandt
Manager
SNAP-21 Program

Issued by
ISOTOPE POWER PRODUCTS

MINNESOTA MINING AND MANUFACTURING COMPANY
ST. PAUL, MINNESOTA 55119

LEGAL NOTICE

This report was prepared as an account of Government sponsored work. Neither the United States, nor the Commission, nor any person acting on behalf of the Commission:

A. Makes any warranty or representation, expressed or implied, with respect to the accuracy, completeness, or usefulness of the information contained in this report, or that the use of any information, apparatus, method, or process disclosed in this report may not infringe privately owned rights; or

B. Assumes any liabilities with respect to the use of, or for damages resulting from the use of any information, apparatus, method, or process disclosed in this report.

As used in the above, "person acting on behalf of the Commission" includes any employee or contractor of the commission, or employee of such contractor, to the extent that such employee or contractor of the Commission, or employee of such contractor prepares, disseminates, or provides access to, any information pursuant to his employment or contract with the Commission, or his employment with such contractor.

[redacted]

DISTRIBUTION

Distribution of this document is in accordance with TID-4500 (50th Edition) category UC33.

BLANK

TABLE OF CONTENTS

Section		Page
1.0	SUMMARY	1-1
2.0	TASK I – 10-WATT SYSTEM	2-1
2.1	System Design and Tradeoff Study	2-1
2.2	Component Design and Development	2-1
2.2.1	Fuel Capsule (Design)	2-1
2.2.2	Biological Shield and Spider	2-7
2.2.3	Insulation System	2-10
2.2.3.1	Linde Subcontract	2-10
2.2.3.2	Transportation of Insulation System	2-25
2.2.4	Segmented Ring	2-29
2.2.5	Pressure Vessel	2-29
2.2.6	Thermoelectric Generator	2-30
2.2.6.1	Design	2-30
2.2.6.2	Generator Fabrication Development	2-31
2.2.6.3	Couple Fabrication	2-36
2.2.7	Power Conditioner	2-36
2.2.8	Electrical Receptacle and Plug	2-36
2.3	Component and Subassembly Testing	2-37
2.3.1	(Test) Fuel Capsule	2-37
2.3.2	Biological Shield	2-37
2.3.3	Insulation System	2-38
2.3.3.1	Offgassing Investigation	2-38
2.3.3.2	Vacuum Seal-Off and Getter Retention	2-45
2.3.3.3	Weld Joint Development	2-51
2.3.3.4	Material Compatibility Test	2-66
2.3.4	Segmented Hold Down Ring	2-68
2.3.5	Pressure Vessel	2-68
2.3.6	Thermoelectric Generator	2-70
2.3.6.1	Cold End Heat Transfer Testing	2-70
2.3.6.2	Leg and Couple Testing	2-74

TABLE OF CONTENTS (Continued)

Section		Page
2.3.6.3	Leg Inspection Development Testing	2-77
2.3.6.4	Generator Development Testing	2-79
2.3.6.5	Phase I Continuation Testing	2-79
2.3.6.5.1	Post-Test Investigation, Prototype Unit P3	2-87
2.3.7	Power Conditioner	2-93
2.3.8	Electrical Receptacle	2-94
2.4	System Fabrication, Assembly and Testing	2-94
2.4.1	Phase I Continuation Testing	2-94
2.4.2	Phase II System	2-94
2.5	Safety Analysis and Testing	2-98
2.5.1	Ocean Exposure Studies of Radioisotope Fuel Capsule	2-98
2.5.2	Laboratory Corrosion Testing of SNAP-21 Material	2-98
2.5.3	Ocean Exposure Studies of Electrically Heated Fuel Capsule Test Systems	2-99
2.5.4	Ocean Fuel Release Studies	2-99
2.5.5	Radiation Testing and Analysis	2-99
3.0	TASK IIA – 20-WATT SYSTEM	3-1
3.1	Conceptual Design	3-1
4.0	EFFORT PLANNED NEXT QUARTER	4-1

APPENDIX A – SNAP-21 PROTOTYPE UNIT THERMAL PERFORMANCE TEST – CALCULATION OF UNIT HEAT LOSS

APPENDIX B – CALCULATION OF ALLOWABLE PROTOTYPE UNIT PRESSURE RISE FOR A ONE-YEAR LIFE

LIST OF FIGURES

Figure		Page
2-1	Temperature Rise of Fueled Capsule with Time	2-2
2-2	Rate of Expansion of Fuel Capsule	2-2
2-3	Typical Gas-Tungsten Arc Weld, 12X	2-4
2-4	Electron-Beam Weld; 150 ms at 30 KV, 18 in/min Travel Speed, 12X	2-5
2-5	Electron Beam Weld; 125 ms at 30 KV, 18 in/min Travel Speed, 12X	2-6
2-6	Tension Rod Support Concept	2-8
2-7	Two Shields to Spider Attachment Concepts	2-9
2-8	SNAP-21 Prototype Unit – Thermal Performance Test Setup	2-12
2-9	SNAP-21 Prototype Unit – Top View of Unit during Thermal Performance Test	2-12
2-10a	SNAP-21 Prototype Thermal Performance Test No. 1	2-13
2-10b	SNAP-21 Prototype Thermal Performance Test No. 2	2-13
2-11	1900°F Heaters	2-15
2-12	SNAP-21 Prototype Thermal Performance Test No. 3	2-18
2-13	SNAP-21 Prototype Unit Pressure Rise	2-18
2-14	Insulation System Shipping Container Showing Method of Support	2-27
2-15	Insulation System Showing Washers Under Spring Bolt Heads	2-28
2-16	Assembly of Generator A10D-2: Method of Holding Followers in Place	2-33
2-17	Assembly of Generator A10D-2: Couple Insertion	2-33
2-18	Assembly of Generator A10D-2: Fiberglass Insulation Sleeving	2-34
2-19	Assembly of Generator A10D-2: Partially Disassembled to Correct Shorting	2-34
2-20	Assembly of Generator A10D-2: Weld Closure	2-35
2-21	Cross Section of Electron Beam Weld	2-38
2-22	Corrected Pressure Rise Curves for Empty Chamber and Chamber with Stainless Steel	2-39

LIST OF FIGURES (Continued)

Figure		Page
2-23	Schematic of Offgassing Cycles	2-41
2-24	Calibration Curve for Philips Vacuum Gauge	2-43
2-25	Pressure Rise Curves for Slope Determination	2-44
2-26	Offgassing Rate of Stainless Steel vs Pressure at 100°F	2-44
2-27	Offgassing Rate of Stainless Steel vs Time at 100°F	2-45
2-28	Schematic of Getter Installation and Seal-Off Apparatus	2-47
2-29	Getter Retainer Material Weld Specimens	2-50
2-30	Getter Retainer Material Welded in Simulated Outer Case	2-52
2-31	Macrograph of Enclosure Girth Weld Specimen No. 3 (5X)	2-54
2-32	Macrograph of Enclosure Girth Weld Specimen No. 4 (5X)	2-55
2-33	Macrograph of Enclosure Girth Weld Specimen No. 5a (5X)	2-56
2-34	Macrograph of Enclosure Girth Weld Specimen No. 5c (5X)	2-57
2-35	Enclosure Girth Weld Tensile Test Specimens After Test	2-59
2-36	Neck Tube Weld Joint	2-60
2-37	Simulated Neck Tube Weld Joints – 2-1/2 Inch O. D.	2-64
2-38	Simulated Neck Tube Weld Joints – 5 Inch O. D.	2-65
2-39	Schematic View Showing the Insulation and Biological Shield Material in Test Chamber	2-67
2-40	Compatibility Test Assembly After 500 Hours on Test	2-69
2-41	U-8% Molybdenum Bars After 500 Hours on Compatibility Test	2-69
2-42	6-Couple Heat Transfer Test Module	2-71
2-43	Cold End Heat Transfer Tests Without Heat Transfer Grease	2-72
2-44	Cold End Heat Transfer Tests with Heat Transfer Grease	2-72
2-45	Performance Data, SNAP-21 6-Couple Module A1	2-80
2-46	Performance Data, SNAP-21 6-Couple Module A3	2-81
2-47	Performance Data, SNAP-21 6-Couple Module A4	2-82
2-48	Performance of Prototype 48-Couple Generator 3M-37-P3, P5, P6, P7 (E = voltage, R = resistance, P = power, x = experimental, C = computer)	2-83
2-49	Arrangement of Couples in Prototype P3	2-89
2-50	Schematic of Electrically Heated Hot Block and Location of Thermocouples	2-95

LIST OF FIGURES (Continued)

Figure		Page
2-51	Taking Radiation Measurements in Test Area	2-101
2-52	Radiation Measurement Points on Mock-Up System	2-103
2-53	Reworked Biological Radiation Shield Showing Material Removed	2-105
2-54	Spatial Relationship of Shield Designs	2-108

BLANK

LIST OF TABLES

Table		Page
2-1	Electron Beam Welding Parameters	2-3
2-2	SNAP-21B Prototype Unit Thermal Test Heater Failure Data	2-14
2-3	Summary of Neck Tube and Tension Rod Support System	2-20
2-4	Comparison of 6ms and 8ms Shock Duration	2-21
2-5	Type 304 Stainless Steel Offgassing Test Data from Mass Spectrometer Analysis for Cycle Identification (see Figure 2-23)	2-42
2-6	Gold "O" Ring Torque Test Data	2-46
2-7	Seal-Off Apparatus - Gold O-Ring Seal Tests	2-49
2-8	Summary of Automatic Girth Weld Tensile Specimens Cut from 6-Inch O. D. Pipe Welds	2-58
2-9	Weld Parameter for Semi-Automatic Neck Tube Edge Weld	2-62
2-10	Leak Rate Data Neck Tube Edge Weld	2-63
2-11	Cold End Heat Transfer In-Line Test Data Summary	2-75
2-12	Cold End Heat Transfer Indium Test Data Summary	2-76
2-13	6-Couple Module Performance Test Data	2-84
2-14	Prototype 48-Couple Generator Performance Test Data	2-85
2-15	Seebeck Voltage of Leg Segments in Prototype P3 T_C = 75°F, T_H = 675°F - results in mv	2-91
2-16	Radiation Survey	2-102
2-17	Film Badge Dosimetry	2-104
2-18	Temperature Measurements During Radiation Tests	2-106
2-19	Shield Thickness Required to Achieve 200 mr/hr Maximum System Surface Radiation	2-107

BLANK

1.0 SUMMARY

1.0 SUMMARY

Significant accomplishments during this report period are summarized below.

- Generator A10D-2 completed assembly.
- The first insulation system was completed.
- Radiation effectiveness of the biological shield was determined from radiation measurements taken with a 200-watt SrO source.
- Fabricated 214 couples, including both the instrumented types and those with output tap assemblies.
- Initiated Task II conceptual design effort.
- Test plans for compatibility testing were completed and the test fixture design completed.
- Initiated development of the power conditioner.
- Test specimens for electrically heated fuel capsules, laboratory corrosion specimens and and galvanic and marine fouling system components were fabricated.

- The results of the ultrasonic tests of the first weld development closures on fuel capsules were evaluated.
- Cold end heat transfer tests 16 through 24 were completed.
- Started post-test investigation of SNAP-21 Prototype Unit P3.

2.0 TASK I– 10-WATT SYSTEM

2.0 TASK I–10-WATT SYSTEM

2.1 SYSTEM DESIGN AND TRADEOFF STUDY

The System Design and Tradeoff Study was completed during the first quarter of 1967 and is fully reported in SNAP-21 Quarterly Report No. 3, MMM 3691-17, published in May, 1967.

2.2 COMPONENT DESIGN AND DEVELOPMENT

2.2.1 FUEL CAPSULE (DESIGN)

a) Capsule Thermal Expansion Analysis

An analysis was performed to determine the minimum allowable time for transfer of the fuel capsule to the shield cavity before interference due to thermal expansion of the capsule occurs. Figure 2-1 shows the temperature rise of the capsule (203 watts) in air. Figure 2-2 indicates the rate of expansion of the capsule. The maximum dimensional tolerance on the capsule and the minimum tolerance on the mating surface of the inner liner (present designs) results in a clearance of 0.002 inch. Interference will occur in less than 6 minutes. Forced convective cooling, where the ambient air is moving at a velocity of about 5 ft/sec, can be used to dissipate 203 watts from the capsule so that no thermal growth occurs. However, a greater clearance (0.020 inch) for insertion is advisable for mechanical handling reasons and, with the greater latitude, capsule expansion should not pose a problem to insertion.

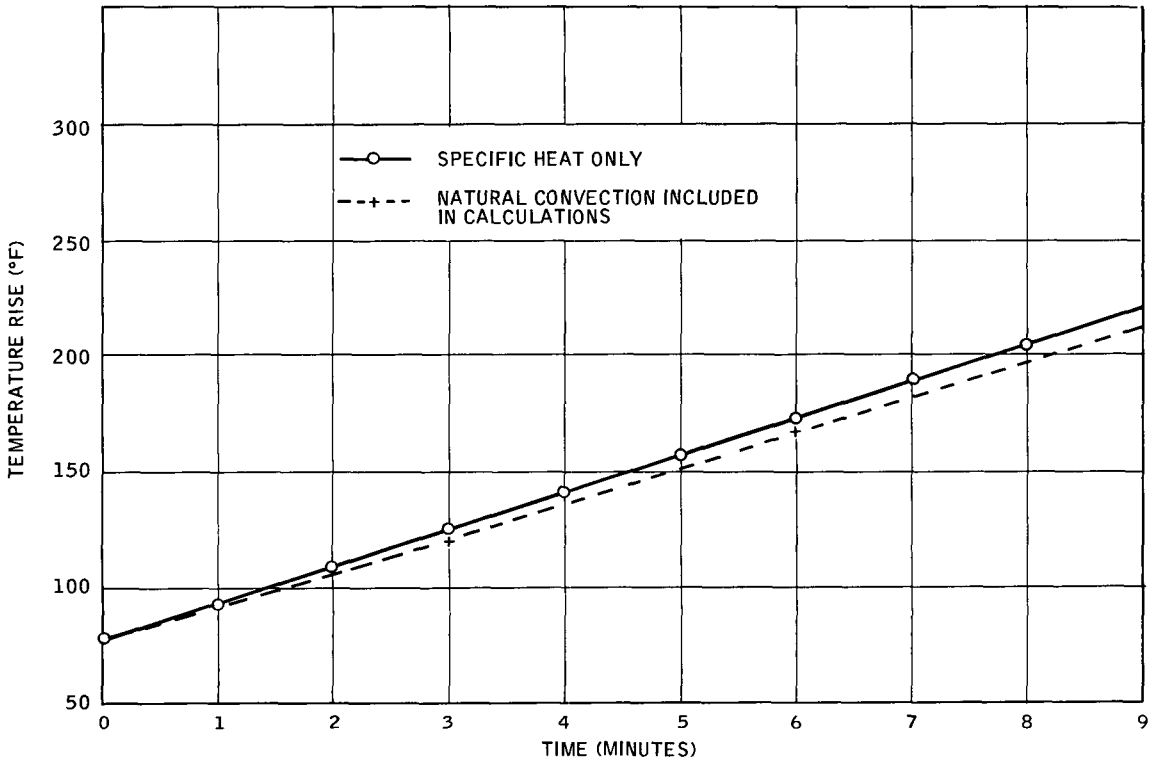

Figure 2-1. Temperature Rise of Fueled Capsule with Time

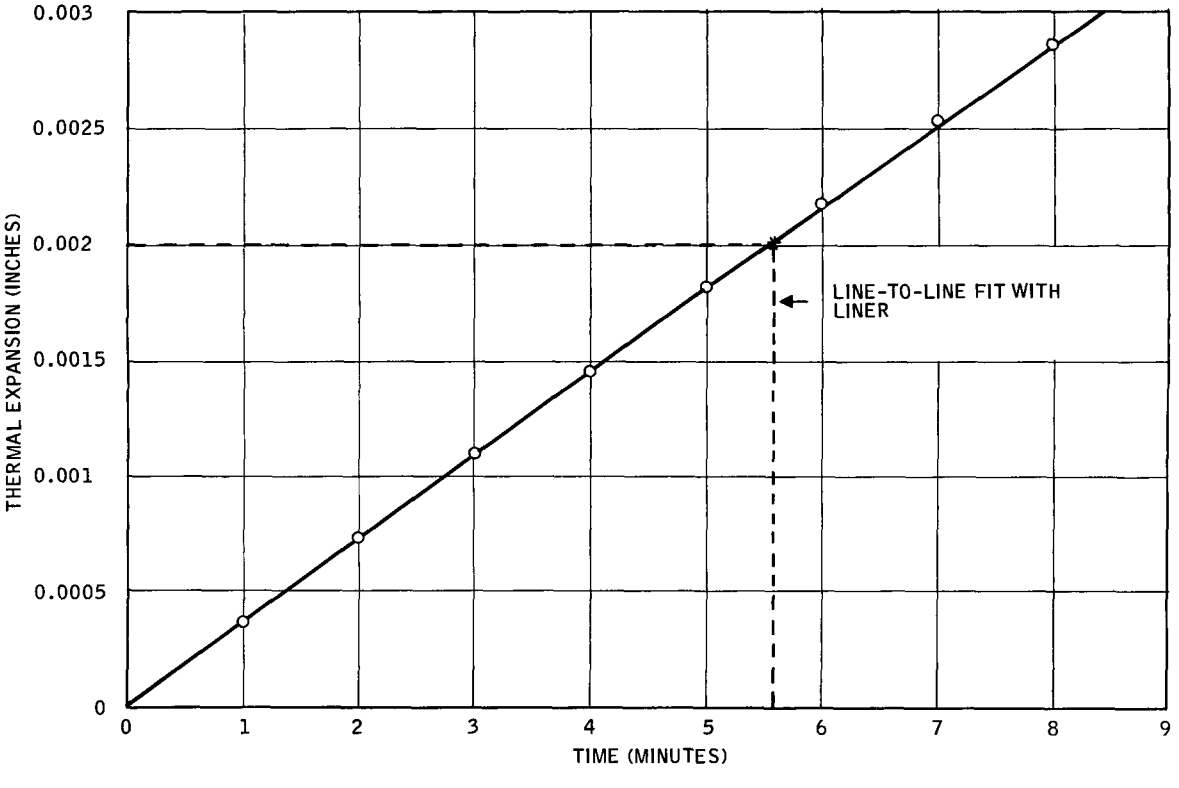

Figure 2-2. Rate of Expansion of Fuel Capsule

b) Weld Analysis

Electron-beam welding was investigated as a capsule closure technique. The equipment used was of the low voltage, 30 kv type. Advantages of this equipment are the relatively low cost and the modular construction which makes it potentially suitable for hot-cell use.

A gas tungsten-arc weld typical of those previously sent to Pacific Northwest Laboratories (PNL) for evaluation is shown in Figure 2-3 for comparative purposes. First attempts at electron-beam welding resulted in welds similar to that shown in Figure 2-4. The conditions were 150 ma at 30 kv and 18 in./min travel speed. Full penetration of the joint is evident; however, gross surface melting has resulted in undesirable weldmetal overhang. Increasing the welding speed to 30 in./min and lowering the current to 125 ma results in somewhat less penetration (Figure 2-5) and no weldmetal overhang.

Three capsules with two joints each were electron-beam welded and sent to PNL for ultrasonic and metallographic examination. Initial results of the examination are described in section 2.3.1. The parameters of these welds are given in Table 2-1.

Table 2-1. Electron Beam Welding Parameters

Welding speed:	30 in./min
Accelerating voltage:	30 kv
Preheating temperature:	None
Chamber pressure:	$\sim 5 \times 10^{-5}$ torr

Capsule	Cap. No.	Current, ma
5	2	125
	18	125
7	10	150
	13	150
8	12	150[a]
	11	150[a]

[a]Much sharper focusing of beam obtained in comparison to previous welds.

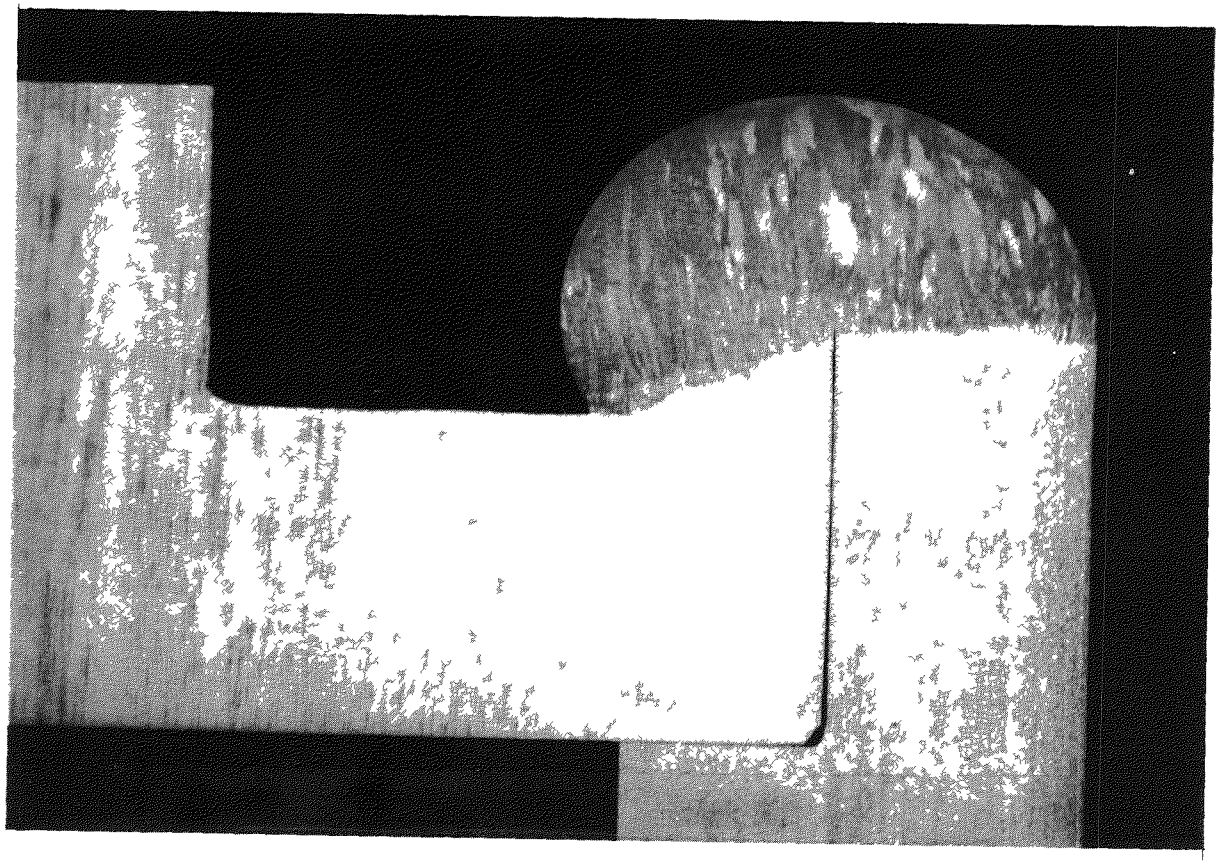

Figure 2-3 Typical Gas-Tungsten Arc Weld, 12X

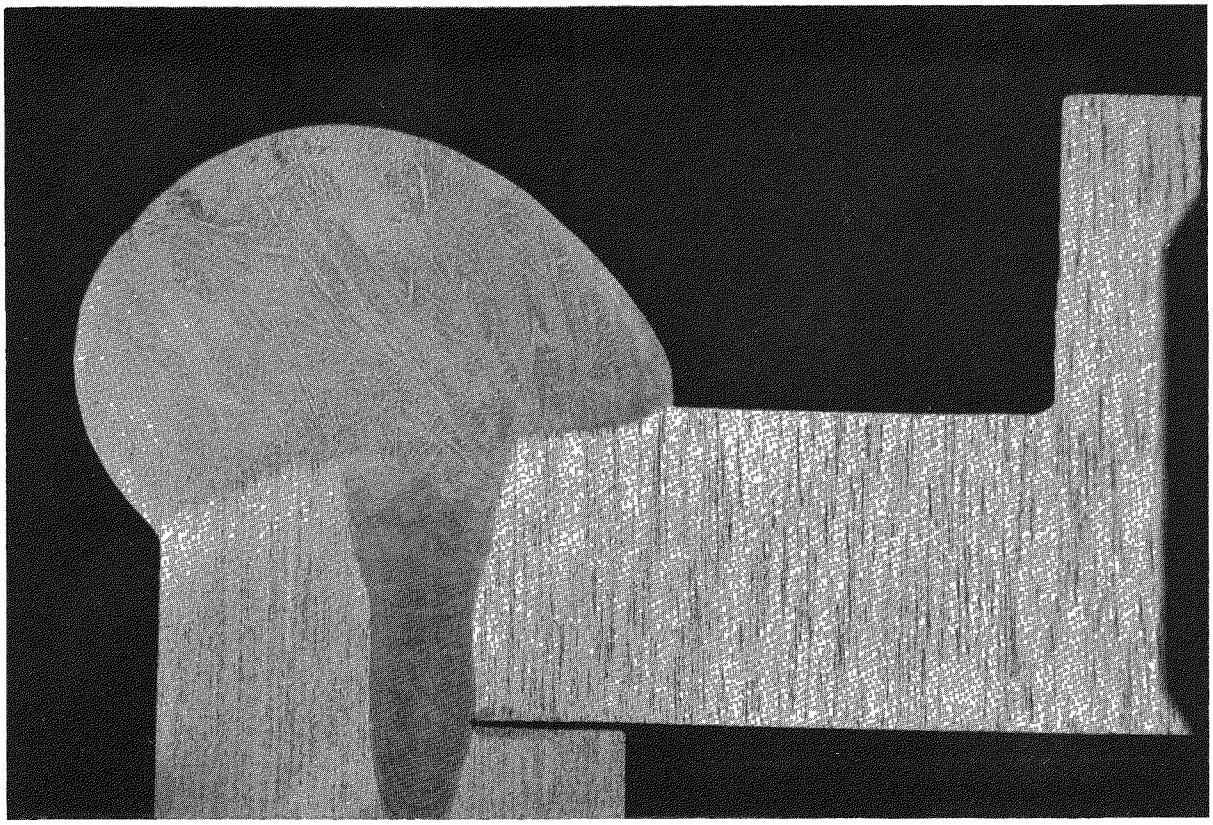

Figure 2-4. Electron-Beam Weld; 150 ms at 60 KV, 18 in/min Travel Speed, 12X

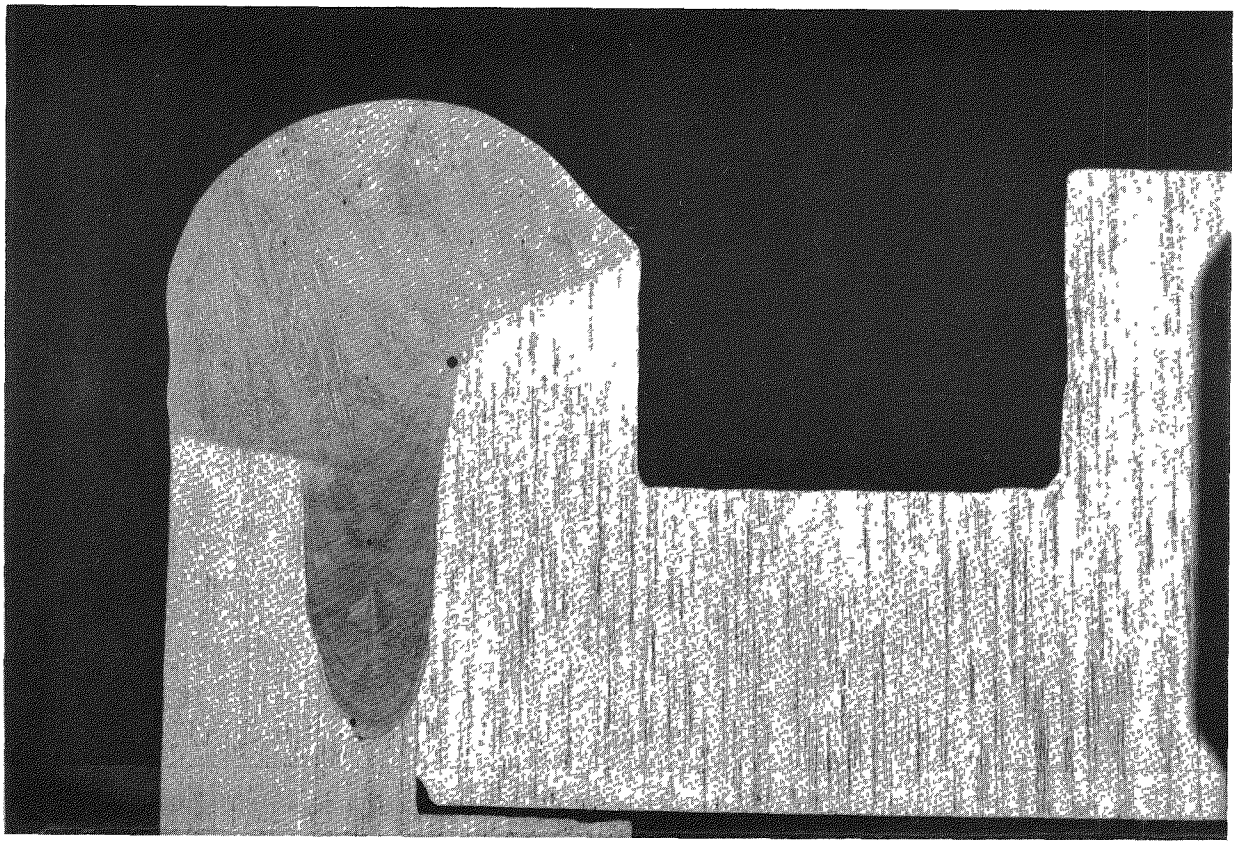

Figure 2-5. Electron Beam Weld; 125 ms at 30 KV, 18 in/min Travel Speed, 12X

More recent electron-beam welding efforts have resulted in joints which are narrower, of full penetration, and which do not exhibit gross surface melting. With these conditions, it is possible to preserve the outside edges of the joint. This is desirable for ultrasonic inspection purposes.

2.2.2 BIOLOGICAL SHIELD AND SPIDER

The primary design effort during the past quarter was concerned with analysis and design of the shield support system. This effort requires accurate knowledge of the "thermo-physical properties" of the shield alloy, U-8 Mo. Since this knowledge is either not available or is of questionable reliability, 3M is having specimens made to determine tensile strength, heat capacity, thermal expansion and creep in elevated temperature conditions. One specimen is a nut and bolt type, designed to simulate the system. The other specimen is to be fabricated according to Federal Test Standard No. 151a. All tests will be conducted at 3M's Central Research Laboratory.

The shield support system must limit movement of the biological shield with respect to the outer case, to prevent the neck tube from buckling. The method selected to meet this requirement is a tension tie rod system in conjunction with a monocoque neck tube, as shown in Figure 2-6. Using the best available data, molybdenum was initially selected as the spider material because its low coefficient of expansion would allow a low tension tie rod angle. This would provide a high ratio of horizontal force to tie rod load, thus permitting a minimum tie rod diameter and, therefore, minimum heat leak. A detailed analysis of the molybdenum spider indicated, however, that because of the large variation in coefficients of thermal expansion between the shield material and the spider, it would be impossible to maintain the minimum relative movement within the system and stay within the elastic range of the spider materials. Because it was impossible to predict the failure point of a structural member being cyclically loaded beyond the yield point, this spider material was abandoned.

Two concepts which were considered for the shield to spider attachment are shown in Figure 2-7. These were unacceptable because it was impossible to design a rigid connector to prevent shield deflection and yet stay within the elastic range of the spider components under cyclic loads. The unknown strength characteristics of materials under cyclic loads at high temperatures makes this technically unacceptable.

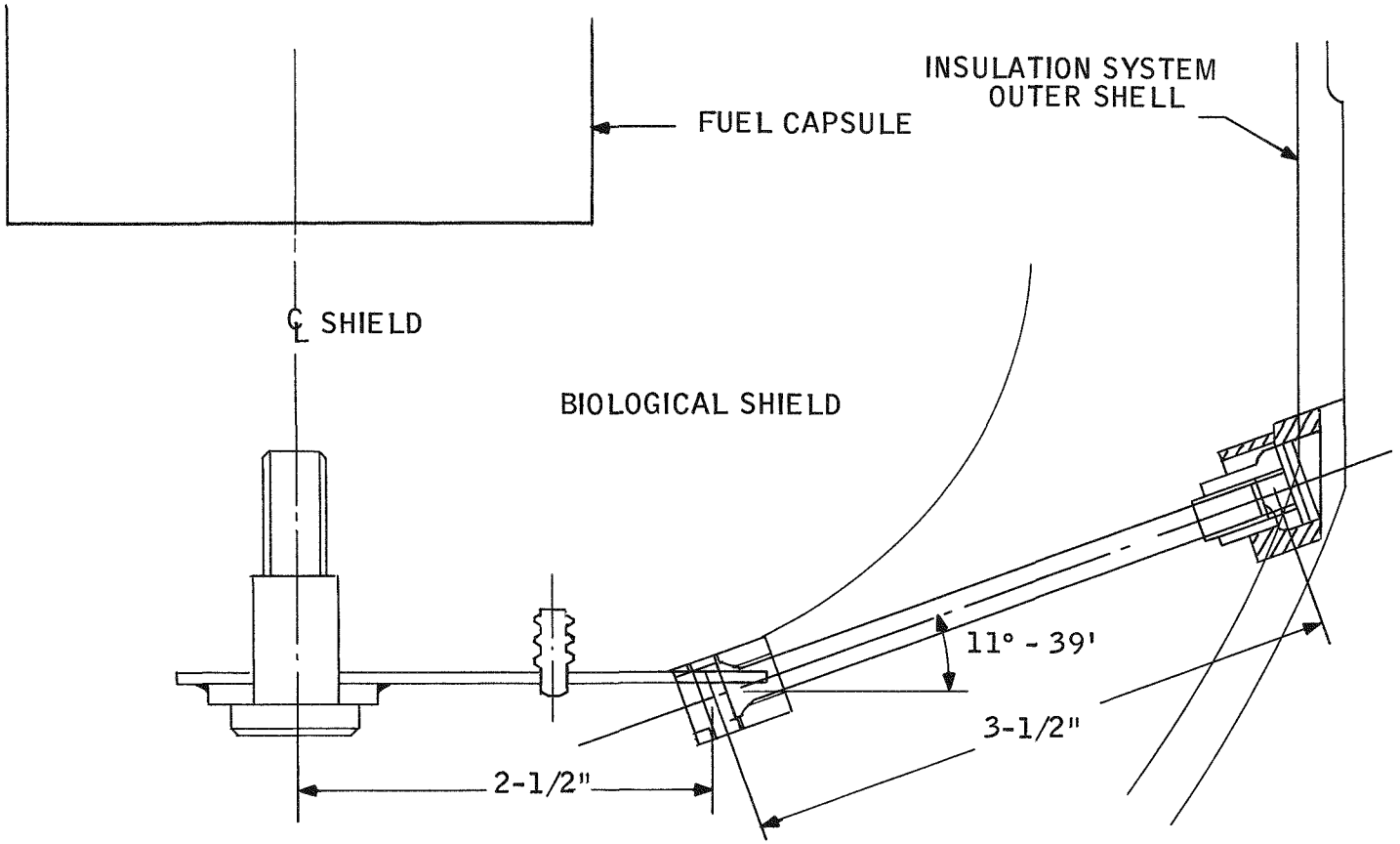

Figure 2-6. Tension Rod Support Concept

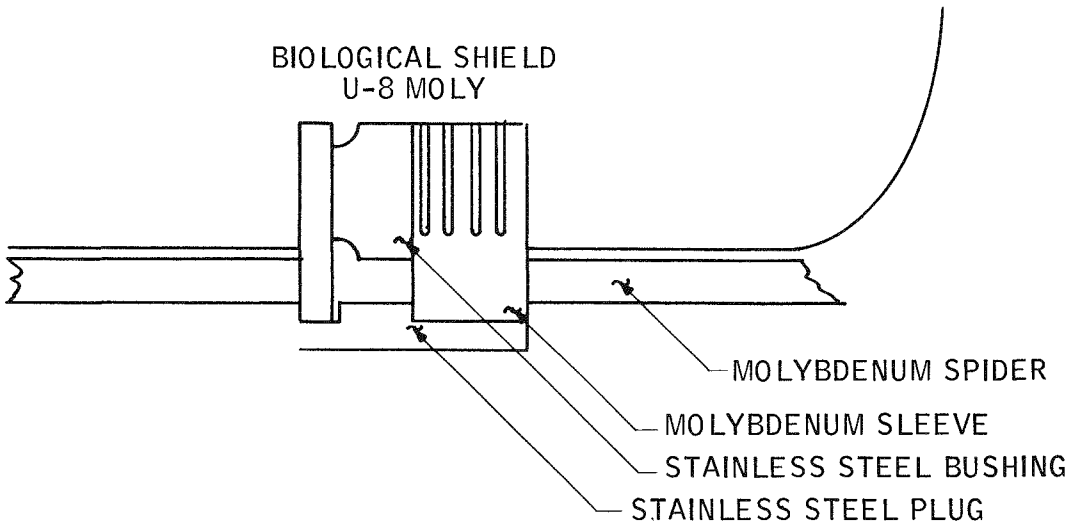

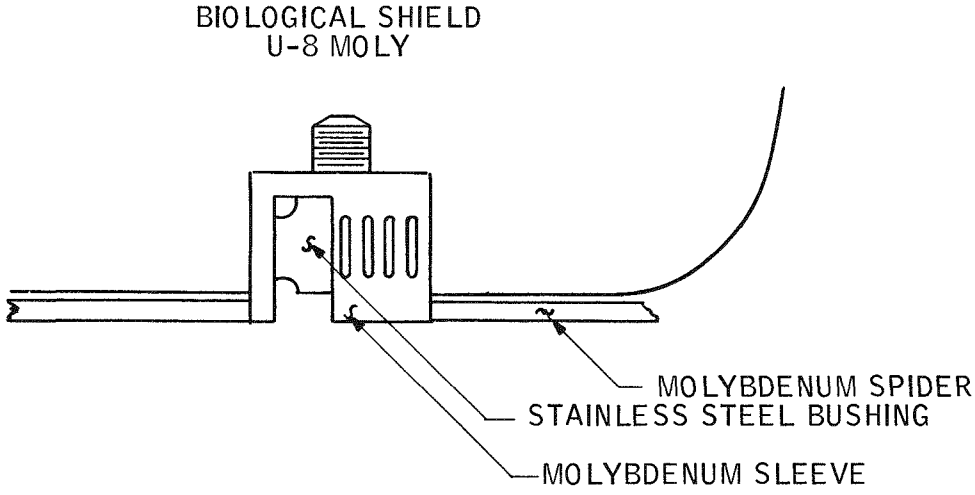

Figure 2-7. Two Shields to Spider Attachment Concepts

Hastelloy-X was then selected as this material has a coefficient of thermal expansion which closely matches that of the U-8 Moly shield. The diameter of the rods will increase somewhat because they must be installed at a greater angle. This will increase the heat leak slightly.

The attachment of the spider to the shield requires that the spider be coated with a barrier material to prevent eutectic formation wherever the Hastelloy-X contacts the U-8 Moly under normal operating conditions.

Maintaining a rigid connection between the spider and the shield under hot and cold conditions requires machining mating parts to close tolerances and assembled under close fits to prevent any movement of the biological shield.

The spider will be attached to the insulation system outer case by three 1/4-inch diameter Inconel-625 rods placed 120° apart. The attachment points will be a ball and socket configuration to allow movement due to thermal expansion of the shield. The angular adjustment and preload of each rod will be controlled by a spherical ball threaded to the rod and seated in a movable socket to allow angular movement of the rod during assembly.

The design of the biological shield plug is nearly complete. Thermal growth calculations have been done and tolerance build-ups were considered to ensure that the plug will have sufficient clearance at elevated temperatures.

Prints for the plug have not yet been released nor has there been a design review.

2.2.3 INSULATION SYSTEM

2.2.3.1 Linde Subcontract

Linde, continuing work under letter subcontract AT(30-1)3691-5511, has completed the SNAP-21B prototype unit. Work has also progressed on the analysis of the structural support of the biological shield, development testing and development test procedures.

a) SNAP-21B prototype

The SNAP-21 prototype insulation system which has been undergoing thermal conditioning is shown on test in Figures 2-8 and 2-9. At the end of the last reporting period, a heater failed while bringing the unit up in temperature A plot of the temperature rise data is shown in Figure 2-10a. The heater block was removed from the unit and was machined so that larger diameter heaters could be used. For the next thermal performance test run, two Watlow LA411 heaters (5/8-inch O.D. x 4 inches long - 250 watts, 115 volts) were used. These heaters were connected in parallel to reduce the heater watt density. An isolation transformer was placed in the circuit. After running for 72 hours and attaining a maximum temperature of 1331°F, this test also had to be discontinued because of decreasing resistance in one of the heaters. The thermal test heater failure data is shown on Table 2-2. A plot of the temperature rise data for this test is shown in Figure 2-10b.

Heater vendors were contacted and informed of the heater failures. 1900°F heaters were purchased for use in the next thermal test. These heaters were delivered to Linde and the third try at a thermal test was initiated. Fifty watts of power was supplied to the heaters; the next day the power input was increased to 70 watts. When the temperature of the unit reached 1200°F the pressure was 1.2 microns. At 1285°F the total heat leak of the unit was determined to be 43.5 watts. The extraneous heat loss has not yet been calculated and, therefore, the unit heat loss has not been determined. At the end of this reporting period the temperature of the unit had reached 1550°F, which is the conditioning temperature.

After the second heater failure, a meeting was held at Linde to discuss the heater problems. It was determined that additional contacts should be made with heater vendors to obtain a heater which would not fail at high temperatures. A trip was made to RAMA Industrial Heater Company, San Jacinto, California, to determine the causes of the heater failures and to get recommendations for heaters to be used in future tests. It was determined that the lava plug at the top of the heater had become carbonized from overheating so that the heater pins shorted out to each other through the lava. Sketches of the standard Ramarod heater and the heater recommended for the 3M application are shown in Figure 2-11.

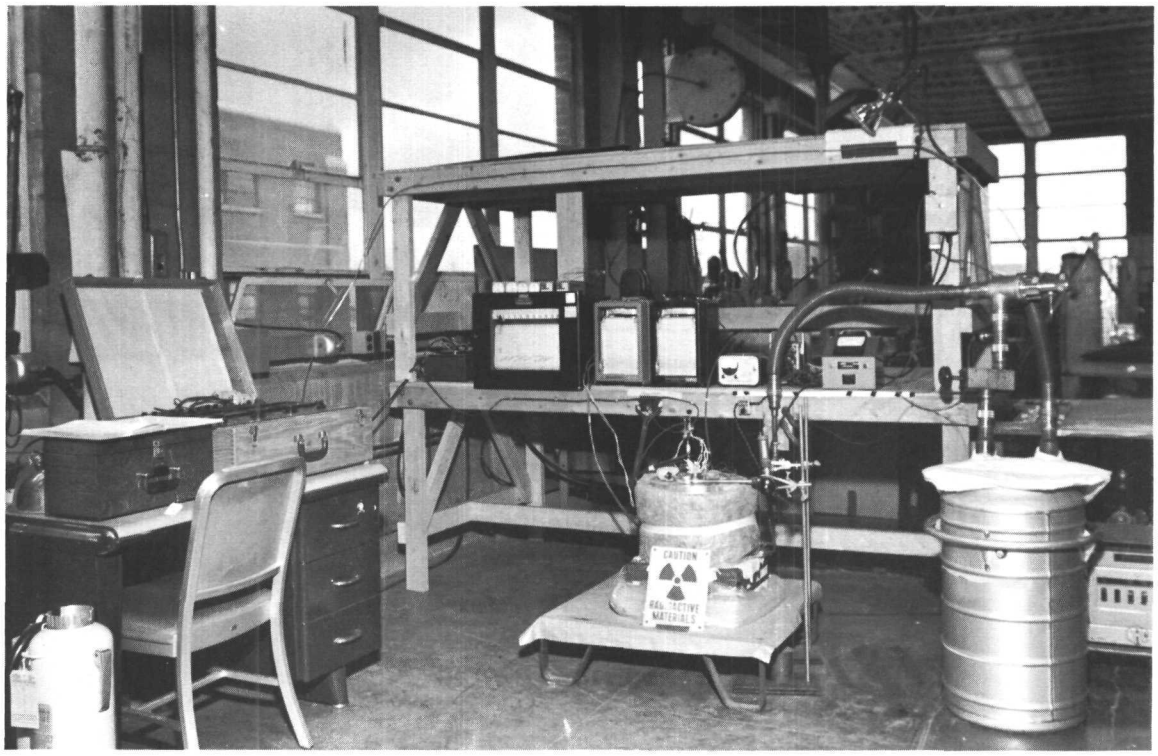

Figure 2-8. SNAP-21 Prototype Unit – Thermal Performance Test Setup

Figure 2-9. SNAP-21 Prototype Unit – Top View of Unit during Thermal Performance Test

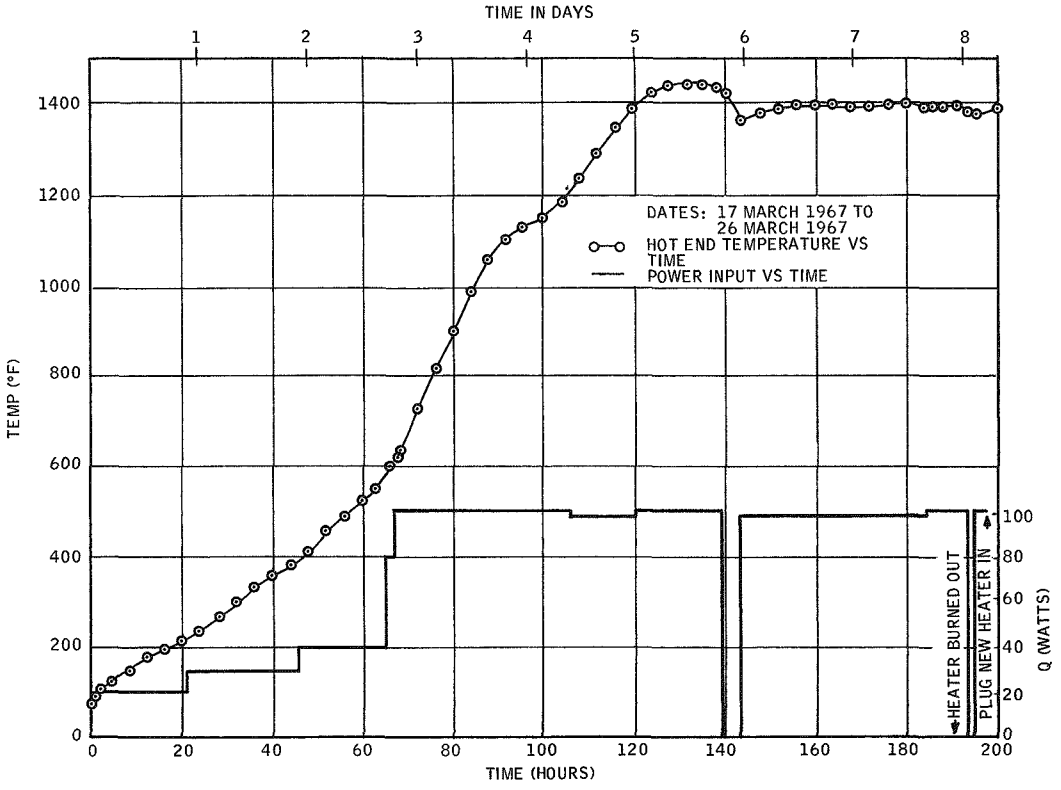

Figure 2-10a. SNAP-21 Prototype Thermal Performance Test No. 1

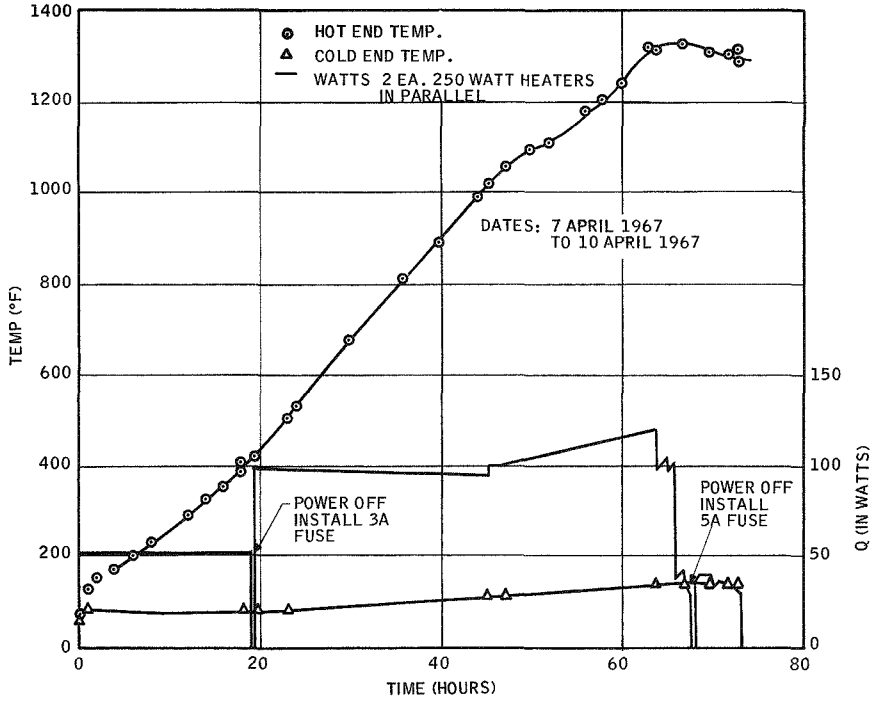

Figure 2-10b. SNAP-21 Prototype Thermal Performance Test No. 2

Table 2-2. SNAP-21 Prototype Unit Thermal Test Heater Failure Data

Heater Name and No.	Size Watts Volts	Type of Circuit	Initial Resistance		Total Operating Time Hours	Max. Power per Heater Watts	Watt Density w/in^2	Max. Hot End N. T. Temp. °F	Heater Dia. OD Inches After Removal	Heater Block Hole ID Inches	Final Resistance		Mode of Failure	Comments
			Heater Ω	Wire Case Ω							Heater Ω	Wire Case Ω		
Test Number 1														
Watlow G-A4D 25-5	3/8" x 4" 250 w 115 v	One Heater	47	5.5×10^6	180	100	21.3	1435	0.373T 0.371M 0.373B	0.371B 0.371M	---	---	Lead wires burned out at heater	After 140 hr. when max. temp. reached and heater failure apparent, resistance of heater = 60Ω, resistance (lead to ground) = 10Ω and 70Ω.
Watlow G-A4D 31-5	3/8" x 4" 250 w 115 v	One Heater	50	∞	<20	100	21.3		0.373T 0.373M 0.373B	0.3715B 0.3715M	---	---	Lead wires burned out at heater	After 140 hr. at temp. without power the resistance of heater was 26Ω. Resistance (lead to ground) = 19Ω and 22Ω.
Test Number 2 – Argon Backfilled														
Watlow LA411	5/8" x 4" 250 w 115 v	Two Heaters in Parallel	47	500-1000 $\times 10^6$	72	50	6.38	1331	0.623T 0.621M 0.620B	0.626T 0.625M 0.623B	49	50-1000 $\times 10^6$	OK	With temp. at ~1300°F after power shutoff. Resist. of parallel heaters = 1.65Ω lead-lead. Resistance (lead to ground) = 4.7Ω and 4.0Ω.
Watlow LA411	5/8" x 4" 250 w 115 v	Two Heaters in Parallel	47	500-1000 $\times 10^6$	Failure started at ~65 hrs.	50	6.38	1331	0.622T 0.621M	0.625T 0.625M	8.2	41×10^4	Decreasing Resistance	

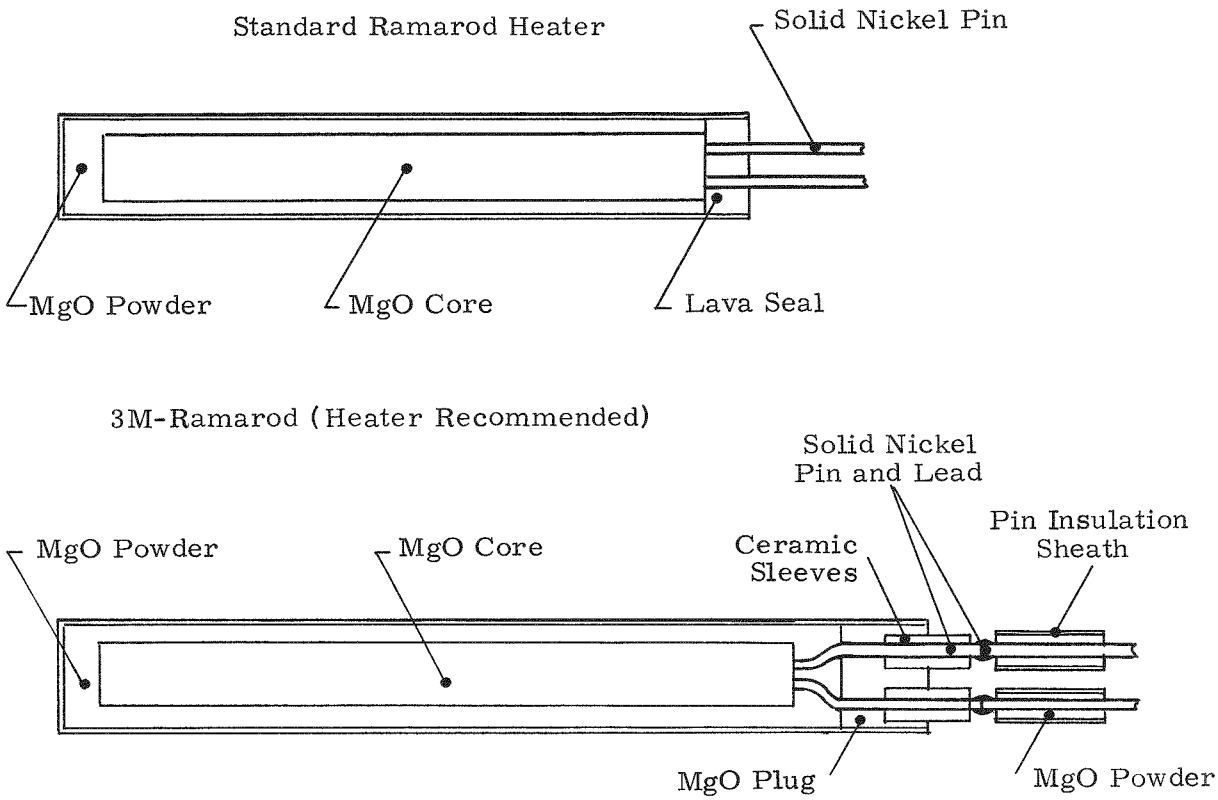

Figure 2-11. 1900°F Heaters

The following recommendations were made by RAMA:

- Separate the pins as much as possible
- Use magnesium oxide (MgO) plug for better dielectric strength in place of lava
- Use isolation transformer so there is no potential to ground (sheath) in new pin position
- Use ceramic sleeves protruding from the MgO plug
- Use welded nickel lead wires
- Centerless grind heaters to ±0.00025 tolerance
- Heater block holes to be held to ±0.001 tolerance

- Oxidize heater surface and heater block holes for better emissivity operating in argon
- Use a slow rate of heat up when the heaters are hot to keep the leads from overheating

A rate of heat up specification was prepared by 3M Company. This procedure was supplied with the heaters to Linde for use with the third thermal test. To preclude heater failure, the power input was limited to 70 watts maximum during the entire test. Power increases were made in small increments as shown on Figure 2-12. In the event of heater failure, it was decided to run the thermal performance test at 1285°F prior to conditioning at 1550°F as the unit has previously been at 1435°F during Run No. 1. The hot end neck tube temperature versus time for the entire run to include the thermal test and conditioning is shown on Figure 2-12.

A steady-state power input of 42.88 watts was required to maintain the unit at 1285°F. To this input power the following subtractions must be made to determine the unit heat loss: neck tube insulation – 4.66 watts; heater wires and insulation – 6.42 watts; and thermocouple wires and insulation – 0.74 watt. This subtraction yields a total unit heat loss of 31.06 watts (see Appendix G to A). This heat loss breaks down to 12.5 watts for the insulation and 18.56 watts for the neck tube. During the thermal test the unit was vacuum pumped and the pressure was 1.4 microns. The cold end neck tube temperature was 135°F while the upper head temperature at the girth weld was 115°F. The lower enclosure temperature at the bottom girth weld was 100°F and the temperature at the center of the bottom enclosure head was 95°F.

Following the thermal performance test, the power was increased (see Figure 2-12) to bring the unit to 1550°F for conditioning of the insulation. The uncorrected power input at 1548°F was 60.5 watts, including all subtractable losses. The insulation pressure was maintained at 5.5 microns while vacuum pumping. In addition, the enclosure was heated with a blanket type heater to promote conditioning. At 1548°F hot end neck tube temperature, the following enclosure temperatures were measured: cold end neck tube, 230°F; enclosure at upper girth weld, 240°F; enclosure at lower girth weld, 200°F; center of bottom enclosure head 170°F.

After 24 hours at 1548°F, the power was turned off and the unit was allowed to cool to 1215°F before removing the neck tube insulation for a rapid cooldown.

During Test Run No. 3, the unit was valved off at two constant temperatures to determine the unit pressure rise rate and thus the unit combined offgassing and leak rate. Figure 2-13 shows the two pressure rise curves. The initial portion of the curve from time zero to approximately 40 minutes is the time required for the unit to reach an equilibrium pressure after the vacuum pump is valved off. Note that the 1285°F pressure rise was performed before conditioning at 1548°F. The pressure rise rate after conditioning would be less. The offgassing plus leak rate can be calculated from the relationship — offgas rate = volume x pressure change/time period. With the prototype unit volume of approximately 0.55 ft^3, the offgassing rate at 1285°F would be:

$$\text{Offgassing rate at } 1285°F = 0.55\ ft^3 \times \frac{28.32\ell}{ft^3} \times \frac{0.1\ \text{micron}}{\text{hr}} = 15.58$$

while the offgassing rate at 1548°F would be

$$\text{Offgassing rate at } 1548°F = 0.55\ ft^3 \times \frac{28.32\ell}{ft^3} \times 0.55\ \text{micron/hr} = 8.55\ \mu\text{-}\ell/\text{hr}$$

For this prototype unit based on the conductance of the getter retainer, getter pumping speed and getter capacity, the allowable pressure rise rate for a one-year unit life has been calculated in Appendix B to be 5.4 microns/hr. Figure 2-13 shows that the actual pressure rise rate is much lower than the calculated maximum; this should allow a unit life longer than one year.

A shipping container for transporting the completed prototype unit was designed and drawings were prepared. One shipping container was fabricated during this reporting period. The container directly supports the biological shield through a solid neck tube plug which is bolted to the shield and the frame of the shipping container. The unit will be completely enclosed in the container with plywood sheet bolted to the container framework.

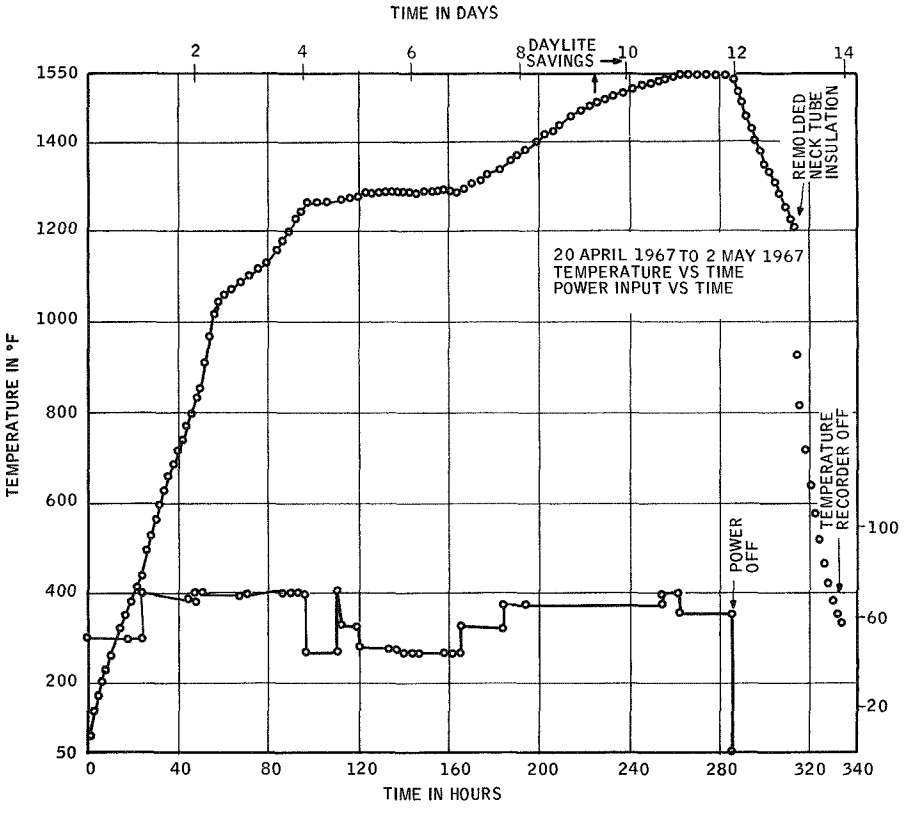

Figure 2-12. SNAP-21 Prototype Thermal Performance Test No. 3

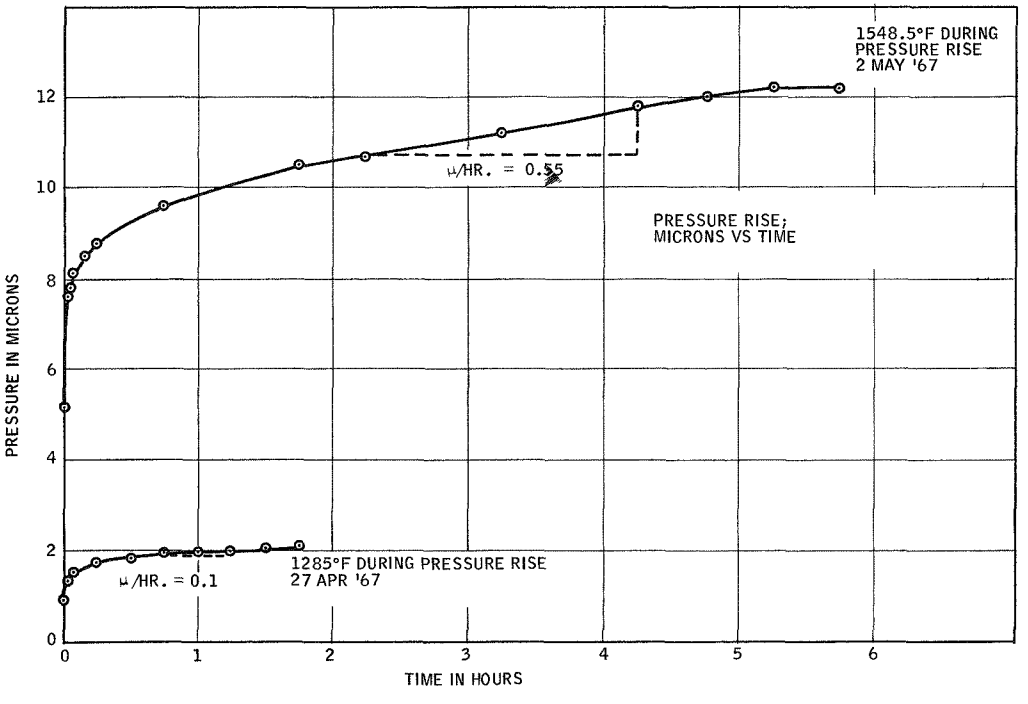

Figure 2-13. SNAP-21 Prototype Unit Pressure Rise

The allowable input g-loading which the HTVIS prototype unit can be subjected to during handling and shipping was calculated for the unit being in the horizontal, vertical, and vertical upside-down positions. The allowable input g-loading to the HTVIS prototype unit during shipping was also calculated when the shield was supported through a support rod inside the neck tube. In this case, the neck tube supports the enclosure only. The results of the calculations are summarized as follows:

Position of Unit During Shipping	Allowable Input g-Loading for 1.5 Safety Factor When Neck Tube Supports Shield	Allowable Input g-Loading for 1.5 Safety Factor When Neck Tube Supports Enclosure
Horizontal	2.3	4.4
Vertical	24.6	33.7
Vertical Upside Down	11.6	70.9

The unit was placed in its shipping container and it was shipped to Oak Ridge National Laboratory, as described in paragraph 2.2.3.2. After the radiation survey was completed, the unit was sent to 3M Company, where it currently is undergoing heat-up for the thermal test.

b) Structural Support of Biological Shield

The analysis of the HTVIS Model A support system consisting of the neck tube and three tension rods was completed for a dynamic loading at 6g in shock and 3g in vibration at 50 cps. Under 1g static loading, the support system is designed to support the load for five year life. The results of the analysis are summarized in Tables 2-3 and 2-4. Table 2-3 gives the results of the analysis for 6 ms shock duration, which is the specified time duration for the shock test. If the 6 ms shock duration were increased to 8 ms, the analysis shows that the total system heat leak is reduced by 3 watts. Table 2-4 compares the results of the 6 ms to 8 ms design. The total system heat leak for the 6 ms design is 44.6-46.1 watts, compared to 41.5-42.9 watts for the 8 ms design. The materials used for the structural supports were: neck tube, Hastelloy-X, tension rods, Inconel 625, hot end spider, molybdenum TZM Alloy. The temperature of the neck tube was 1285°F at the hot end and 150°F at the cold end. The temperature of the tension rod was 1430°F at the hot end and 50°F at the cold end.

Table 2-3. Summary of Neck Tube and Tension Rod Support System

6g Shock and 3g Vibration 6ms	
Total supported weight	289 lb.
Angle between tension rod and axial centerline	76° 32'
Top and bottom neck tube wall thickness for 1.5 safety factor	0.010 inch T 0.011 inch B
Natural frequency	888 Rad/sec.
Deflection of shield at center of gravity	2.93×10^{-3} inch
Amplification factor due to shock	1.19
Amplification factor due to vibration	
Horizontal	1.14
Vertical	1.08
Vertical upside down	1.04
Tension rod diameter	0.212 inch
Load in tension rod	959.4 lb.
Allowable stress in tension rod	27,222 psi
Maximum applied stress in tension rod	27,194 psi
Shear load on neck tube	801 lbs.
Allowable shear stress in neck tube for 1.5 safety factor (cold end)	10,942 psi
Allowable shear stress in neck tube for 1.5 safety factor (hot end)	9,403 psi
Maximum applied shear stress in neck tube (cold end)	10,369 psi
Maximum applied shear stress in neck tube (hot end)	9,423 psi

Table 2-4. Comparison of 6ms and 8ms Shock Duration

Model A HTVIS		
	6ms Shock Duration	8ms Shock Duration
Load on neck tube	801 lb.	813 lb.
Load on tension rod	933 lb.	921 lb.
Neck tube wall thickness	0.010 inch top 0.011 inch bottom	0.0095 inch top 0.0105 inch bottom
Tension rod diameter	0.212 inch	0.195 inch
Neck tube heat loss	17.8 to 19.2 watt	17.0 to 18.3 watt
Tension rods heat loss	17.7 to 17.8 watt	15.4 to 15.5 watt
Insulation heat loss	9.0 watt	9.0 watt
Total heat loss	44.6 to 46.1 watt	41.5 to 42.9 watt
Amplification factor (shock)	1.19	1.00
Natural frequency	888 rad/sec	836 rad/sec
Detection of shield at CG	2.93×10^{-3} inch	3.32×10^{-3} inch

The thermal expansion of the structural components due to a temperature increase from ambient to the given end temperatures of the neck tube (150°F and 1285°F) and the tension rods (50°F and 1430°F) were as follows: neck tube – 0.020 inch, tension rods – 0.016 inch, shield (in the axial direction) – 0.093 inch, spider (in the radial direction) – 0.013 inch. The temperature distribution in the neck tube and in the tension rods was calculated by using the one dimensional heat conduction equation with variable thermal conductivity. The temperature distribution in the neck tube was also calculated more accurately by including the effect of heat transfer by radiation from the multi-layer insulation to the neck tube and the heat transfer from the inside of the neck tube through the MIN-K insulation powder. Knowing the temperature distribution in the neck tube and tension rods, and the thermal expansion coefficient as a function of temperature, the thermal expansion was calculated by numerical integration. For the numerical integration the neck tube and tension rod lengths were divided into 25 increments. As a result of the thermal expansion of

the neck tube, shield, tension rods and the spider, it was found that the tension rod must rotate 2°30' during the heating or cooling cycle in order to follow the movement of the shield and neck tube. To avoid high bending stresses in the tension rods, free rotation of the tension rods was provided by using spherical ball joints at the tension rod ends. It was also found that the tension rods have to be installed with a 76°32' angle between the tension rods and the axial centerline of the shield in order to support the shield in the cold and hot condition without causing thermal stresses in the tension rods. The effect of change in this angle on thermal stresses in the tension rods was evaluated due to dimensional tolerances between the cold end and hot end of the tension rods. It was found that for ±0.062 inch dimensional variation between the hot end and cold end of the tension rods in the axial direction, the required 76°32' angle of the tension rod will vary by ±1°20'. This variation in the calculated rod angle will cause 20,800 psi tensile stress in the rod when the variation in angle is +1°20' and will cause the rod to be loose by 0.0025 inch when the variation in the angle is -1°20'. The reason for the tension rods being loose for negative angle variation is that they are designed with end connectors which allow only tensile loads to be transmitted to the rods. When the rods are subject to compressive loads, they become loose. To avoid high tensile stresses or looseness in the tension rods due to axial tolerance build-up, a sliding adjustment was provided at the cold end of the rods. Thermal stresses or looseness due to radial tolerance variations are prevented by a radial adjustment. This is done by varying the thickness of the spherical washer used in the tension rod assembly. With the adjustments provided both in the axial and radial directions at the cold end, the rods can be installed at an angle of 76°32' with a tolerance of ±0°7' allowed for measurement limitations. The tensile stress corresponding to the +0°12' tolerance limit is 3000 psi; the looseness corresponding to the -0°12' tolerance limit is 0.00036 inch (0.00036 inch elongation corresponds to 3000 psi compression). The rod will be prestressed to 3000 psi to prevent the looseness at the -0°12' tolerance limit, and to allow the +0°12' tolerance, the allowable stress in the rod for load carrying capacity is reduced by 3000 psi.

The method of installation described will prevent excessive tensile stresses and loseness at the cold and hot conditions of 50°F and 1430°F. However, at the intermediate temperatures during heating or cooling, or at temperatures above 1430°F (the unit will be heated to 1550°F for insulation conditioning), the rods will loosen. The 3000 psi prestressing will compensate for this.

The tension rod connector parts were designed for 1.5 safety factor based on the yield strength of the material. The thread size determined for the tension rod was 1/4-28 UNF with a required thread engagement length of 0.250 inch. The bearing pressure between the spherical washer and the ball of the rod was one half of the allowable tensile stress based on the yield strength of the material. Since the rod must rotate during heating or cooling, clearances were provided in the connector parts to allow the 2°30' rotation without interference.

In addition to sizing the connector parts, the deflection of each part was calculated under 1000 lbs. maximum load in the rods. This was done to determine the combined deflection of the tension rod and the tension rod connector parts.

The forces acting in the tension rods and in the neck tube were determined for the unit in three possible positions: vertical, vertical upside down, and horizontal. This was done by equating the deflection of the tension rod end of the shield, as determined by deflection of the neck tube end of the shield, and the corresponding angle to the deflection of the tension rods when corrected for the rod angle.

In the vertical position (neck tube open end up) the neck tube carries 1680 lbs. and the tension rods carry 54 lbs. At 6g static loading the 3000 psi prestress and 3000 psi tensile stress in the tension rods due to +0°12' tolerance on the tension rod angle will reduce the tensile forces in the neck tube. The maximum tensile stress occurs in the neck tube when the 3000 psi prestress is offset by the 3000 psi compressive load due to -0°12' tolerance on the angle. The maximum tensile stress under these conditions at 6g static loading was 14,500 psi which gives a 2.6 safety factor at the hot end of the neck tube. This figure is based on the yield stress of the material.

In the vertical upside down position (neck tube open end is down) the neck tube is in compression. The 3000 psi prestress and the 3000 psi tensile stress due to 0°12° tolerance on the rod angle is causing compressive stresses in the neck tube in addition to the compressive loads due to the weight of the shield. Under the maximum compressive loading at 6g static loading, the neck tube has a safety factor of 3.8 in pure compression and 2.9 and 2.6 in buckling in combined compression and internal pressure at the hot end and cold end of the neck tube, respectively.

The critical loading condition for the neck tube and tension rod support system occurs when the unit is in the horizontal position. In this position, the neck tube carries 801 lbs. and the tension rods carry 933 lbs. of the total load. It is assumed that under the worst condition, the 933 lb. load will be carried by only one tension rod. The neck tube was designed in combined shear and bending buckling. The critical mode of failure is in shear buckling since the bending moment on the neck tube with one end of the shield supported by the tension rod is small. The failure in shear buckling would occur by formation of diagonal wrinkles on the side of the neck tube. The critical shear stress at which failure occurs was calculated from experimental data obtained from the literature. It was determined that for 1.5 safety factor in shear buckling, the neck tube must have a minimum wall thickness of 0.011 inch at the hot end and 0.010 inch at the cold end. The required tension rod diameter was 0.212 inch. The allowable stress in the tension rod was based on the proportional limit rather than on the yield strength. The reason for this was that the 0.002 in/in permanent set obtained at 0.2 percent offset is significant compared to the total deflection of the tension rods. Deflection of the tension rod under 6g loading was 0.003 inch. With this deflection of the tension rods, the neck tube had a safety factor of 1.5 in shear buckling. The amplification factor due to shock loading was 1.2 for 6 ms. This amplification factor was factored into the strength of the neck tube and tension rods.

The amplification factor in vibration of 3g dynamic loading at 50 cps was 1.14 for the unit when vibrated in the horizontal position. The amplification factors in the vertical and vertical upside down positions were 1.08 and 1.04.

The rupture life of both the neck tube and tension rods was greater than the required 5-year life. The total heat leak for this system, including 9 watts insulation heat leak, was 44.6 watts minimum and 46.1 watts maximum.

It was found that if the time duration can be increased to 8 ms, the amplification factor due to shock reduces to unity and the neck tube wall thickness and tension rod diameter will be reduced. The neck tube wall thicknesses for this design were 0.0095 inch at the cold end and 0.0105 inch at the hot end. Tension rod diameter was 0.195 inch. The total heat leak for this system was 41.5 watts (minimum) to 42.9 watts (maximum).

Enclosure Analysis

Top Flange Design

The required wall thickness of the top flange was 0.375 inch. The design at the top flange thickness was based on deflection of the flange under 6g loading for the unit being in the horizontal position. The rotation of the neck tube and shield at the tension rod end due to the deflection of the top flange was 6 percent of the total deflection of the tension rods. A safety factor of 10 was calculated for the top flange at 6g loading. The calculation was based on the yield stress of the material.

Upper Head Design

The required thickness of the upper head was 0.250 inch. The safety factor of the upper head at 6g loading was 1.7.

Outer Shell Cylindrical Wall

The required wall thickness of the cylindrical wall is 0.109 inch. The safety factor in compression loading was 16.

Outer Shell Lower Head

The required wall thickness for the lower head was 0.250 inch. Assuming that the total axial load acts on a 2 inch diameter circle at the bottom of the head, the maximum load stress at 6g loading was 21,485 psi. The safety factor based on the yield stress was 1.5.

2.2.3.2 Transportation of Insulation System

The radiation test performed at ORNL used the insulation system assembled from residual Phase I parts.

The fragile nature of this particular insulation system (maximum horizontal shock – 2.3 g'sunsupported) required extreme care in handling, and rather than trust the unit to commercial carriers, it was decided that transportation from Buffalo to the test site at Oak Ridge should be under the direct supervision of responsible 3M

technical personnel. A station wagon fitted with a heavy plywood floor was selected as the best means of transport. The Linde Company supplied a steel shipping container (Figure 2-14) which supported the insulation system by a suspension prong which connected to and carried directly the weight of the shield. This arrangement greatly reduced the load carried by the insulation system inner liner. The vacuum was checked before transporting the unit and was recorded at less than 0.1 microns of Hg. The unit within the shipping container was then mounted approximately midway between the front and rear wheels and bolted to the floor. Prior to actual loading of the unit, the vehicle was driven over rough pavement and railroad tracks to determine what shock loads might be expected during transit. A recording accelerometer indicated less than 0.5g maximum shock (vertical). This same accelerometer was mounted on top of the shipping container during actual transit.

A recommended AAA route was followed. This routing followed the best surfaced roads and consisted of about 60 percent freeway or tollway driving.

Auxiliary equipment was air freighted to Oak Ridge. Delay in assembly of the system mock-up occurred because the mounting ring had been assembled at Linde using the pressure springs. The presence of the springs required a means of compression such that the ring would not interface with the insulation getter tube. External steel bands attached to the vacuum envelope were used to apply this compressive force (Figure 2-14). However, these bonds prohibited insertion of the insulation system into the pressure vessel. A means of compression was devised using washers under the spring bolt-heads (see Figure 2-15), whereby the bands could be removed and the system was assembled without further delay. Here again the vacuum was checked and measured at less than 0.1 microns of Hg.

No unusual situations developed during transportation and the unit was returned in good condition to 3M. The maximum shock recorded during transportation was 0.1g.

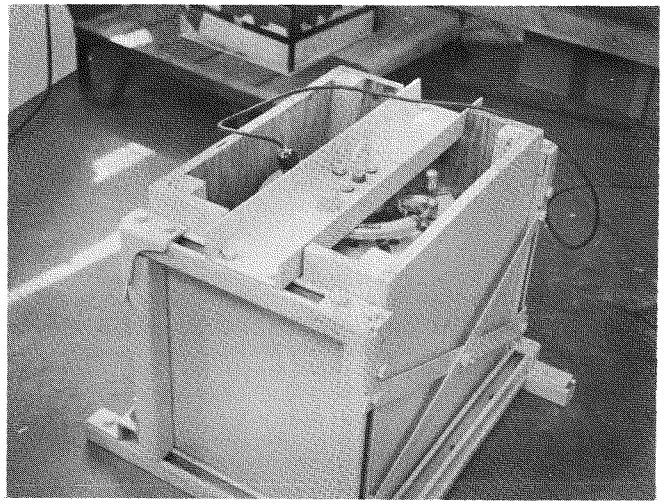

a) Container with System

b) Channel and Insulation System

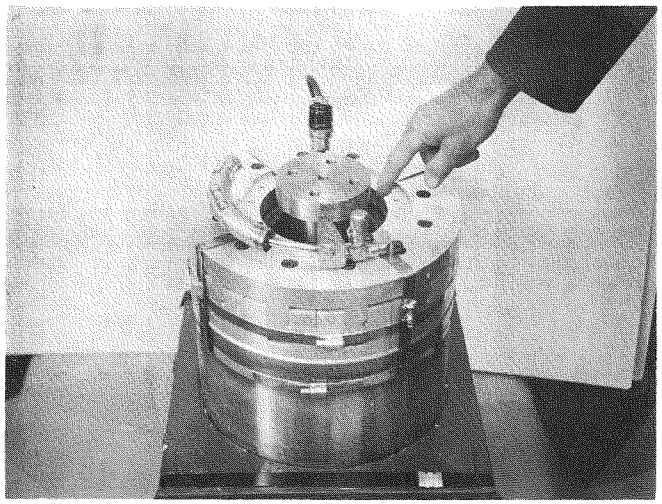

c) Main Center Support

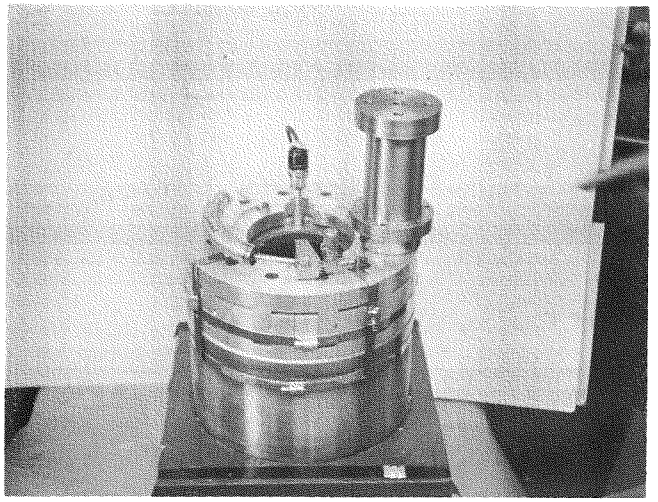

d) Main Center Support Removed

Figure 2-14. Insulation System Shipping Container Showing Method of Support

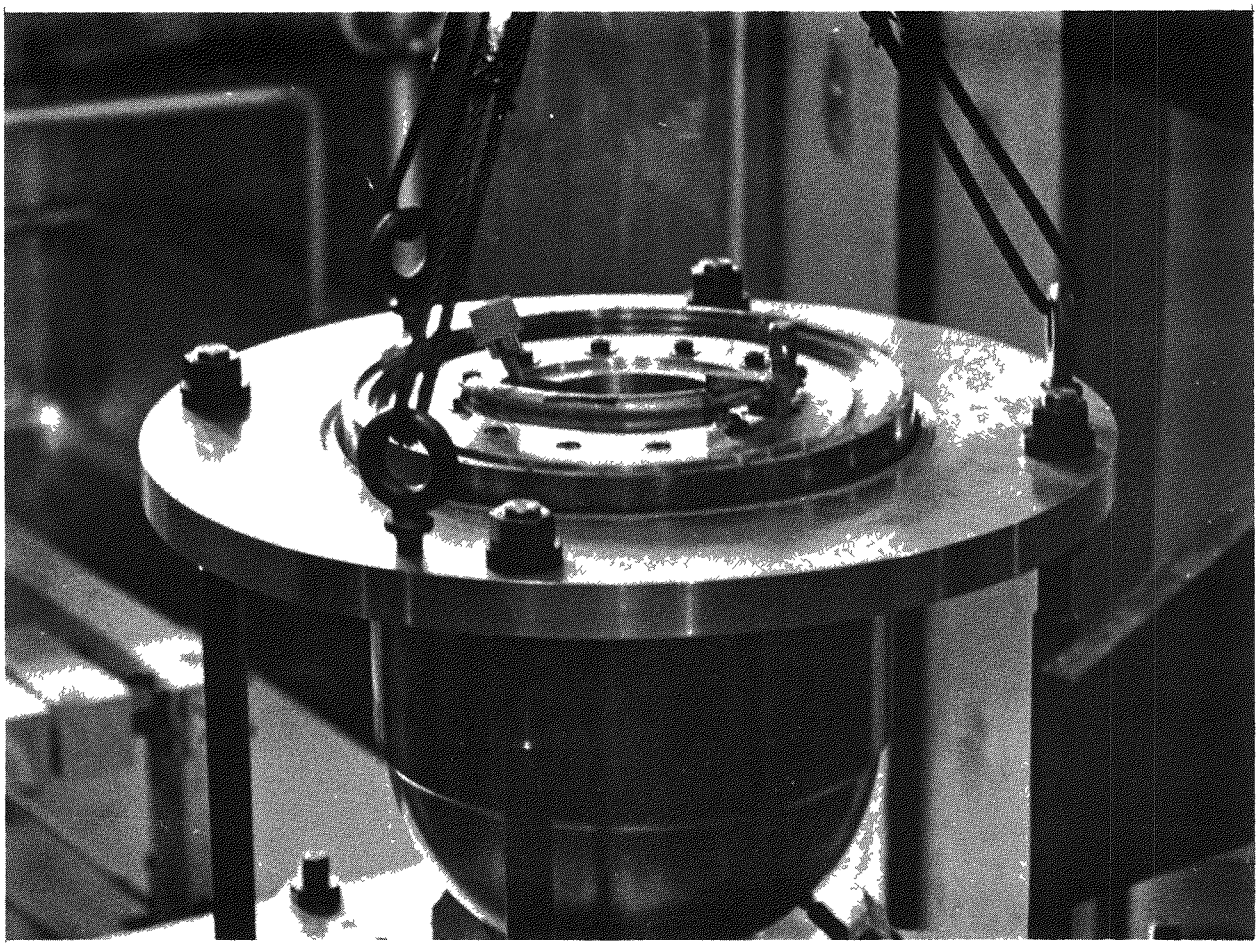

Figure 2-15. Insulation System Showing Washers Under Spring Bolt Heads

2.2.4 SEGMENTED RING

No effort was expended on this subtask this reporting period.

2.2.5 PRESSURE VESSEL

a) Design

The material to be used for the pressure vessel, titanium 6-2-1-0.8 (6A1, 2Cb, 1Ta, 0.8 Mo, generally referred to as 621-8 moly titanium alloy) was selected during the last reporting period. Calculations show that the wall thicknesses of the body and pressure vessel will be increased slightly because the strength properties of the 621-8 titanium alloy are lower than the 721 alloy. Because it is improbable that this change is significant enough to affect the results of the Phase I subscale tests, no further subscale tests are planned with this alloy. The minimum wall thickness for the cylindrical body was determined to be 1.121 inches and the small cover thickness 0.582 inch. Comparable dimensions for the 721 alloy are 1.085 inches for the cylindrical body and 0.502 inch for the small cover. The large cover wall thickness remains to be determined. A meeting is being planned between 3M and David Taylor Model Basin personnel to review the pressure vessel stress analysis.

A test forging of the pressure vessel cover using 621-8 moly titanium billet stock was forged by Taylor Forge and Pipe Works. Test samples were cut from the forging and mechanical property testing conducted on these samples.

Drawings were prepared by 3M showing the positions on the forging where specimens would be cut for future mechanical property testing.

The test data from the mechanical property testing will be evaluated and compared with data obtained from 721 alloy testing and marine engineering laboratory report 506/66.

2.2.6 THERMOELECTRIC GENERATOR

2.2.6.1 Design

The primary design effort during this report period consisted of incorporating the changes resulting from the analysis of problems encountered during the fabrication of components for the first four Phase II generators. The major areas in which design changes were considered were the thermoelectric couples, the sequence of fabrication of the cold frame assembly, and the interfaces between the long case and the hot frame and short case.

a) Thermoelectric Couples

The physical and electrical characteristics of the thermocouple components were 100 percent inspected to enable post-manufacture evaluation with respect to thermoelectric performance, ease of fabrication, and inspection. This evaluation resulted in minor changes in the physical dimensions of both legs and couples. These changes will be incorporated into Design No. 2.

The Seebeck voltages of the completed segments were analyzed and compared well with the design requirements. Minor adjustments were made to the data reference points and the equipment setup.

The resistivity technique was employed on the segments destined for use in the first four units, but later segments will be qualified by a maximum total resistance. On the segmented legs for the first four units, the R vs L check was replaced by the total resistance technique. While R vs L check is a measure of the bond resistance increase with respect to total resistance, the total resistance technique provides a resistance value which includes that of the bonds and the thermoelectric materials. This value is more easily obtained, requires less inspection time, and is more meaningful. Also, since the total resistance value is not so easily affected by surface conditions, the possibility of accepting inferior legs is lower than for the R vs L check.

The thermoelectric legs were bonded to the cold cap assemblies with a solder preform disk which produces a cleaner, more uniform joint. The cold caps were bonded to the jumper wire by inserting a braze preform into the tooling hole which was

extended to meet the jumper wire hole. This technique allows better bonding material flow than was obtainable when tin solder was used to bond the caps to the wire. These bonds were ultimately rebonded to the caps when the legs were bonded to the caps. This may have caused the joints to weaken.

b) Generator Components

The cold frame drawings were revised to change the sequence of fabrication. This was done to assure correct dimensions at the final subassembly level and requires a final machining of the copper cold frame and short case after they are brazed together.

c) Generator Design Variables

The design variables to be evaluated in the first four generators were determined during this period. The variables to be evaluated include argon vs xenon backfill gas and followers with hardcoated sockets vs followers with non-hardcoated sockets. Indium plated followers were also considered as a method to increase cold end heat transfer. These were ruled out because of relatively limited test data and the absence of material compatibility information. All generators will have soft nose P-legs and precision ball and socket cold end hardware.

2.2.6.2 Generator Fabrication Development

Quality Control and the Program Office reviewed process routings written during the first quarter. Final routings, incorporating the addition and corrections made, were approved by Manufacturing Engineering, Quality Control, and the Program Office.

Manufacturing Standard Instructions were written for:

- Processing of Fiberglass Insulation Sleeving
- Processing of Micro-Quartz
- Ultrasonic Precleaning of Metals
- Alkaline Cleaning of Non-Ferrous Metals
- Cleaning of Stainless Steel by Passivating
- Cleaning of Stainless Steel by Pickling
- Part Identification and Marking, General

In addition to these, a welding specification was written for the welding of the generator long case at the hot and cold ends to hermetically seal the generator.

All hardware relevant to the assembly of Generator A10D-2 was completed in this quarter; actual assembly started on June 9, 1967. The decision was made not to use vacuum grease in the assembly process of this generator. (Previously, a thin film of vacuum grease was applied to the follower prior to assembly to hold the follower in position.) Instead, rubber bands were used to hold the followers in place, as shown in Figure 2-16. This led to some difficulties during the assembly of the thermopile due to the increased pressure required to shove the follower up for couple insertion and resulted in some broken thermoelectric couples. The method of inserting the couples is shown in Figure 2-17. Another approach to the assembly of the thermopile is now being considered whereby couples can be assembled without contact with the follower. This would allow total assembly of the thermopile before the hot end is adjusted to its proper relation to the cold end.

The assembly of Generator A10D-2 was completed on June 22, 1967, and was found to have short circuits in some of the instrumentation. The shorts were attributed to fiberglass insulation sleeving (see Figure 2-18). It was partially disassembled (Figure 2-19) on June 23, 1967, to correct the shorting problems by putting additional micro-quartz insulation behind the fiberglass sleeving where contact with the copper cold frame was made. During the process of assembly, disassembly and reassembly, instrumentation to two of the followers was lost. Continuity checks were performed once again and the generator was accepted. Weld closure of the generator was made on June 23, 1967. The method of welding is shown in Figure 2-20.

Effort during the next quarter will be the completion of Generators A10D-4, which will be insulated and welded in a controlled atmosphere. Assembly of the three generators using the in-line follower concept, A10D-5, -6, and -7, is also planned for the next quarter.

Process routings, flow plans and Manufacturing Standard Instructions will be constantly updated to reflect any changes or improvements as assembly continues.

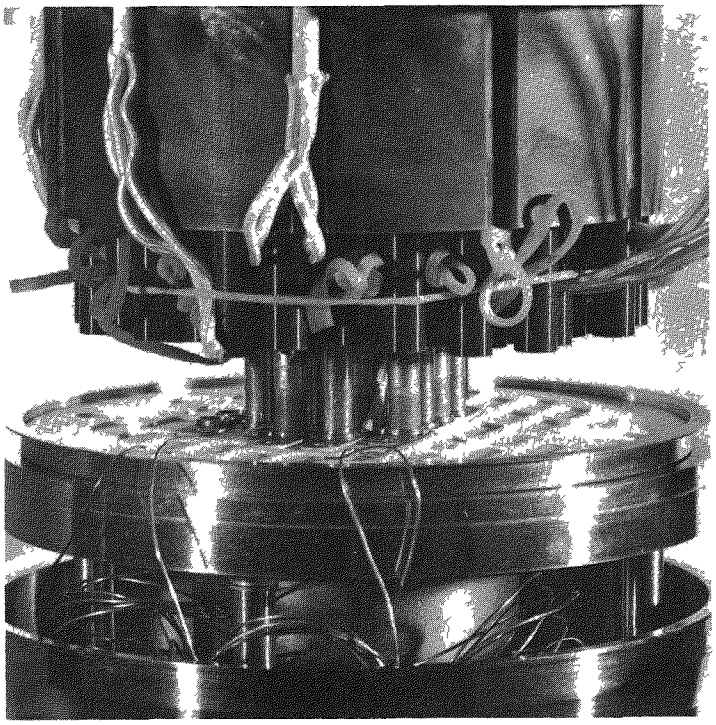

Figure 2-16. Assembly of Generator A10D-2 Method of Holding Followers in Place

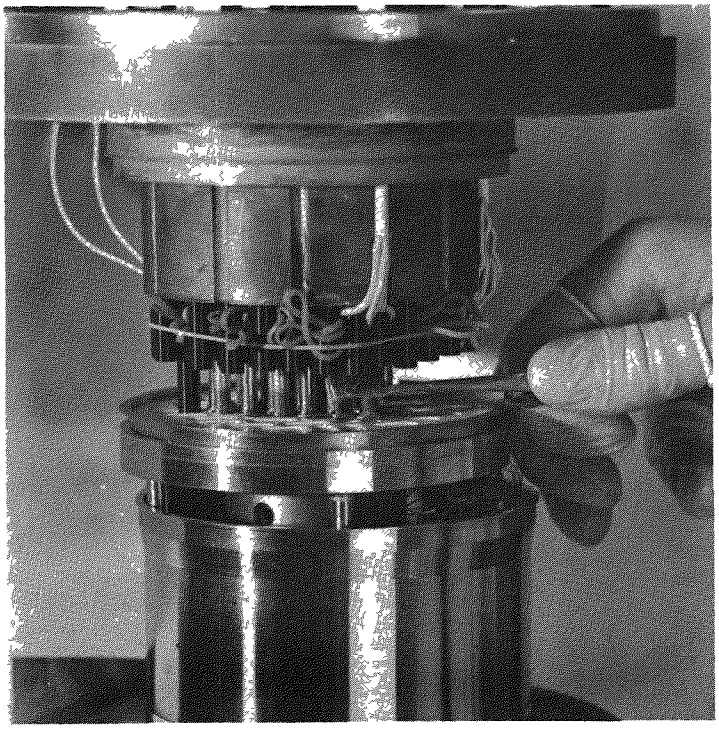

Figure 2-17. Assembly of Generator A10D-2 Couple Insertion

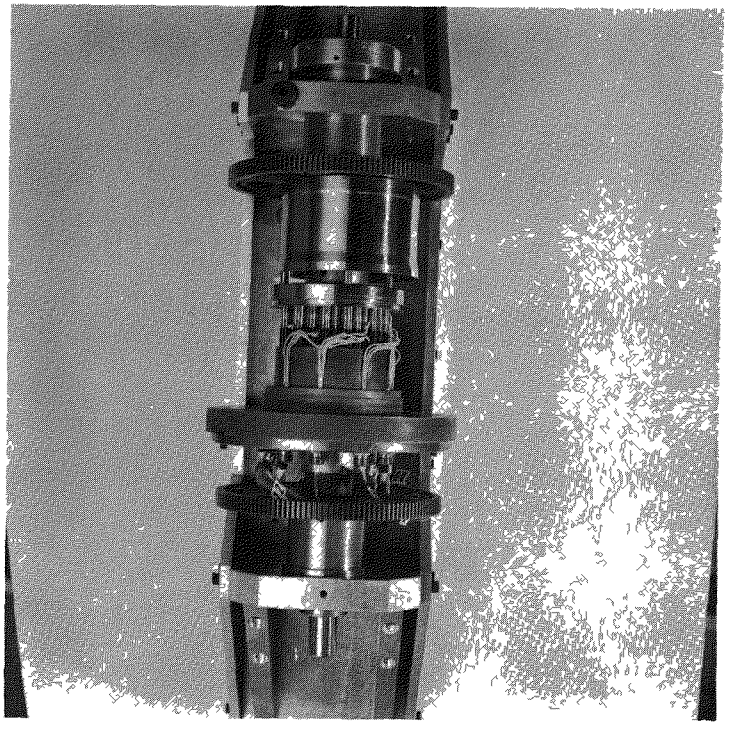

Figure 2-18. Assembly of Generator A10D-2: Fiberglass Insulation Sleeving

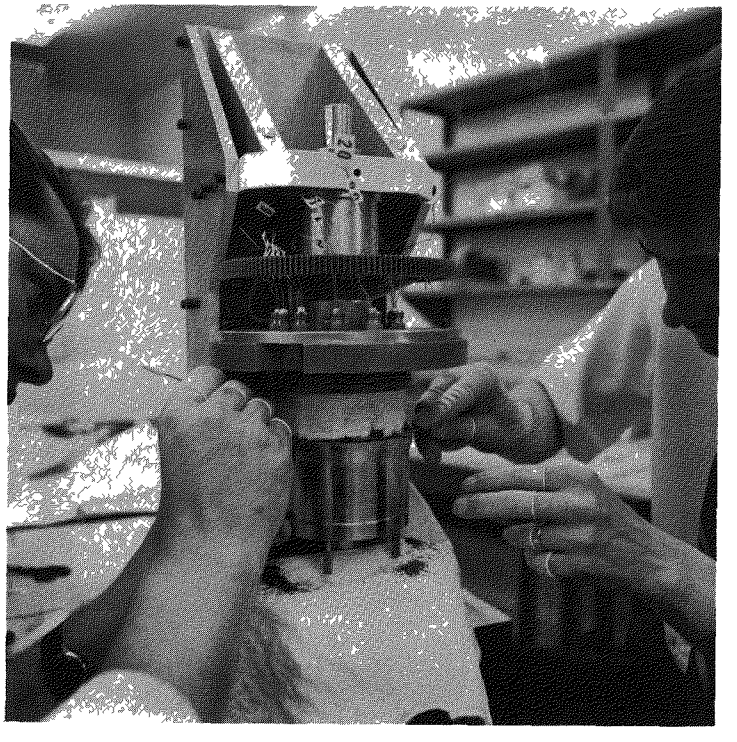

Figure 2-19. Assembly of Generator A10D-2: Partially Disassembled to Correct Shorting

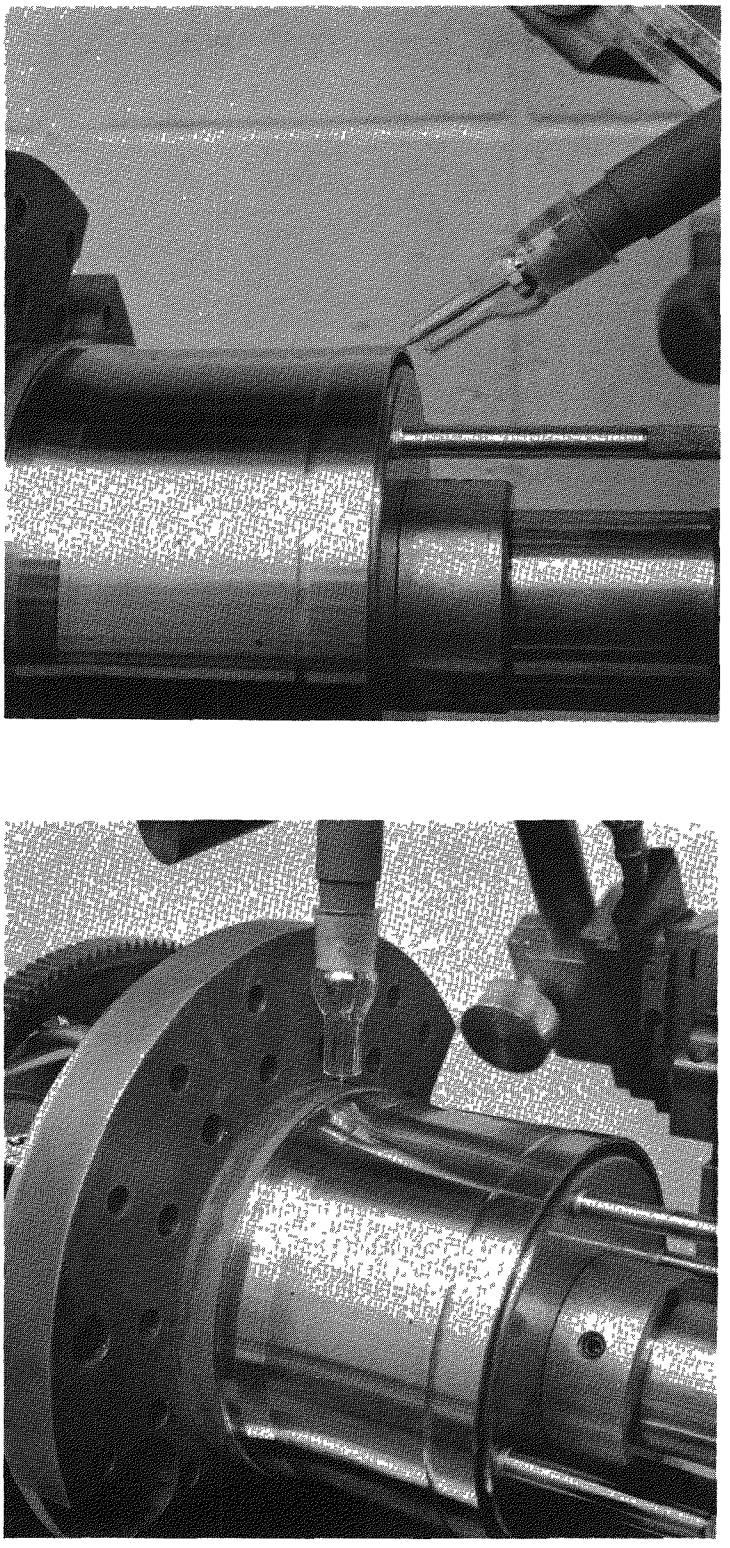

Figure 2-20. Assembly of Generator A10D-2: Weld Closure

2.2.6.3 Couple Fabrication

A total of 214 couples were fabricated during this quarter, including both instrumented and output tap assemblies. During the fabrication of this first group of couples manufacturing breakage was higher than expected. This breakage occurred at the N-leg and P-leg segment interface and the N- and P-leg segment to cold cap interfaces.

Development work is continuing to improve the physical strength of the bond during the bonding of the N- and P-leg segments (XTPO-193-A). The leg segments to cold cap bonds were improved by more thorough cleaning techniques and improved temperature control. Work is continuing to improve the physical strength of this joint through improved fabrication techniques (XTPO-204-A).

Some trouble was experienced in the fabrication of the instrumented couples. Investigation will be initiated to overcome this trouble by either changing the instrumenting wire size or changing the fabrication techniques.

2.2.7 POWER CONDITIONER

Design effort for the power conditioner was initiated during this quarter. Effort to date has consisted of initiating a review of the Phase I electronic component drawings to ensure that they are adequate for re-procurement and of contacting vendors who supplied the electronic components during Phase I to verify that the component is still being manufactured and to determine procurement lead times. A search is also being conducted for other electronic component suppliers to determine the availability of identical components that have demonstrated reliability.

Development tests on the existing power conditioner circuit are being performed to determine the adequacy of the existing circuit under certain off-design conditions. Results of these tests will determine whether or not circuit design moficiations are required. Details of the tests being performed are presented in section 2.3.7.

2.2.8 ELECTRICAL RECEPTACLE AND PLUG

No effort was expended on this sub-task during this report period.

2.3 COMPONENT AND SUBASSEMBLY TESTING

2.3.1 (TEST) FUEL CAPSULE

Development of ultrasonic methods for measurement of weld penetration and detection of flaws in peripheral end-cap welds on SNAP-21 capsules is continuing. Metallographic analysis verified the ultrasonic detection of (a) lack of penetration on the TIG welded samples, (b) porosity in the electron beam welded samples, and (c) a crack in the seam weld on Sample 9.

Abnormalities observed in the ultrasonic reflections during the measurement of weld penetration on the TIG welds appear to be caused by mechanical bonding of the unwelded joint. Comparison of metallographic and ultrasonic data showed anomalies between the two measurements of weld penetration where the mechanical bonding existed. The ultrasonic test procedure is being modified to compensate for this variance.

Increased emphasis is being placed on development of ultrasonic techniques for the classification of voids and the measurement of weld penetration on the electron beam weld configuration. Initial evaluation of ultrasonic data indicates porosity size and location in the electron beam weld volume can be effectively monitored. Metallographic analysis will be performed to verify these ultrasonic indications.

A supplementary effort to the weld development program being conducted at ORNL was undertaken. A specialty house was engaged to perform weld closures on three capsules using electron beam techniques.

Excellent results were obtained. Full penetration with no apparent voids or cracking was obtained.* (See Figure 2-21.) While these welds were performed with a high voltage electron beam welder (Hamilton-Standard) it should be possible to obtain equivalent results with the low voltage equipment (Brad-Thompson) available at ORNL.

The weld conditions for the weld shown were:

Acceleration voltage – 125,000

*Weld penetration obtained: 0.305 inch.

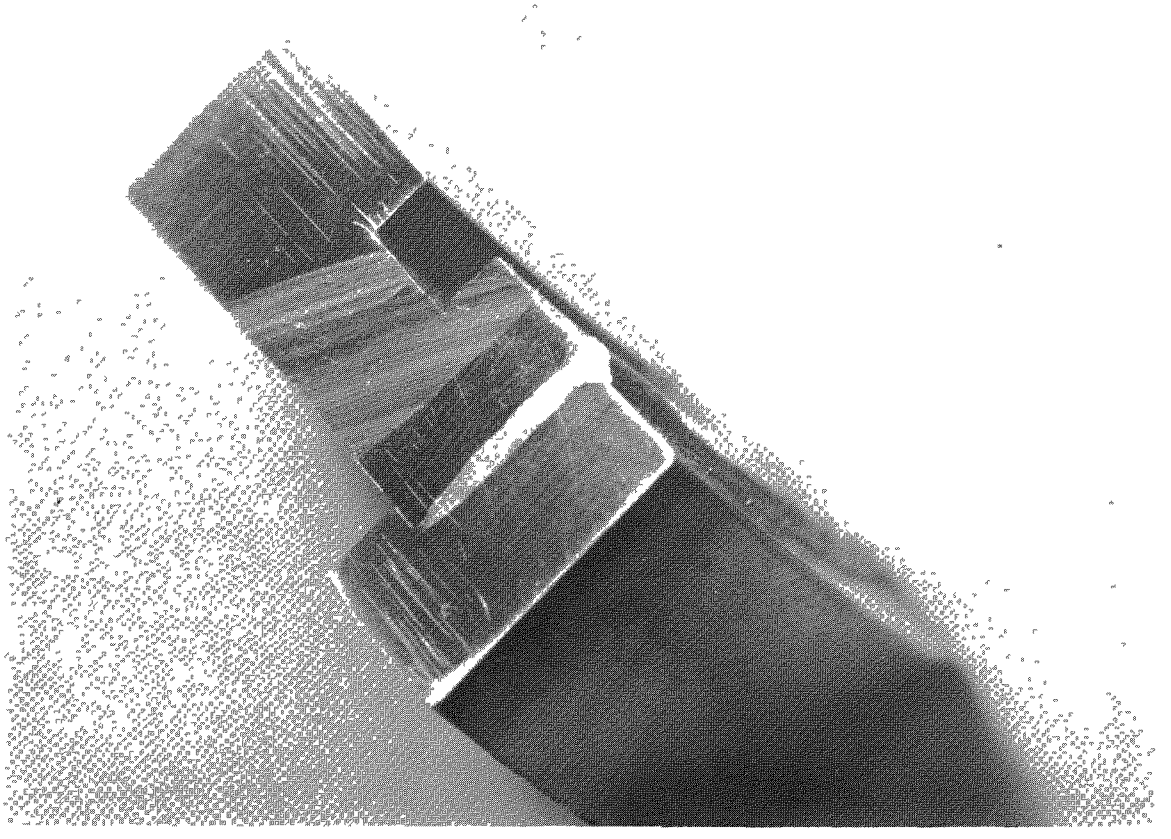

Figure 2-21. Cross Section of Electron Beam Weld

Beam current — 3.5 ma (tack welds)
— 15.2 ma

Welding speed — 16-17 sec/rev

Filament voltage — 1.58

Focal distance — 607 inches

2.3.2 BIOLOGICAL SHIELD

No work was done in this area during the past quarter.

2.3.3 INSULATION SYSTEM

2.3.3.1 Offgassing Investigation

Tests to determine the offgassing rate and offgas constituents of type 304 stainless steel were completed during this reporting period. The stainless steel tests followed the offgassing tests on the biological shield material. Because the shield tests contaminated the offgassing chamber it was necessary to decontaminate the

chamber by wiping the walls with a dilute solution of hydrochloric acid (1 part acid + 4 parts H_2O) followed by the application of 320 grit emery cloth and a final wipe with distilled water.

Following the chamber decontamination the empty chamber was maintained at 1550°F for 72 hours while vacuum pumping instead of the 1800°F for 48 hours as was originally planned. This change was made because it was felt that the 1550°F temperature would provide adequate conditioning for the stainless steel runs to be conducted at 100°F. At the conclusion of the conditioning, two empty chamber cycles were performed to determine the pressure rise characteristics of the empty chamber. Figure 2-22 presents the pressure versus time characteristics of the empty chamber. It can be seen that the second empty chamber run produced a lower pressure rise than the first run indicating that the chamber is more fully conditioned. Both empty chamber runs exhibited characteristics different from the empty chamber runs recorded during the prior offgassing work in that when the chamber was valved off at the start of the run the pressure was sharply reduced initially before it started a gradual rise. This phenomenon may be explained by the fact that the chamber had been conditioned at 1550°F and was therefore very clean for the runs at 100°F. For the low temperature offgassing cycle of stainless steel (condition at 350°F – run at 100°F), the chamber was most probably initially acting as an adsorber.

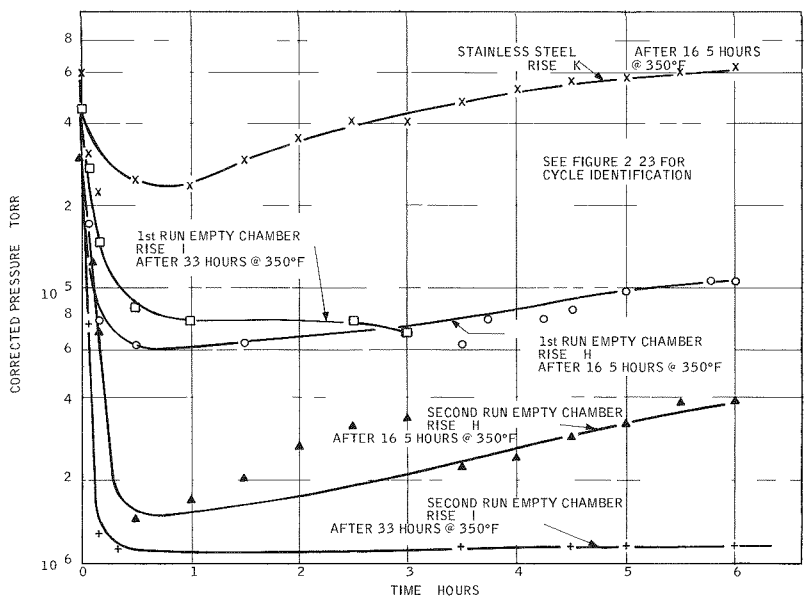

Figure 2-22. Corrected Pressure Rise Curves for Empty Chamber and Chamber with Stainless Steel

After the two empty chamber runs were completed, 20 square feet surface area of type 304 stainless steel was loaded into the offgassing chamber and the offgassing cycle shown in Figure 2-23 was conducted. Rise K at 100°F after 16.5 hours conditioning at 350°F is shown in Figure 2-22. The stainless steel sample was then conditioned at 350°F for an additional 16.5 hours and pressure rise L was started. After five minutes of rise L, the chamber temperature controller failed causing the chamber to be rapidly heated to 950°F and thus rise in pressure terminating the offgassing run. The pressure time history for rise L was as follows:

Time	Pressure (True) (Torr)	
8:30 a.m.	2.6×10^{-5}	
8:31 a.m.	1.9×10^{-5}	
8:32 a.m.	1.6×10^{-5}	
8:33 a.m.	9.3×10^{-6}	
8:34 a.m.	4.2×10^{-6}	
8:35 a.m.	4.1×10^{-6}	
8:36 a.m.	4.5×10^{-6}	(temperature controller failure)
8:37 a.m.	9.3×10^{-6}	
8:38 a.m.	1.13×10^{-5}	
8:39 a.m.	1.7×10^{-5}	
8:40 a.m.	2.9×10^{-5}	
8:45 a.m.	7.0×10^{-4}	

A comparison of this pressure-time history with rise K on Figure 2-22 shows that the additional 16.5 hours at 350°F initially reduced the offgassing rate of stainless steel by a considerable amount. If the rise could have been completed it is possible that the stainless steel would have been found to be an adsorber. At this point it was dediced not to rerun rise L since the empty chamber cycles would have had to be rerun as well. Since the surface area of the stainless steel in the actual units is small, a conservative estimate of the getter requirement for stainless steel offgassing can be based on rise K which was taken after 16.5 hours of conditioning. Table 2-5 shows the results of the mass spectrometer gas analysis for both the empty chamber and the chamber with the stainless steel sample. Figure 2-23 shows the offgassing cycles schematically.

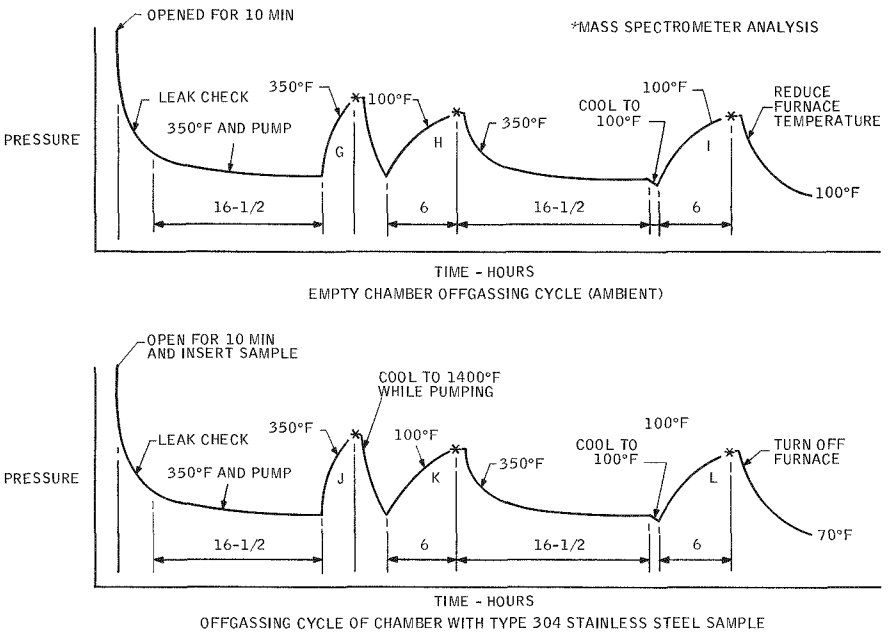

Figure 2-23. Schematic of Offgassing Cycles

At the completion of the stainless steel offgassing investigation as described above, the Philips type vacuum gauge used for all the offgassing runs except the quartz paper was removed from the offgassing test apparatus and calibrated against a McLeod type absolute vacuum gauge in air. Figure 2-24 shows the Philips gauge pressure versus the McLeod gauge pressure. The Philips gauge readings of the offgassing tests, corrected using Figure 2-24 are called P true (pressure true). Because the major constituent gas of the offgassing tests is hydrogen, P true was further corrected to account for the hydrogen in the gauge as follows:

$$*P_{corrected} = \frac{P_{true}}{0.4\,(X_H) + X_{rest}} \qquad \text{where}$$

X_H = Mole-fraction of hydrogen and hydrocarbon gases in the offgassing.

X_{rest} = Mole-fraction of the rest of the gases present in the offgassing.

*From communication with Consolidated Vacuum Corporation.

Table 2-5. Type 304 Stainless Steel Offgassing Test Data from Mass Spectrometer Analysis for Cycle Identification (see Figure 2-23)

Date	Time Hours	Temp. °F	Percent Composition							Cycle	Remarks
			CO_2	H_2	Ar	H_2O	N_2-CO	Hydrocarbon	O_2		
March 29, 1967	0930	350	0.630	35.40	---	53.60	9.66	---	0.68	G	Empty Chamber
March 29, 1967	1630	100	--	20.65	---	60.60	18.68	---	---	H	Empty Chamber
March 30, 1967	1600	100	0.613	21.20	0.435	68.90	8.85	---	---	I	Empty Chamber
April 5, 1967	0930	350	--	28.16	0.974	59.50	11.26	---	---	G	Repeat Empty Chamber
April 5, 1967	1630	100	0.540	19.40	0.527	73.60	5.82	---	---	H	Repeat Empty Chamber
April 6, 1967	1600	100	--	20.60	0.798	70.00	8.54	---	---	I	Repeat Empty Chamber
April 11, 1967	0930	350	3.750	33.30	---	48.70	14.20	---	---	J	304 Stainless Steel
April 11, 1967	1630	100	1.300	76.75	---	16.46	5.47	---	---	K	304 Stainless Steel

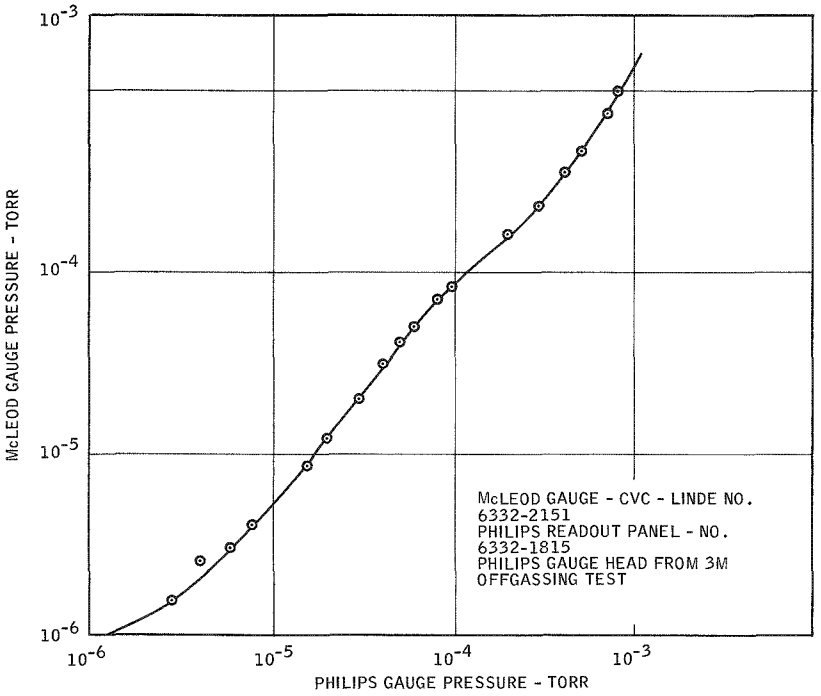

Figure 2-24. Calibration Curve for Philips Vacuum Gauge

as $X_H + X_{rest} = 1$, $P_{corrected}$ may be expressed as

$$P_{corrected} = \frac{P_{true}}{(1-0.6\,X_H)}$$

The offgassing rate for the stainless steel specimen was calculated at 100°F after 16.5 hours at 350°F. Figure 2-25 shows the corrected pressure rise versus time for Rise K plotted on rectangular coordinates to determine the slope of the curve. Because the empty chamber pressure rise was low compared to the chamber with stainless steel, it was not possible to subtract the empty chamber slope from the chamber with sample slope at an equal pressure. For calculating the stainless steel offgassing rates, as shown in Figure 2-26, plotted against pressure, and in Figure 2-27 plotted against time, the slope of the empty chamber was assumed to be zero.

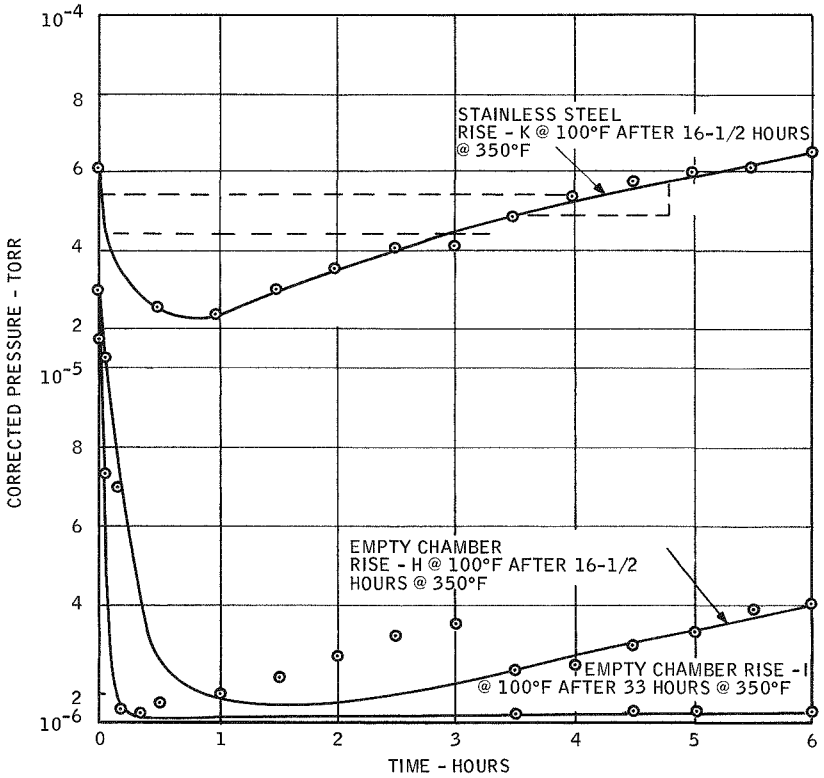

Figure 2-25. Pressure Rise Curves for Slope Determination

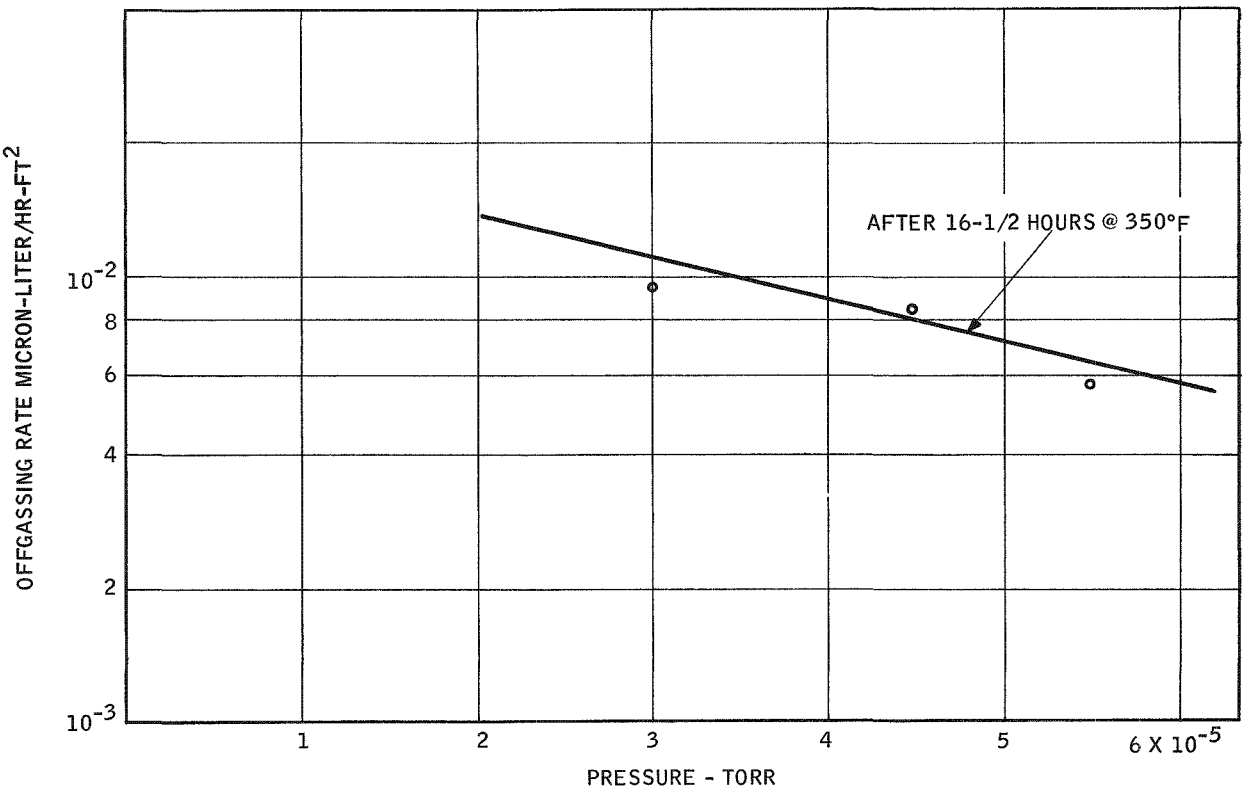

Figure 2-26. Offgassing Rate of Stainless Steel vs Pressure at 100°F

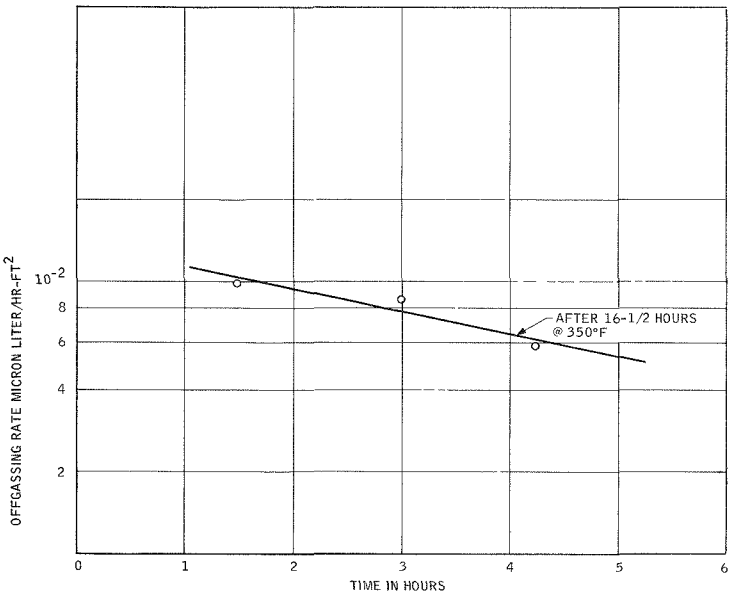

Figure 2-27. Offgassing Rate of Stainless Steel vs Time at 100°F

2.3.3.2 Vacuum Seal-Off and Getter Retention

Torque tests were performed on gold "O" rings which were purchased from an outside vendor. Two of the rings tested had raised beads at their joints; these two had earlier been declared unacceptable. Table 2-6 shows the results of the torque test on the "O" rings.

Because of the relatively uniform leak rates established during these tests, rings 6 and 7 were declared acceptable. The "O" ring acceptance standards are being re-evaluated in light of the tests in Table 2-6.

A simulated getter fill and temporary seal-off test was performed using modified test apparatus. The modification to the basic fill and seal-off apparatus included the installation of a 3/4-inch vacuum ball valve and a Hoke vacuum valve in the getter feed tube. This allowed using the basic seal-off device to evacuate a unit during conditioning and thermal performance testing without the necessity that the glass getter fill tube be in position during this time. A schematic of the modified getter fill and seal-off apparatus is shown in Figure 2-28.

Table 2-6. Gold "O" Ring Torque Test Data

Item	Torque (Ft. Lbs.)	Leak Rate (Std cc/sec air)	Remarks
1	25	5.26×10^{-11}	
2	40	5.27×10^{-11}	
3	30	5.8×10^{-11}	
4	30	4.75×10^{-11}	
5	15	5.26×10^{-11}	
6	45	4.75×10^{-11}	Raised bead at joint
7	30	4.53×10^{-11}	

For this test a simulated getter was prepared using 35 grams of talcum powder plus 5 grams of santocel powder to give a bulk density of 0.34 gm/cc. The bulk density of the getter is in the range of 0.30 to 0.35 gm/cc. Simulated getter was used in place of actual getter because getter cannot be exposed to air without a reaction. Therefore, it was dediced that for this first demonstration test it would be safer to use a simulated getter until the apparatus performance had been demonstrated.

Prior to the test the glass bulb containing the simulated getter was evacuated while heating with an electric blanket for several hours to remove the residual moisture. The test procedure as presented in the development test plan was modified as follows:

a. Close ball valve and evacuate system to a pressure of 1 micron.

b. Insert glass getter fill tube into quick connect coupling and evacuate glass tube through Hoke vacuum valve.

c. Open ball valve and close Hoke valve. Slide glass tube into female portion of seal of device.

d. Open glass stop cock valve and allow simulated getter to flow into getter reservoir.

e. Close glass valve and withdraw getter fill tube just past ball valve and close ball valve.

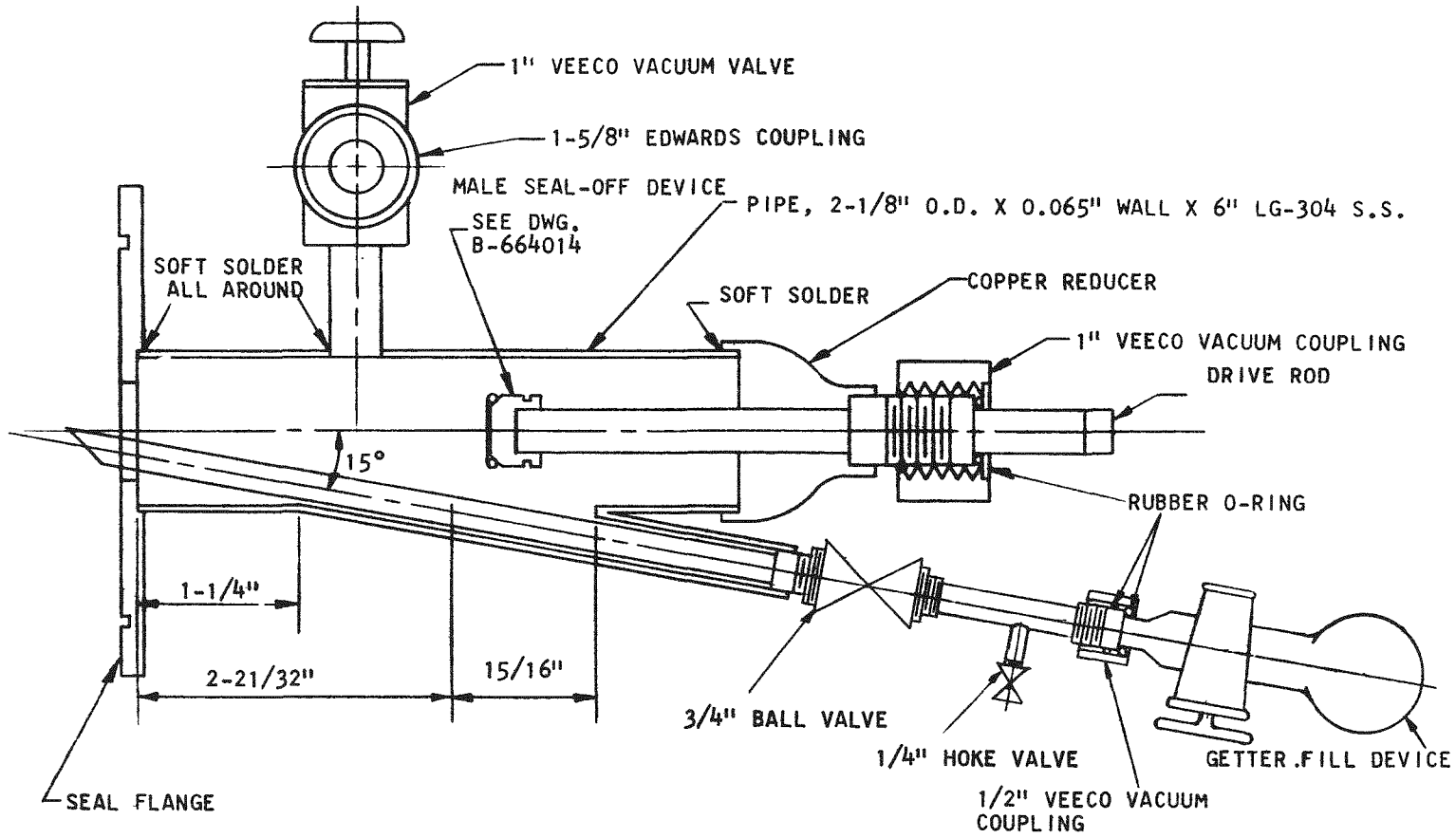

Figure 2-28. Schematic of Getter Installation and Seal-Off Apparatus

f. Open Hoke valve and complete withdrawal of glass getter capsule.

g. Traverse male plug push rod to engage seal-off device threads and apply required torque to seal.

During the test it was observed that the simulated getter powder tended to pack just above the glass valve, stopping the flow into the unit. To resume the flow an electric Vibograder tool was applied to the quick connect coupling sealing the glass tube. It has been observed qualitatively that the actual getter flows much more freely than the simulated powder used for this test, therefore, this packing should not be a problem in the actual units.

To provide the temporary seal for this test, performed gold O-ring No. 1 as presented in Table 2-7 was used. The seal-off torque was 70 ft-lbs. After the evacuation, getter fill and seal-off, the apparatus was removed and the temporary seal was leak checked with a Veeco MS-9 leak detector. After 1 hour and 25 minutes with helium on the non-vacuum side of the seal, the leak rate was determined to be the non-vacuum side of the seal, the leak rate was determined to be 2.81×10^{-10} std cc/sec-air.

Upon opening the test unit, it was noted that the simulated getter powder was piling up in the getter enclosure in the form of a pyramid directly below the fill hole, obstructing the flow path of the simulated getter. Further development work will be performed to eliminate the possibility of a getter pile-up.

As a result of the vacuum conductance and getter retention tests performed previously, Huyck Metal Company, Feltmetal No. FM-215 porus metal sheet (Type 347 stainless steel, 0.050 inch thick, with average pore size of 13 microns and with a Type 347 stainless steel screen sinter bonded on one size) was selected for the tests to determine methods to weld the getter retainer into the lower enclosure head. It is estimated that this material will have a similar conductance as the FM 627 previously tested, however, a conductance test will be performed to determine the actual vacuum conductance in the free molecular flow regime. The bonded stainless steel screen makes this material considerably more rigid than the FM 627. Before starting the weld test, the approximate location of the getter retainer was determined and it was found that the retainer would intersect the lower head wall at approximately a 30 degree angle. This angle was used when making simulated retainer material welds as discussed below.

The weld development was started by welding a 1-1/2 inch long by 1 inch wide FM 215 sample directly to a 3/8 inch thick type 304 stainless steel plate. The FM 215 material was placed at a 30 degree angle with the stainless plate and a manual heliarc fillet weld was performed on the screen side of the sample. The same procedure was followed by welding on the plain side of the sample. This weld is shown in Figure 2-29, No. 1. Because this material does not wet the surface and ball up during welding, severe cracks were noted along the weld joint. This could allow the leakage of getter into the insulation space.

Table 2-7. Seal-Off Apparatus – Gold O-Ring Seal Tests

As fabricated gold rings – 0.060 inch diameter 24 carat wire, batch annealed at 750°F for 30 minutes in a salt bath and air cooled.

Ring No.	Torque Required ft-lb.	Leak Rate std. cc/sec. air
1	27.5	$< 5.10 \times 10^{-11}$
2	22.5	$< 5.57 \times 10^{-11}$
3	50.0	$< 5.57 \times 10^{-11}$
4	37.5	$< 5.57 \times 10^{-11}$
5	No seal at 50	----------
6	70.0	$< 4.84 \times 10^{-11}$
7	37.5	$< 4.40 \times 10^{-11}$
8	50.0	$< 4.40 \times 10^{-11}$
Second run using above rings in a new seal-off device.		
1 (repeat)	22.5	$< 5.10 \times 10^{-11}$
2 (repeat)	25.0	$< 4.75 \times 10^{-11}$
3 (repeat)	40.0	$< 4.20 \times 10^{-11}$
4 (repeat)	No seal at 65	----------
5 (repeat)	75.0	$< 4.92 \times 10^{-11}$
6 (repeat)	25.0	$< 4.46 \times 10^{-11}$
7 (repeat)	55.0	$< 4.46 \times 10^{-11}$
8 (repeat)	30.0	$< 4.92 \times 10^{-11}$

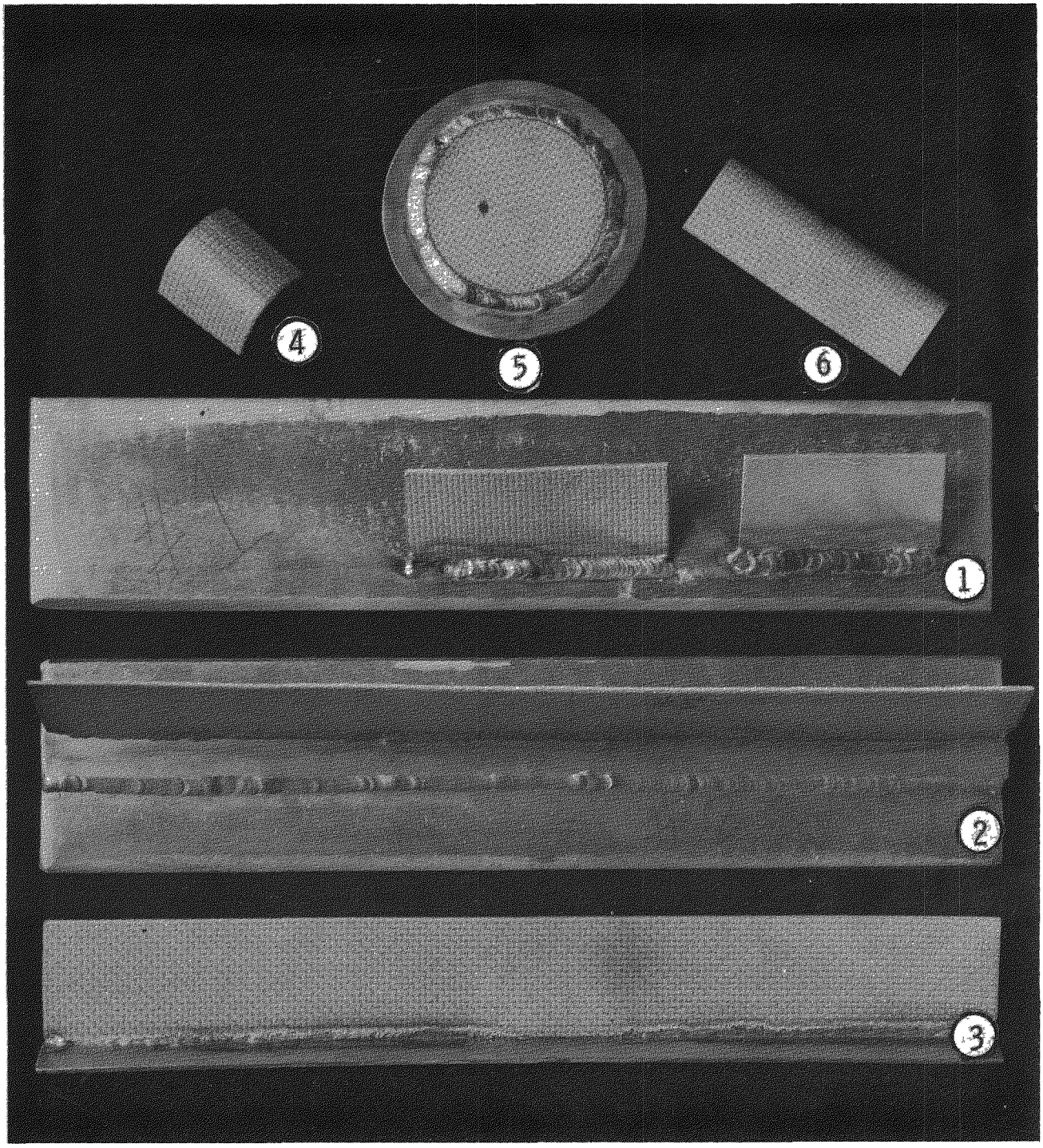

Figure 2-29. Getter Retainer Material Weld Specimens

To provide a better heat sink a thin strip, 0.050 inch thick by 9 inches long by 1/2 inch wide, type 304 stainless steel was welded directly to the FM 215 sample and specimen over a copper block during actual welding. This weld was very satisfactory with no cracks being observed. This type of weld, using a transition strip at a 30 degree angle, was performed on both the plain and screen side of the specimen with equally successful results. The stainless steel transition strip was then fillet welded to the 3/8 inch thick type 304 stainless steel plate with good results as shown in Figure 2-29, No. 2. To use this method, the stainless steel transition piece will be cut and formed into a conical section to fit the radius of the lower enclosure head before welding the FM 215 specimen.

To simplify the process of making a transition piece, a washer type transition piece was cut from type 304 stainless steel, 1-3/4 inch O. D. by 1.0 inch I. D. by 0.050 inch thick, and the FM 215 retainer material was flat fillet welded to the washer using a chill on the porous metal sample. This method also produced an acceptable weld and is shown in Figure 2-29, No. 5.

To simulate the weld at the radius of the lower enclosure head, two getter retainers were welded in 4 inch I. P. S. schedule 40 pipe caps. Transition rings made of 304 stainless steel material were fillet welded to the porous metal sheet. One of the transition rings was formed into a conical section (Figure 2-30, bottom) and the other ring was made like a flat washer type transition ring (Figure 2-30, top).

These fillet welded composite discs were made on the bench by providing appropriate chill to the weld and under argon gas shielding. These discs were, in effect, fillet welded to the 4 inch I. P. S. Schedule 40 pipe.

2.3.3.3 Weld Joint Development

a) Girth Weld

Activities conducted during this reporting period to complete the girth enclosure weld development included making macrographs of the girth weld joint, tensile tests of these weld joints and demonstration of ability to repair a deliberately made leak in the joint.

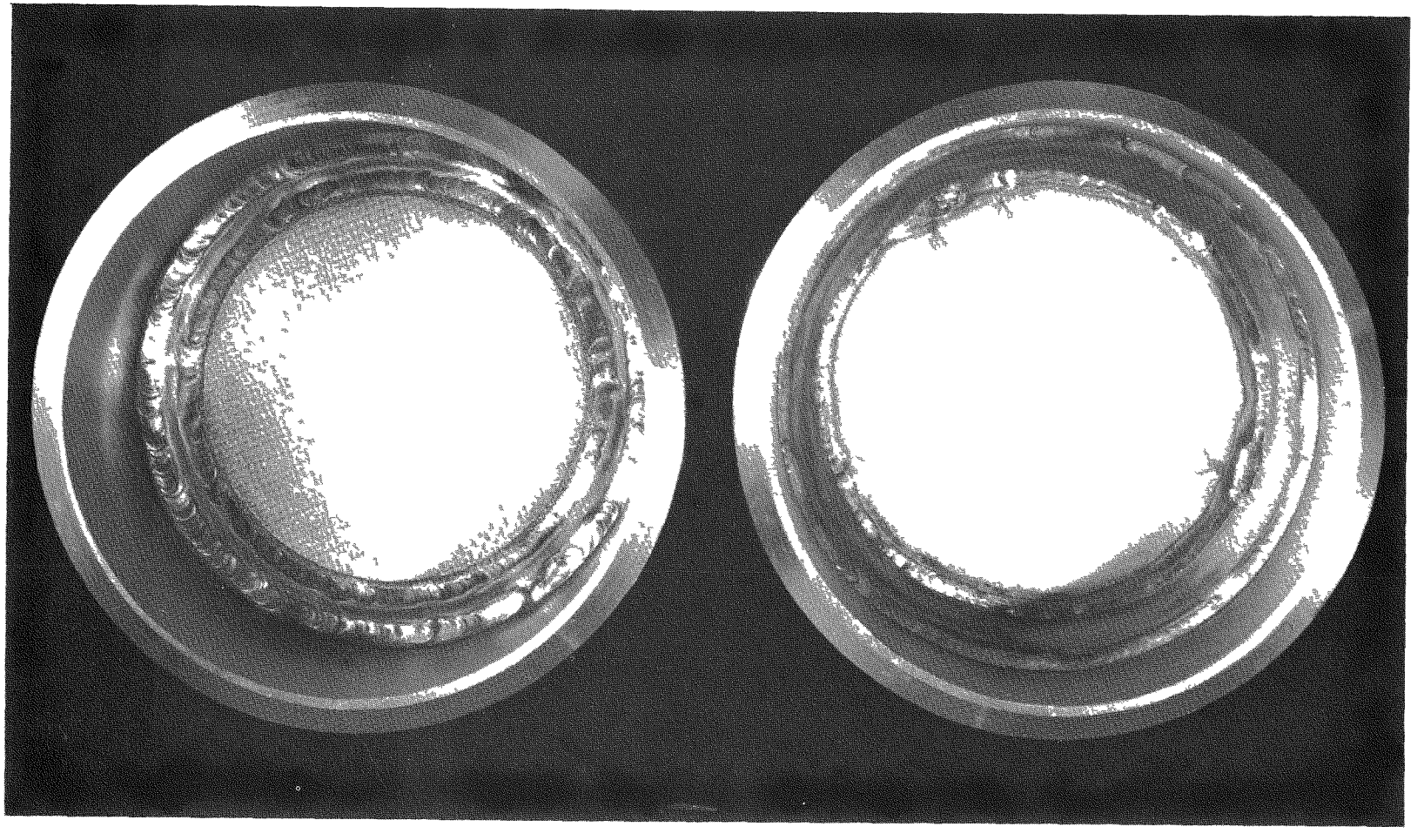

Figure 2-30 Getter Retainer Material Welded in Simulated Outer Case

To show the enclosure weld joint in greater detail specimens were cut from the 6 inch O. D. pipe weld specimens Nos. 3, 4, and 5. The macrographs are shown in Figures 2-31 through 2-34. The two macrographs were made from specimen No. 5 to show the uniformity of the weld. They show that penetration into the backup strip was accomplished without burnthrough. It can also be seen that there is no porosity or gross cracking in the weld zone and that there is good penetration of the second pass into the first pass without cold shunts or cracking.

A tensile specimen was prepared from each of the five 6 inch O. D. pipe girth weld joints. The specimens were too short (7-1/2 inch long) to provide an adequate tensile test machine jaw grip area so a six inch long by 3/8 inch thick 304 stainless steel plate was butt welded to the end of each specimen for the test.

Each specimen was tensile tested. The results are presented in Table 2-8; Figure 2-35 shows the pulled specimens. All failures were through the weld joint where there is minimum cross section area. The welds were not built up higher than the parent material in order to eliminate any need for grinding the weld to meet dimensional tolerances. The ultimate stress, which in all specimens was greater than 87, 600 psi, was based on thickness measurements through the weld in the estimated fractured area.

To demonstrate a leak repair technique, one of the 3 inch diameter pipe girth weld joints was drilled with a No. 43 drill through the weld bead. To repair the leak, the drilled hole area was ground out to a depth of approximately 3/16 inch and 1-1/4 inch long. Repair was made by manual heliarc welding using an HW-20 torch with 25 CFH argon shielding and 3/32 inch diameter type 308 filler wire. Three passes were required to repair the leak with the weld parameters as follows:

Pass No.	Amps	Volts
1	114 – 126	12. 5 – 13. 5
2	150 – 168	11. 5 – 13. 0
3	102 – 108	10. 5 – 11. 5

After the repair was accomplished the joint was leak checked with a Veeco MS-9 helium leak detector and found to be leak tight within the sensitivity of the leak detector (leak less than 5.3×10^{-11} std cc/sec-air).

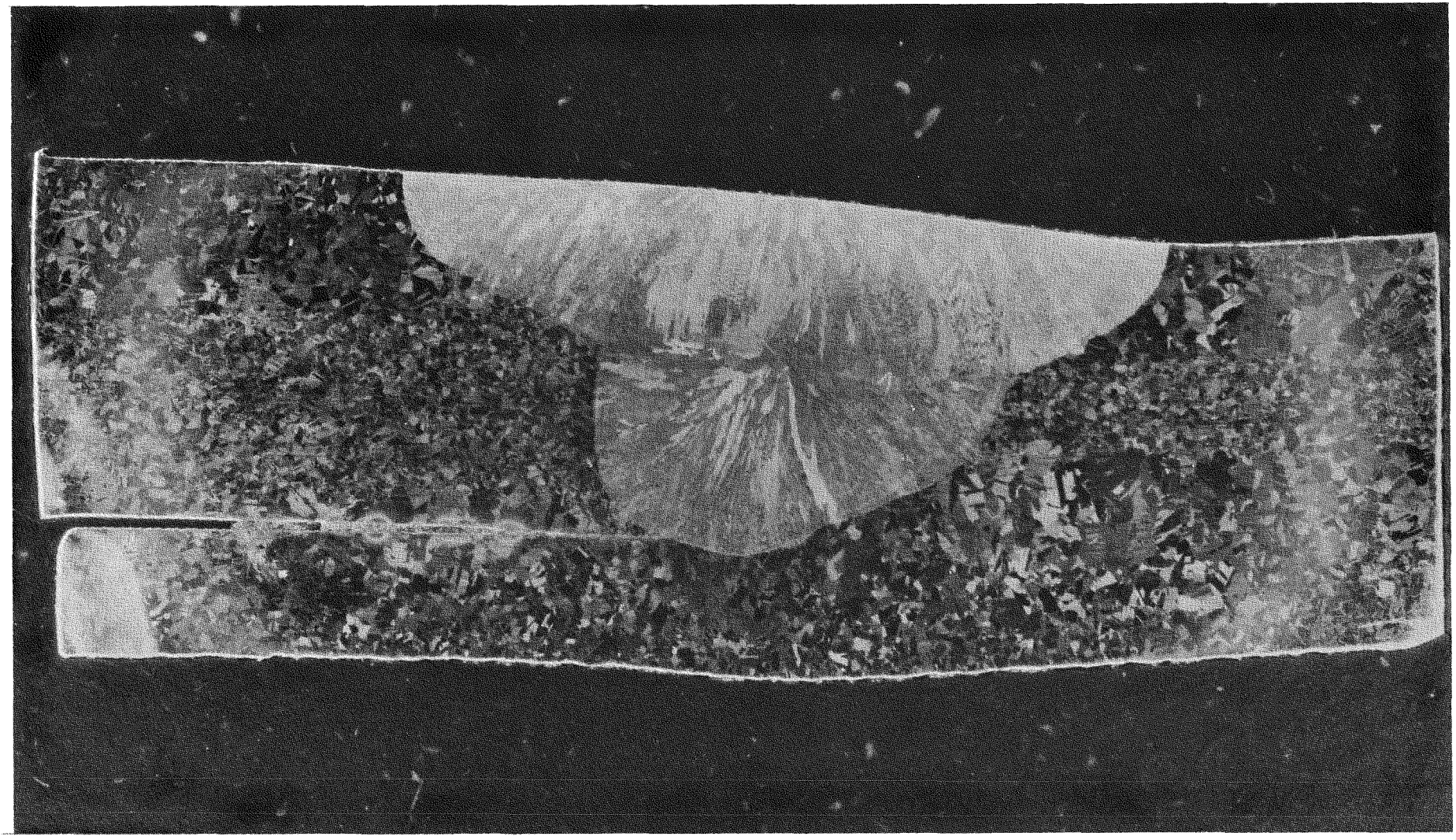

Figure 2-31. Macrograph of Enclosure Girth Weld Specimen No. 3 (5X)

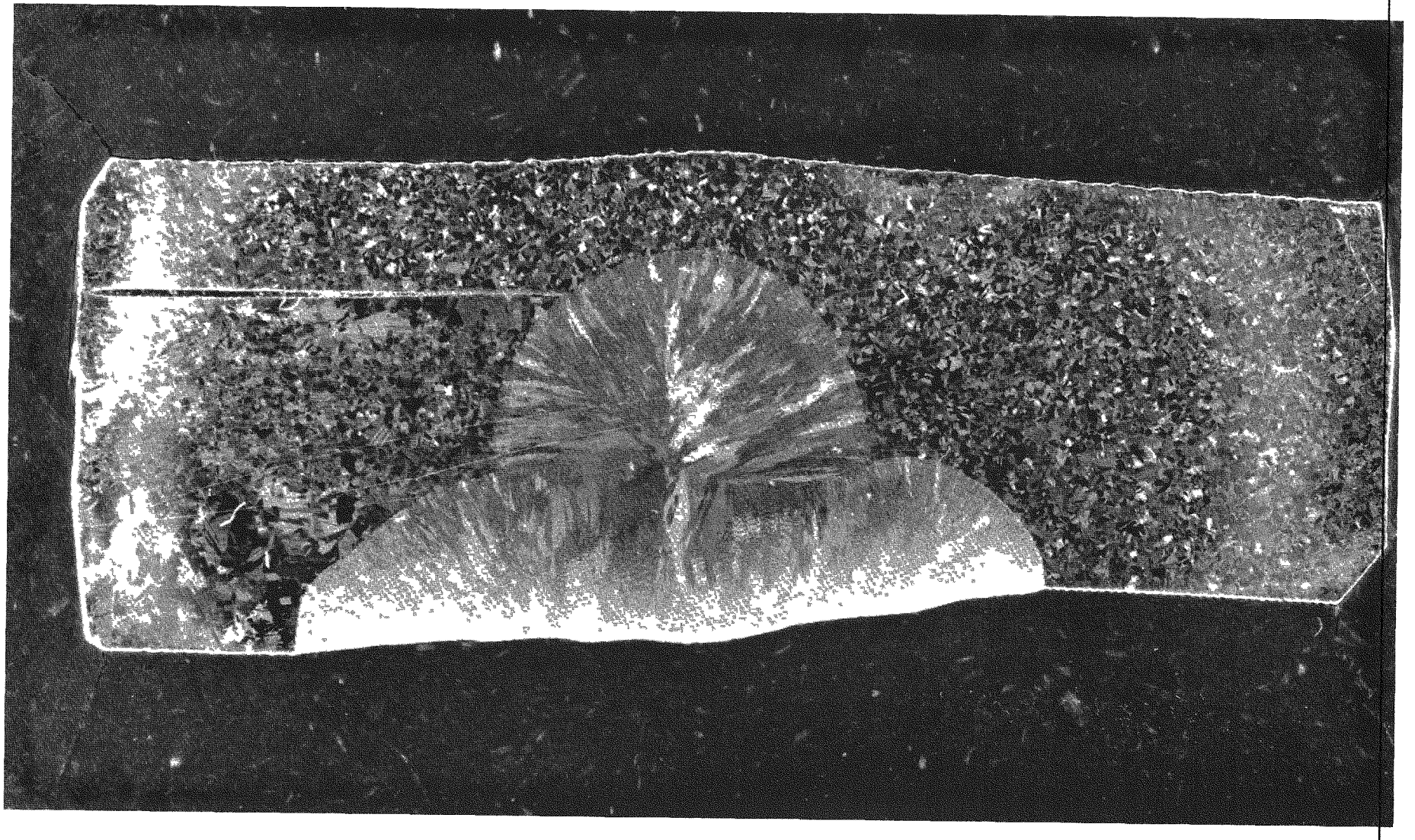

Figure 2-32. Macrograph of Enclosure Girth Weld Specimen No. 4 (5X)

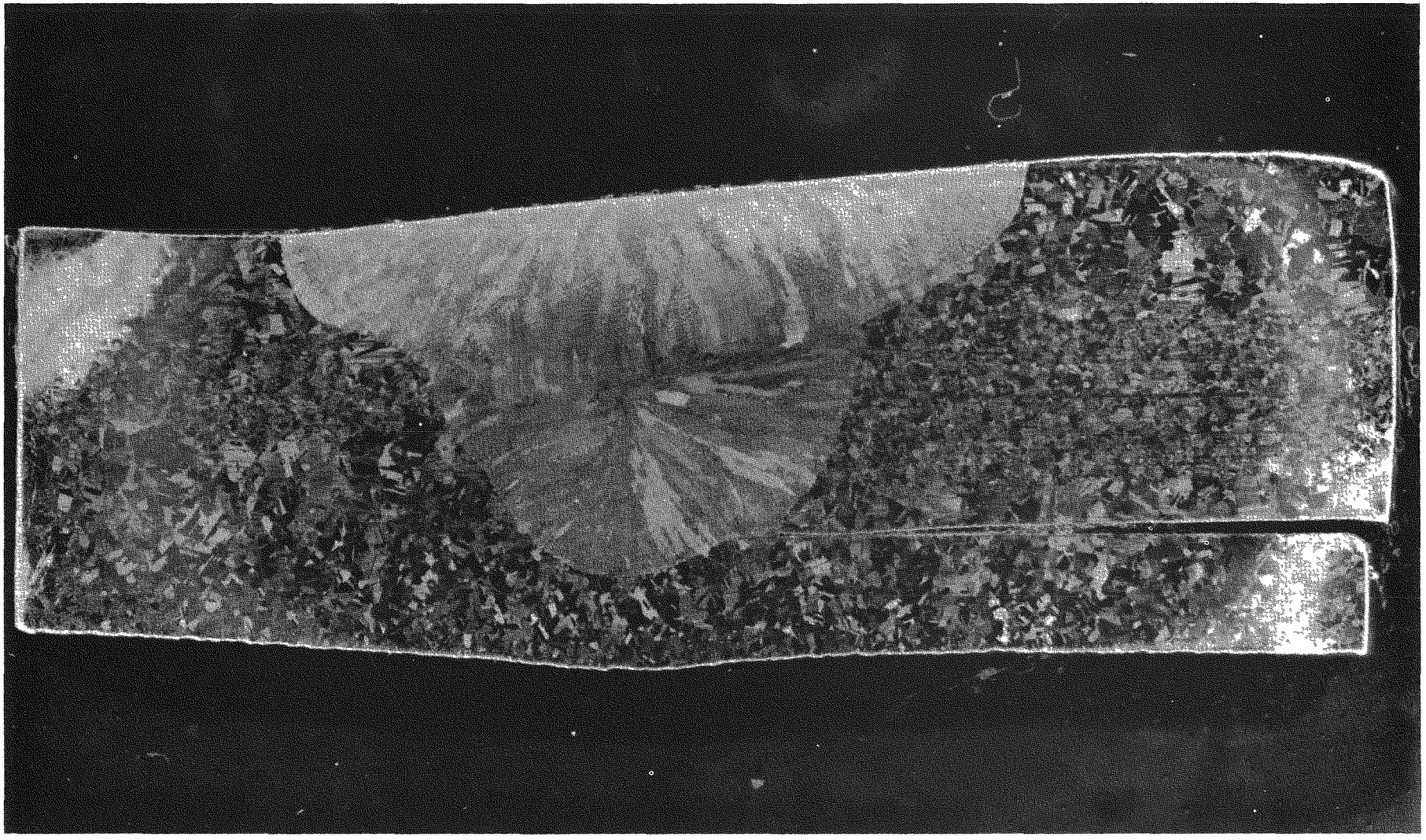

Figure 2-33. Macrograph of Enclosure Girth Weld Specimen No. 5a (5X)

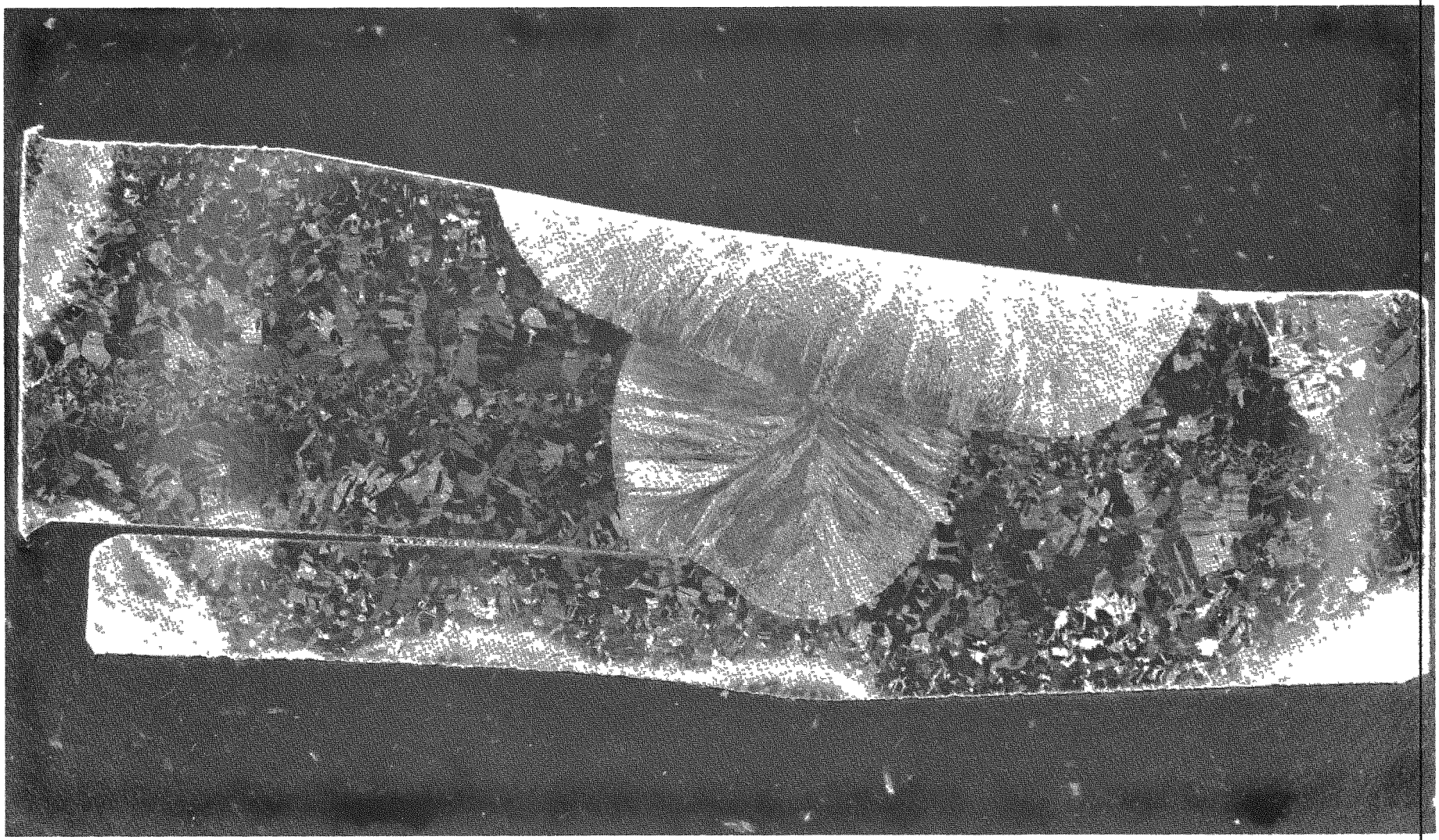

Figure 2-34. Macrograph of Enclosure Girth Weld Specimen No. 5c (5X)

Table 2-8. Summary of Automatic Girth Weld Tensile Specimens Cut from 6-Inch O. D. Pipe Welds

Description	Unit Nos.				
	1	2	3	4	5
Base Material	304 S. S.	304 S. S.	304 S. S.	304 S. S.	304 S. S.
Filler Material	308 Elec.	308 Elec.	308 Elec.	308 Elec.	308 Elec.
Weld Process			Automatic Heliarc		
Test Temp. °F	75°F	75°F	75°F	75°F	75°F
Cross Sectional Area	0.279 Sq. In.	0.298 Sq. In.	0.301 Sq. In.	0.290 Sq. In.	0.292 Sq. In.
Width	1.502 In.	1.502 In.	1.499 In.	1.499 In.	1.502 In.
*Thickness	0.186 In.	0.199 In.	0.201 In.	0.194 In.	0.195 In.
Ultimate Strength (load) lbs.	25,100	26,100	26,650	25,700	26,050
Ultimate Stress Psi	89,900	87,600	88,200	88,600	89,200
Failure Location	Weld	Weld	Weld	Weld	Weld

*Thickness measurements are through weld in estimated fractured area.

b) Neck Tube Weld

Simulated neck tube joint welds between the Hastelloy-X neck tube material and the Type 304 stainless steel top flange material were made to determine the required weld parameters for an acceptable joint. Three joints each of 2-1/2 inch diameter and 5 inch diameter were semi-automatic heliarc welded. The weld geometry is shown in Figure 2-36.

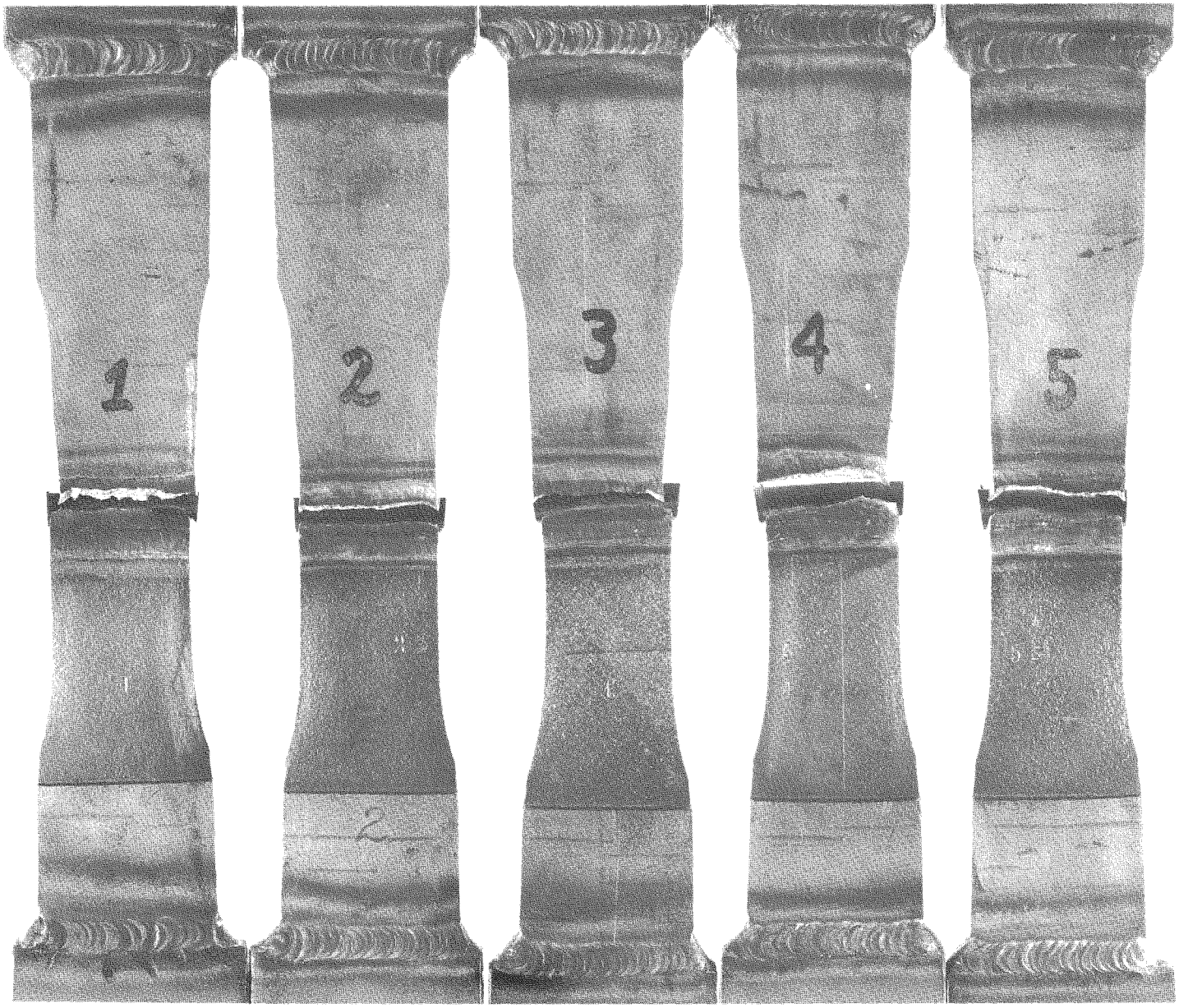

Figure 2-35. Enclosure Girth Weld Tensile Test Specimens After Test

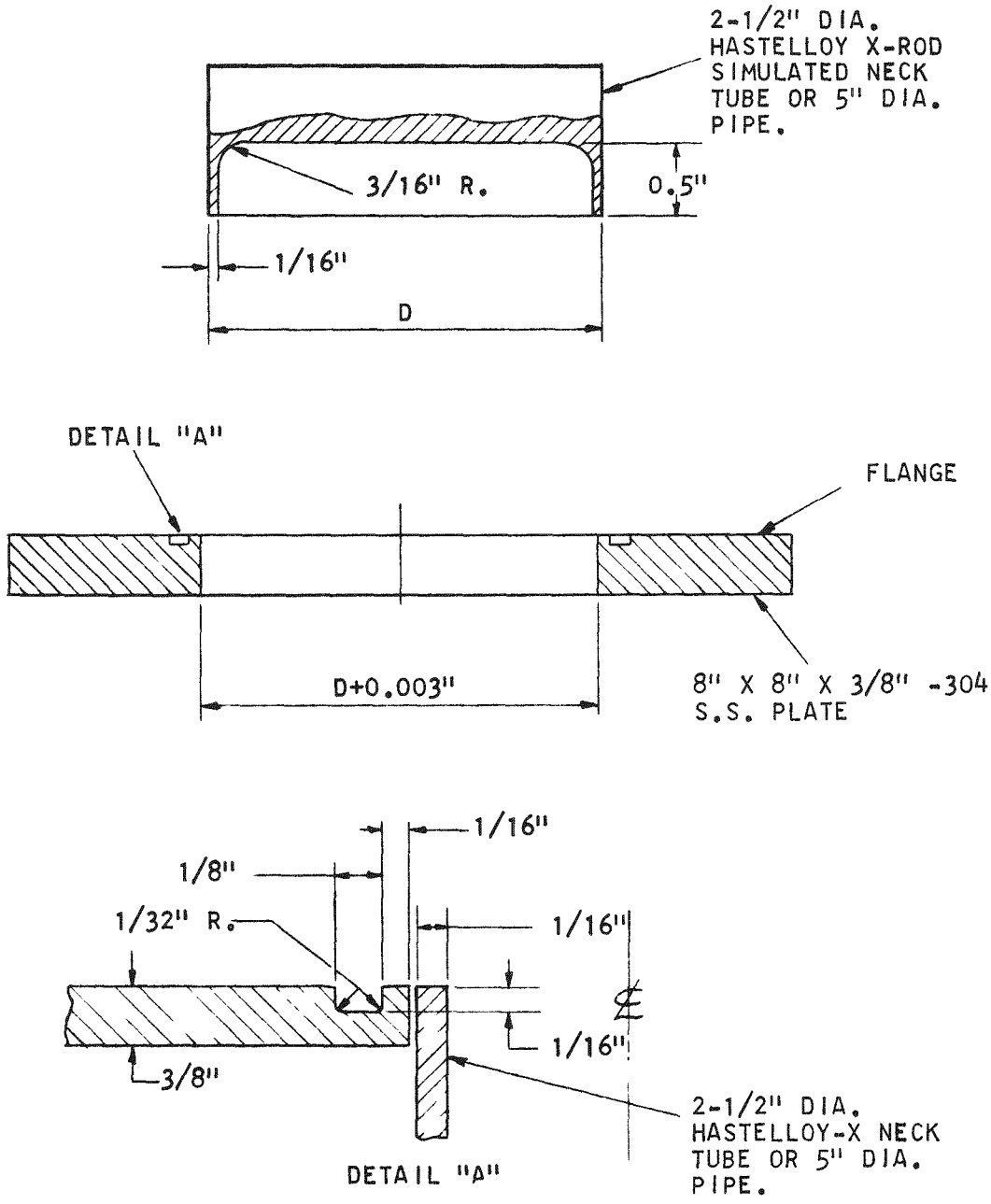

Figure 2-36. Neck Tube Weld Joint

The three 2-1/2 inch joints, Nos. 1, 2 and 3, were semi-automatically welded changing the weld parameters for each weld to determine the most desirable weld conditions. The parameters are shown in Table 2-9. The three specimens were then leak checked with a Veeco MS-9 leak detector with no indicated leakage within the sensitivity of detectors (less than 4.9×10^{-11} std cc/sec-air). Table 2-10 presents the leak rate data; the welded specimens are shown in Figure 2-37.

To demonstrate the capability to repair a leak in the neck tube weld joint, specimen No. 3 was drilled with a No. 57 drill through the center of the weld to a depth of 3/16 inch to cause a leak. The leak was prepared for repair by grinding the weld bead 1/16 inch deep by 3/8 inch in length. The repair was made by manual heliarc welding using a 0.045 inch diameter 308 ELC filler rod, 25 CFH argon shield gas with an HW-20 torch. Two passes were required each employing 36-42 amps and 8.0 - 9.0 volts. Following the leak repair the specimen was again leak checked with the result of no detectable leakage (Table 2-10).

Because of the solid bottom cut shaped configuration of the 2-1/2 inch diameter neck tube joint specimens X-ray pictures of the weld joint could not be made. They were instead tensile tested to the maximum loads given in Table 2-10. All the specimens exhibited maximum loads greater than 23,600 pounds. Specimen No. 3 was not properly aligned in the tensile test machine and therefore failed at a load somewhat lower than would be expected. The ultimate stress for these specimens was not calculated due to inability to accurately determine the cross section area prior to testing. For the purpose of this development testing the maximum load per inch of weld is all that is required to determine that the joint has sufficient strength capability to support the nuclear radiation shield under 6g dynamic shock conditions.

Following the weld parameter development and tests on the 2-1/2 inch diameter neck tube joints, the 5 inch O.D. diameter edge weld joints were made to further refine the weld parameters for the actual size weld joint. These specimens (Nos. 4, 5, and 6) were semiautomatic heliarc welded with the parameters as shown in Table 2-9. The parameters used for specimen Nos. 4 and 5 are those selected for use on the development units. The welded specimens are shown in Figure 2-38. In this figure specimen No. 5 is shown prepared for a leak check with a flat plate soldered to the Hastelloy-X neck tube material to seal off the open end of the tube.

Table 2-9. Weld Parameter for Semi-Automatic Neck Tube Edge Weld

Date	Specimen No.	Hastelloy-X Neck Tube Size in Inches			304 Stainless Steel Flange Size in Inches			Travel Speed, Inches per Minute	Power		Avg. Heat Input Kilojoules	Maximum Load Lbs.	Comments
		O. D.	I. D.	Wall	I. D.	O. D.	Wall		Amperes	Volts			
4-24-67		2.498 to		0.063 to									Weld bead heavy-considerable roll over on I. D., poor gas
4-24-67	1	2.500	2.373	0.065	2.506	2.632	0.063	5	80-82	10.5-12.5	11.18	34,700	cover on I. D. S. S. flange edge favored during weld.
4-25-67	2	2.502	2.374	0.062 to 0.063	2.500 to 2.510	2.633 to 2.603	0.061 to 0.062	10	70-72	10.5-11.5	4.69	24,900	Weld bead medium light-very little roll over, 5 CFH argon auxiliary flow on I. D. of tube.
4-25-67	3	2.478	2.350	0.063 to 0.065	2.483	2.667	0.063 to 0.064	7.5	70-72	9-11	5.69	23,600	Weld bead heavy-roll over on I. D., some high points along I. D., auxiliary argon flow 5 CFH on I. D.
5-2-67	4	4.904	4.780	0.062	4.910	5.034	0.062	7.5	71-73	11.0-12.5	6.7	No Tensile Test Made	Excessive roll over, some high spots, S. S. side melted down to bottom of groove.
5-2-67	5	4.904	4.780	0.062	4.910	5.034	0.062	10	71-73	11.0-12.5	5	No Tensile Test Made	Uniform bead-slight roll over on Hastelloy-X side, S. S. side melted down approximately 1/32"
5-2-67	6	4.904	4.780	0.062	4.910	5.034	0.062	10	71-73	11.0-12.5	5	No Tensile Test Made	Uniform bead same as Specimen No. 5 Beautiful weld.

General Note: All welds contain 4 tacks. Melt down pass, no filler added, edge set flush

Table 2-10. Leak Rate Data Neck Tube Edge Weld

Instrument: Veeco MS9AB Helium Mass Spectrometer
Minimum Detectable Leak Scale Reading = 0.01

Date	Description of the Test Specimen	Time-Leak Check Observed Minutes	Std. Leak Value Std. cc/sec. air	Std. Leak Scale Reading	Leak Rate Std. cc/sec. air Less Than	Remarks
April 11, 1967	3 inch Pipe Girth Weld Repair Leak Check	15	2.9×10^{-8}	5.4	5.35×10^{-11}	No Detectable Leak
April 26, 1967	No. 1 Neck Tube Weld; 2-1/2 inch diameter Hastelloy-X	30	2.9×10^{-8}	6.2	4.67×10^{-11}	No Detectable Leak
April 27, 1967	No. 2 Neck Tube Weld; 2-1/2 inch diameter Hastelloy-X	30	2.9×10^{-8}	7.0	4.14×10^{-11}	No Detectable Leak
April 26, 1967	No. 3 Neck Tube Weld; 2-1/2 inch diameter Hastelloy-X	30	2.9×10^{-8}	5.9	4.91×10^{-11}	No Detectable Leak
April 27, 1967	No. 3 Neck Tube Repair Joint	30	1.2×10^{-8}	2.7	4.44×10^{-11}	No Detectable Leak
May 2, 1967	No. 6 Neck Tube Joint 5 inch diameter Hastelloy-X Tube	30	2.9×10^{-8}	6.6	4.39×10^{-11}	No Detectable Leak
May 9, 1967	No. 5 Neck Tube Joint 5 inch diameter Hastelloy-X Tube	30	2.9×10^{-8}	5.5	5.27×10^{-11}	No Detectable Leak
May 10, 1967	No. 4 Neck Tube Joint 5 inch diameter Hastelloy-X Tube	30	2.9×10^{-8}	5.2	5.27×10^{-11}	No Detectable Leak

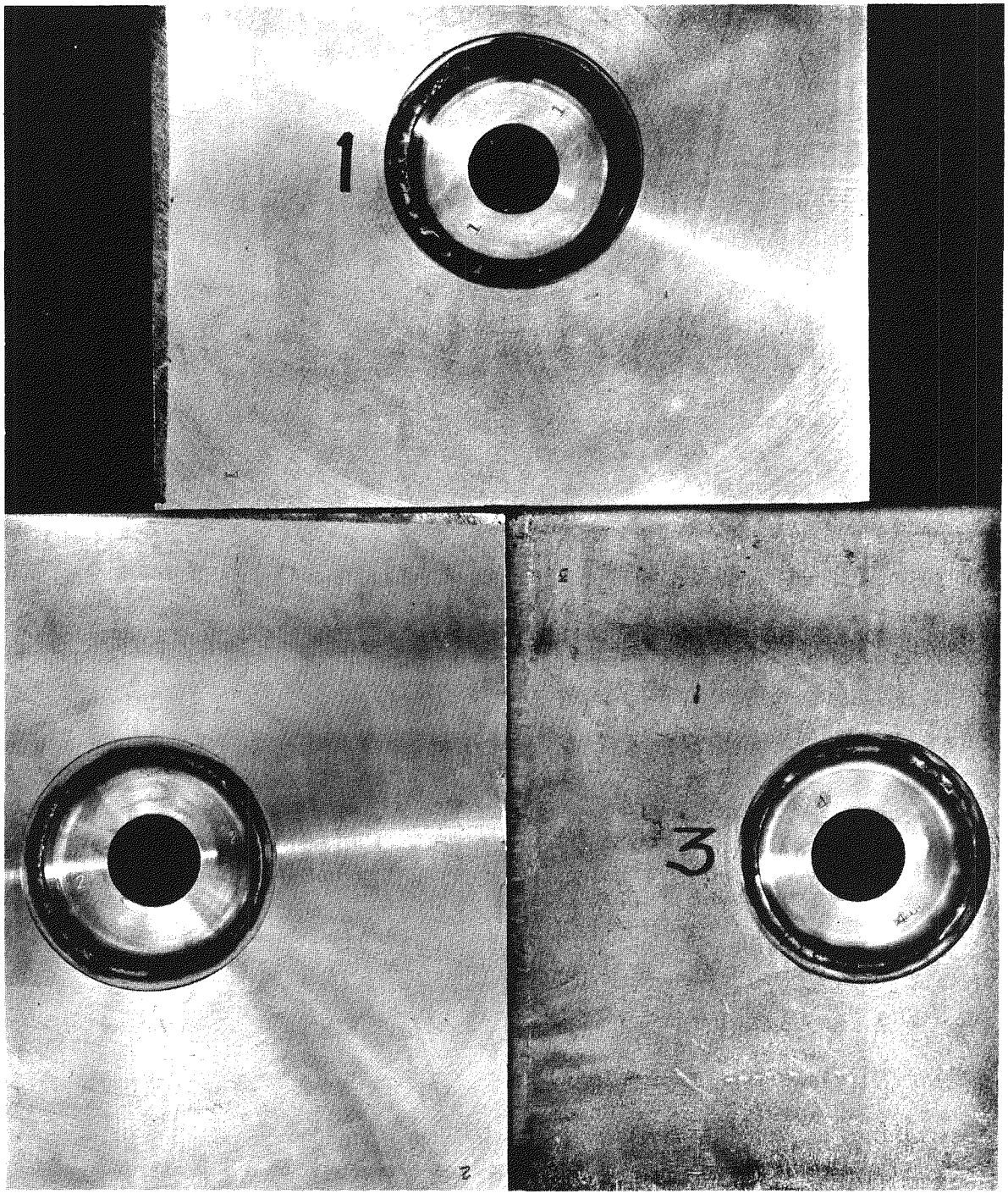

Figure 2-37. Simulated Neck Tube Weld Joints – 2-1/2 Inch O. D.

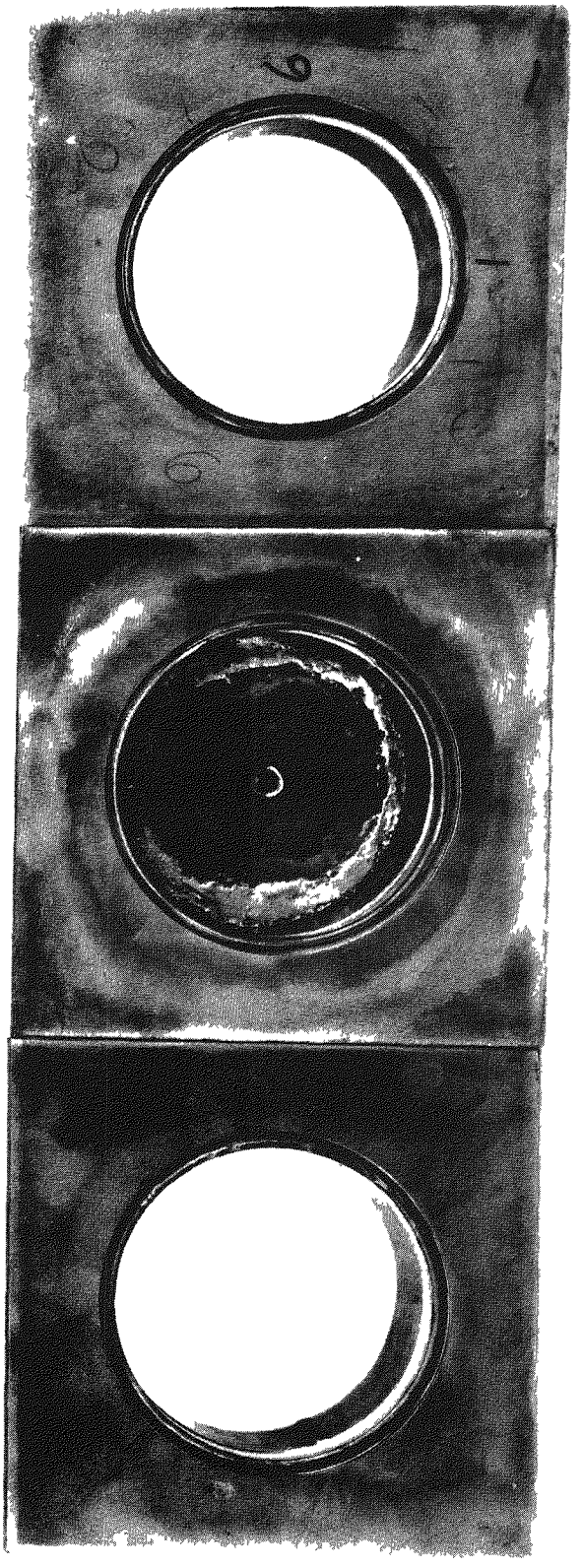

Figure 2-38. Simulated Neck Tube Weld Joints – 5 Inch O D.

All three weld specimens were leak checked with the Veeco MS-9 leak detector, there was no detectable leakage (leak rate less than 5.57×10^{-11} std cc/sec-air, see Table 2-10. The 5 inch O. D. specimens were not tensile tested but were X-rayed. The results of the X-rays leave much to be desired as it was necessary to shoot the weld from above and to the outside in order to preclude the prepared edge on the flange from being in the picture. However, X-rays taken at a 45° angle were clear, indicating that there was no porosity in the weld.

2. 3. 3. 4 Material Compatibility Test

A multi-layer insulation was applied to the 1 inch diameter stainless steel water cooled tube of the compatibility test apparatus. The test section is composed of three test zones, each approximately 4 inches long. Each zone was wrapped with the following materials:

Cold Side	2 turns	0. 0005 inch Nickel foil
	3 alternate turns	0. 005 inch Quartz paper 0. 0005 inch Nickel foil
	52 alternate turns	0. 003 inch 106 paper 0. 0002 inch Aluminum foil
	55 alternate turns	0. 005 inch Quartz paper 0. 0005 inch Copper foil
	46 alternate turns	0. 005 inch Quartz paper 0. 00062 inch Nickel foil
Hot Side	2 turns	0. 005 inch Quartz paper

The test setup is shown schematically in Figure 2-39.

The average outside diameter of the test zone was 3-7/8 inches. Quartz string was used to secure the multi-layer insulation in place. The nickel and aluminum foils were unprocessed while the copper foil, quartz paper, and 106 paper were processed prior to application. The area on the ends of the three test zones was also insulated with multi-layer insulation, as shown in Figure 2-39.

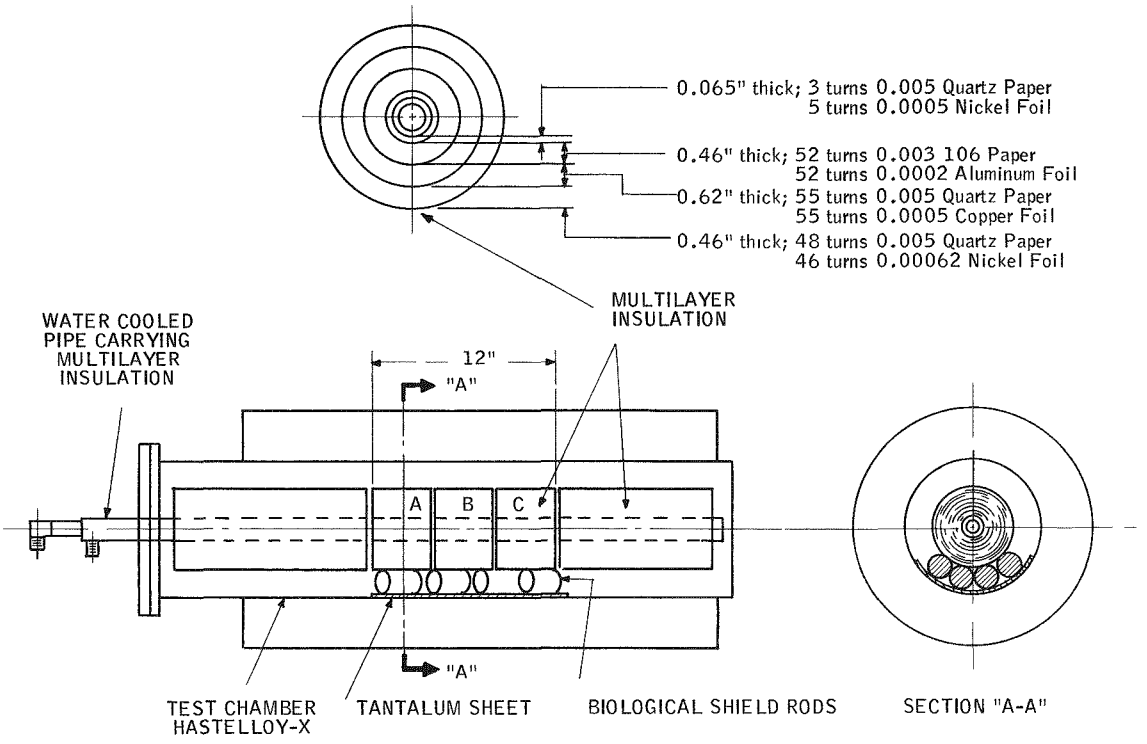

Figure 2-39. Schematic View Showing the Insulation and Biological Shield Material in Test Chamber

To determine the installed comparative reflectance measurement, samples of each radiation shield material were taken at the beginning and the end of each wrap. One sample was taken from the nickel adjacent to the cold surface. Seven samples were taken from each insulation zone, making a total of 21 samples for the test.

A sheet of Hastelloy-X, 0.012 inch thick by 12-1/2 inches long by 7-1/2 inches wide, was rolled to fit the inside diameter of the Hastelloy-X chamber. A tantalum sheet (3 inches by 6 inches by 0.020 inch thick was rolled to fit the Hastelloy-X sheet and located one inch from the edge of the Hastelloy-X sheet. Two thicknesses of 0.0003 inch thick tantalum foil covered the remaining exposed area of the Hastelloy-X sheet as shown in Figure 2-40. The 15 U-8 moly rods, each approximately 1/2 inch in diameter by 3 inches long, were placed on the tantalum (Figure 2-40). These rods contact the tantalum and the outside layers of quartz paper. The tantalum, Hastelloy-X sheet, biological shield material, and the chamber were cleaned with isopropanol alcohol prior to inserting the sample lay

up in the chamber. The Hastelloy-X sheet with samples was placed in the center of the chamber located so that the U-8 moly bars would contact the test zones. The multi-layer insulation was then inserted into the chamber and set on the bars and the vacuum flange was sealed with a copper gasket.

After the compatibility test had been in progress for 500 hours, the furnace was opened and one set of samples was examined. There were no signs of incompatibility between any of the materials in the sample. When the furnace was opened, it was found that several of the U-8 moly rods were not on the tantalum sheet but rather were resting against the Hastelloy-X furnace. The Hastelloy-X reacted with the U-8 moly and caused a pit to develop in one of the rods.

Figure 2-40 shows the compatibility test assembly with one section removed after 500 hours on test. Figure 2-41 shows the U-8 moly bars after 500 hours on test. The flattened areas are where the bars came into contact with the Hastelloy-X.

The test is continuing on the remainder of the samples. The 2000 hour test will be completed in mid-July.

2.3.4 SEGMENTED HOLD DOWN RING

No effort was expended on this sub-task during the period.

2.3.5 PRESSURE VESSEL

Requests for quotes were drawn up for pressure vessels made of Titanium alloy 621.8 and also of beryllium copper, Berylco 165, and sent to:

Ladish Co.
Taylor Forge and Pipe Works
Cameron
Wyman-Gordon

These quotes will be evaluated when received and surveys will be made by vendor qualification teams.

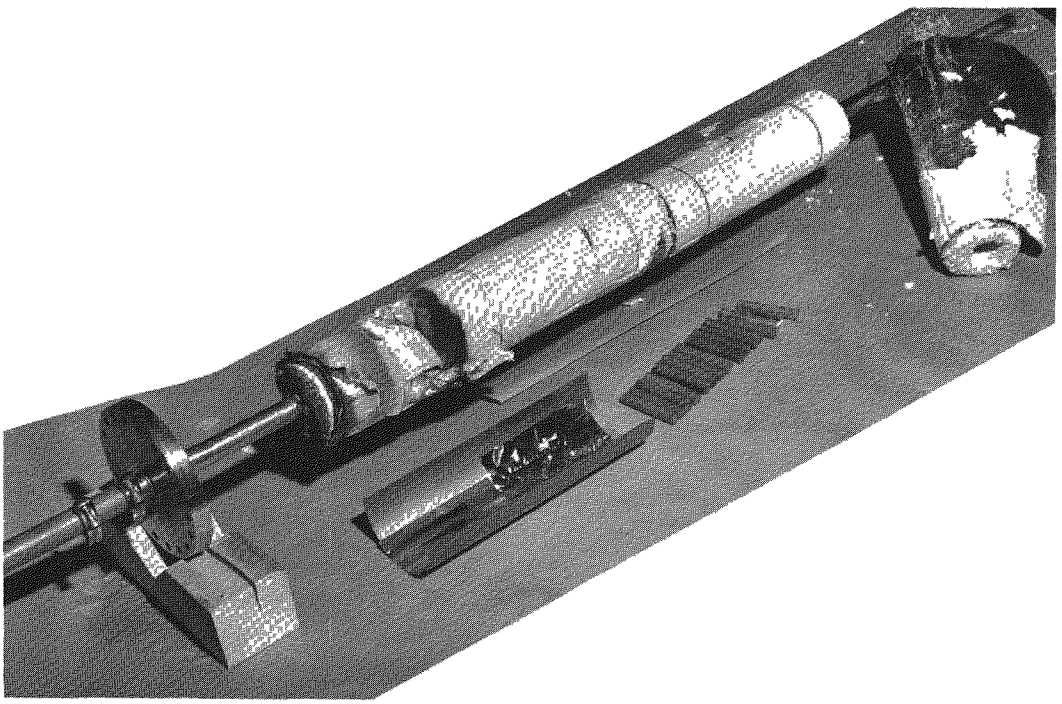

Figure 2-40. Compatibility Test Assembly After 500 Hours on Test

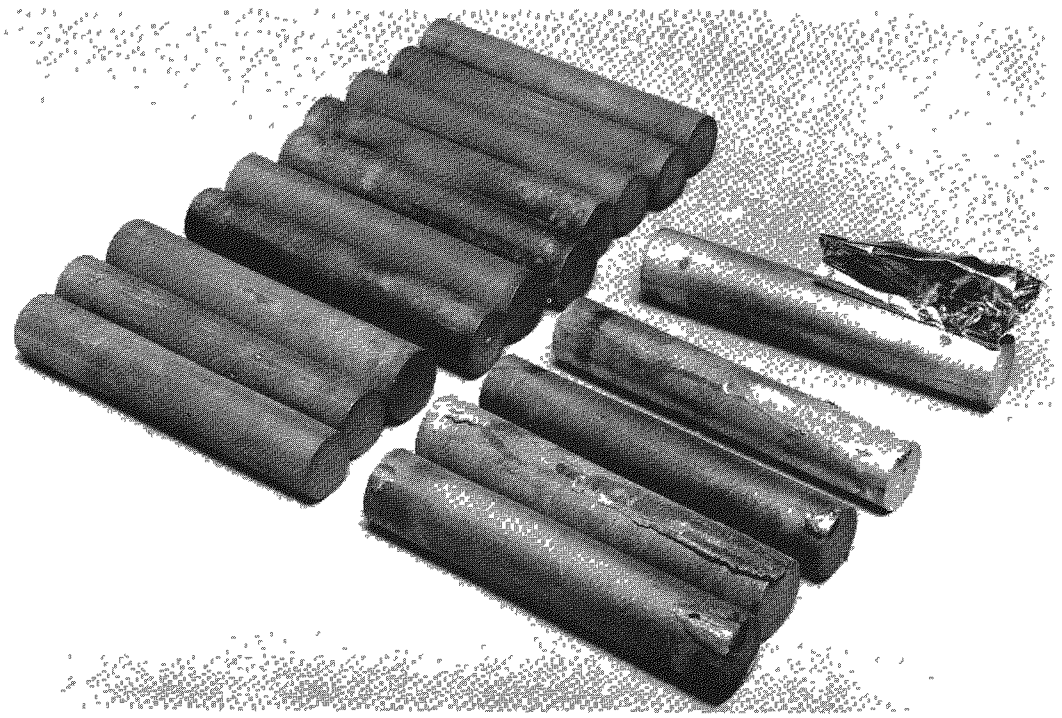

Figure 2-41. U-8% Molybdenum Bars After 500 Hours on Compatibility Test

2.3.6 THERMOELECTRIC GENERATOR

2.3.6.1 Cold End Heat Transfer Testing

Generator cold end heat transfer development testing in the second quarter of 1967 included nine ingradient tests, tests #16 through #24, and the design and fabrication of two new 6-couple modules (Figure 2-42).

The following is a description of tests #16 through #24 and their results:

a. Test #16 investigated the effect of changing follower length without heat transfer grease. Followers with a nominal diameter of 0.2465 inch were used, two 0.75 inch long and two 1.10 inches long. As in test #15*, the hot button protrusions were filed off to allow more flexibility at the hot end. This method is used in tests #17 and #18 also. After test #18, it was found that one leg had bad alignment and the protrusions were left on for the following tests. The holes in the hot strap were opened up to about 1/16 inch to give this flexibility. Test #16 shows that in the range of 0.75 to 1.10 inches, length has no significant effect on heat transfer when no grease is used.

b. Test #17 was the first in-line test to use heat transfer grease. It compared long, large diameter (0.75 inch, 0.2495 inch) followers with shorter, smaller diameter (0.50 inch, 0.2465 inch) ones. In cases such as this, where more than one variable is changed, some of the proposed legs broke in assembly and other available ones were substituted rather than hold up the test to solder new ones. Since only Module No. 2 was used for tests using grease and only Module No. 1 was used when no grease was present, results between different tests can be compared, as in Figures 2-43 and 2-44.

   Results of test #17 show that neither diameter nor length affect heat transfer when grease is present. Only one point was obtained for the long, large diameter followers as the other leg was found broken upon disassembly. The one point obtained for these followers is questionable as additional data (see Figure 2-44) and does not support the argument that length has no effect when using grease.

*Tests No. 4 through No. 15 are reported in SNAP-21 Quarterly Report No. 3, MMM 3691-17, published in May 1967.

1. LAVA HOT BLOCK SUPPORT
2. ELECTRIC HEATER
3. HOT BLOCK
4. SUPPORT ROD
5. BORON NITRIDE INSULATOR
6. CONTAINER SHELL
7. COLD FRAME
8. COOLING BLOCK

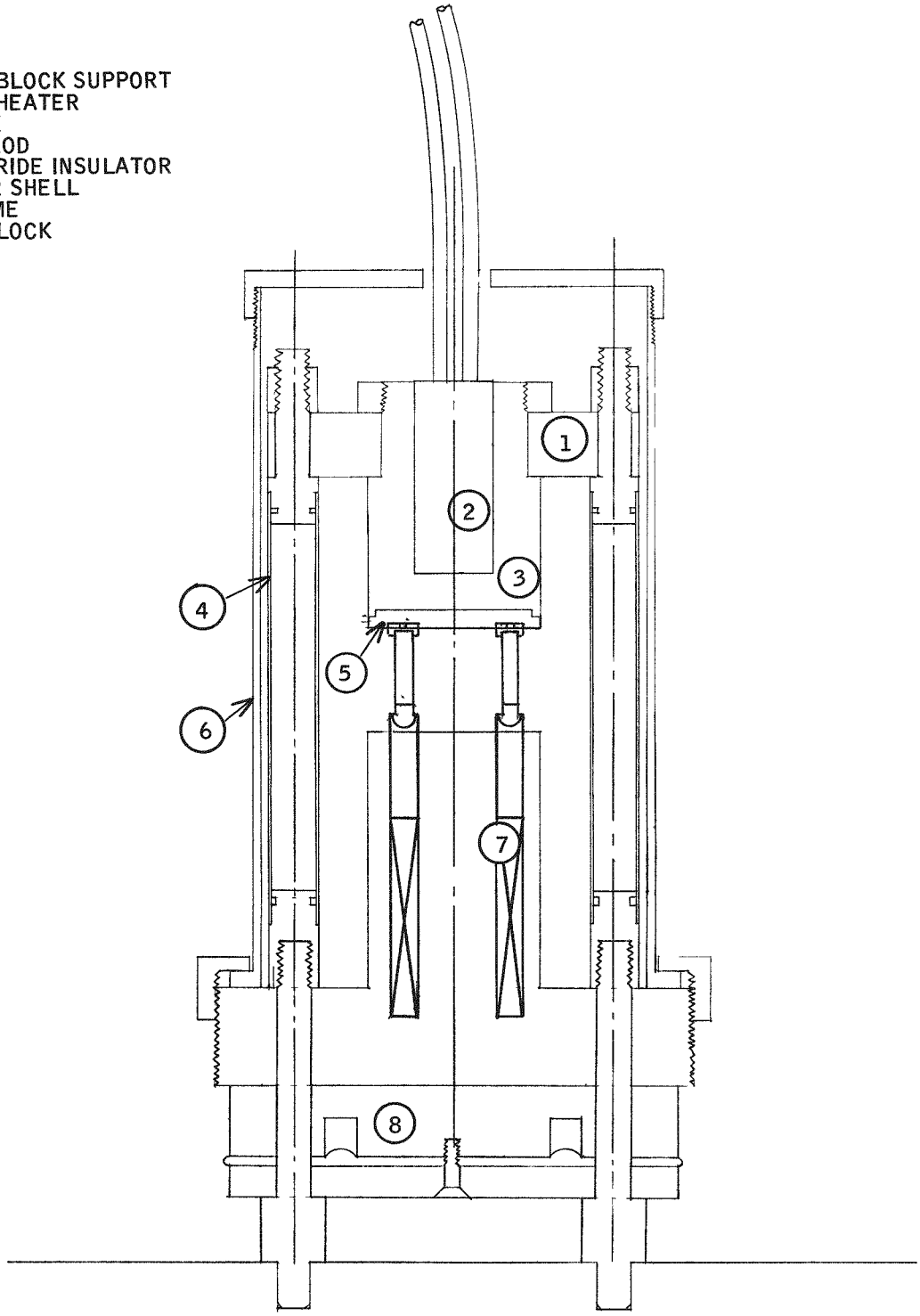

Figure 2-42. 6-Couple Heat Transfer Test Module

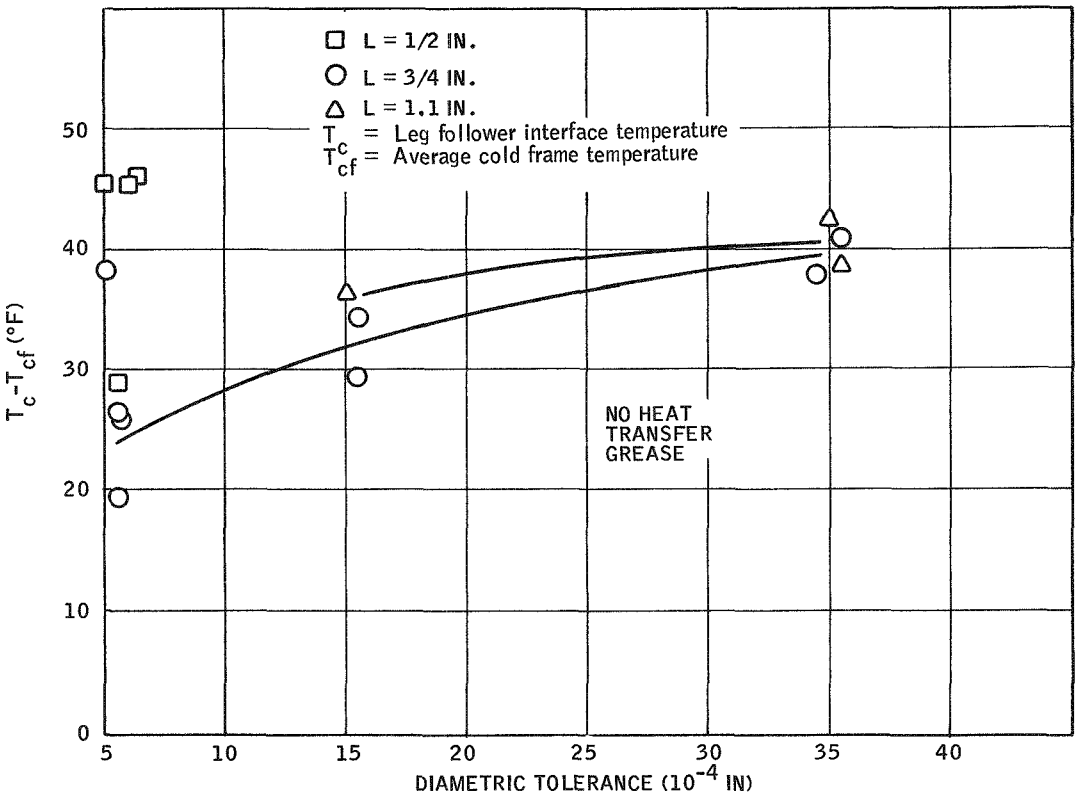

Figure 2-43. Cold End Heat Transfer Tests Without Heat Transfer Grease

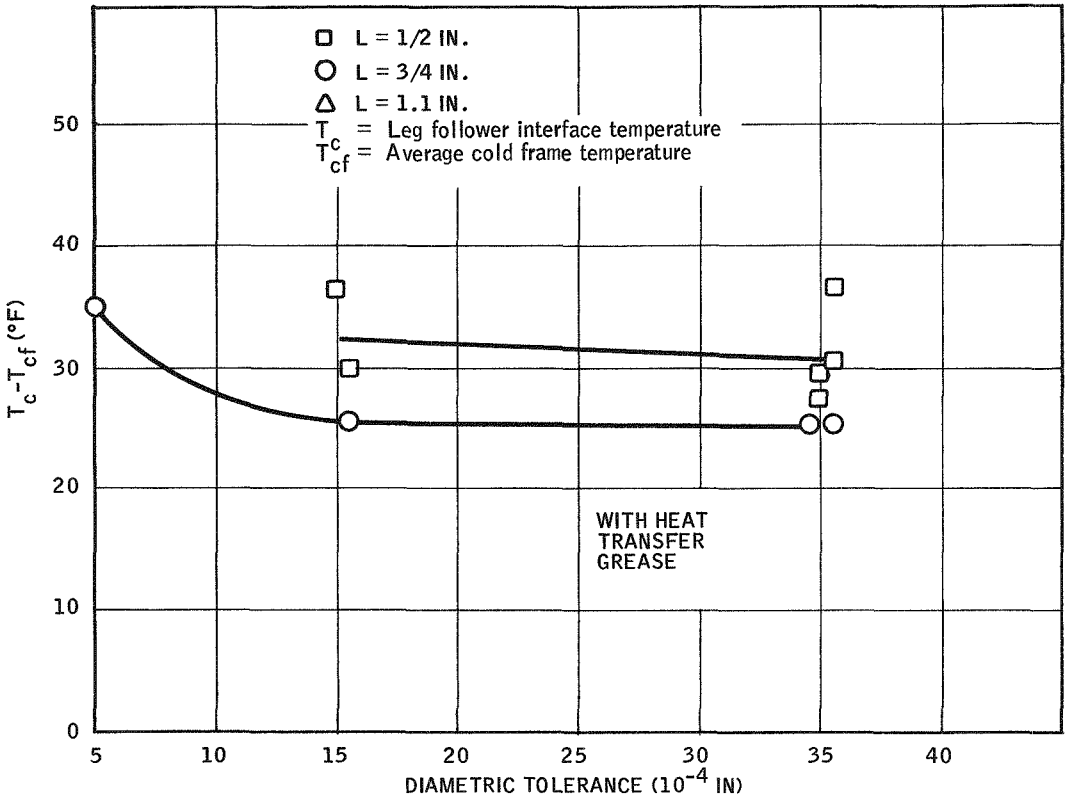

Figure 2-44. Cold End Heat Transfer Tests with Heat Transfer Grease

c. Test #18 compared 0.2495 inch by 0.75 inch long followers with 0.2485 inch by 1.10 inch long ones without heat transfer grease. One of the longer legs was found broken upon disassembly.

The results of test #18 showed that the larger diameter followers, though shorter, showed better heat transfer.

d. Test #19 used 0.75 inch long followers and compared 0.2465 inch diameters with 0.2485 inch diameters, with heat transfer grease. The test showed that diametral effects are negligible when using heat transfer grease. The temperatures at the leg-follower interface were the same except for the leg in location four. During the post-test inspection it was found that a considerable amount of solder was present on the thermocouple wires for a considerable distance away from the interface. It is felt that an extraneous junction was thus formed and the temperature reading is not trusted.

e. Test #20 compared short, 0.50 inch, large diameter, 0.2495 inch, followers to longer (0.75 inch), smaller diameter (0.2485 inch) ones. The leg in location 4 (0.2485 inch diameter by 0.75 inch length) was found broken upon disassembly. The results of test #20, though only three points were taken and a large spread was present in the data on the two similar followers, reinforced the hypothesis that diametral clearance is the prevailing parameter when no heat transfer grease is used. When compared with other tests (Figure 2-42), length appears to have an effect in the 0.50 inch range even though it does not when 0.75 inch is compared to 1.10 inches. Apparently, a lower boundary for follower length had been crossed.

f. Test #21 compared 0.2485 inch diameter followers with 0.2465 inch followers with heat transfer grease using 0.50 inch length pieces only. This test supported earlier data in showing diametral effects negligible when using heat transfer grease.

g. Test #22 is the first ball and socket test using the indium plated cold caps. Two hardcoated and two bare aluminum socket followers were used.

The results of this test show that the use of indium plating improves heat transfer significantly on the hardcoated followers. This can be seen by comparison with the results of tests #1 and #3*. In the case of the bare sockets, the transfer is only slightly improved over a nonplated cap which is perfectly matched to the follower, but is significantly improved when the spherical radii are mismatched.

h. Tests #23 and #24 used the same hardware. In-line followers 1.1 inches long were used; two were 0.2465 inch in diameter, the other two 0.2495 inch. Test #23 utilized heat transfer grease and test #24 used silicone vacuum grease.

These tests showed excellent heat transfer as expected when the long followers were used with the heat transfer grease. Test #24 showed that the vacuum grease is very nearly as good as the heat transfer grease (the average temperature drop was only 1° higher than when using heat transfer grease).

Tables 2-11 and 2-12 summarize the cold end heat transfer test data for test #16 through test #24. For convenience tests #14 and #15, though reported previously, are included so that the table will contain all in-line data to date. Figure 2-43 compares all data (except that from legs which were found broken and the point with the suspected extraneous thermocouple junction) where heat transfer grease is not used. Figure 2-44 is a plot of data gathered when heat transfer grease is used. In both cases, the temperature difference between the thermoelectric leg-follower interface and the average cold frame temperature is plotted as a function of the difference between the cold frame hole diameter and follower diameter.

2.3.6.2 Leg and Couple Testing

SNAP-21 production couples are on test at this writing. All thermal and electrical characteristics are being monitored. The module is undergoing processing identical to that performed on the development generators.

Samples from each lot and batch used in the generator are being sealed in an inert atmosphere and stored for future reference.

*Tests No. 1 through No. 3 are reported in SNAP-21 Quarterly Report No. 2, MMM 3691-12, published in March 1967.

Table 2-11. Cold End Heat Transfer In-Line Test Data Summary

Leg No	Test Description and Number	Follower to Hole Clearance (diam-inch)	Follower Length (in)	Diameter (in)	Hot Button Temp T_h (°F)	Leg-Follower Interface Temp T_c (°F)	Ave Cold Frame Temp T_{cf} (°F)	Seebeck Voltage (mv)	$T_c - T_{cf}$ (°F)	Internal Gas Pressure psig	Comments
1	14 No	0 0006	0 748	0 2494	1095 5	127 0	75 5	126 05	51 5	3 6	Leg broken
2	Heat	0 0005	1 112	0 2495	1098 0	108 0	75 5	126 80	32 5	3 6	Leg broken
3	Sink	0 0006	0 749	0 2494	1105 0	104 0	75 5	126 65	28 5	3 6	Leg broken
4	Compound	0 0005	1 112	0 2495	1103 0	138 0	75 5	126 35	62 5	3 6	
1	15 No	0 0006	0 748	0 2494	1103 0	94 0	74 5	127 10	19 5	3 35	
2	Heat	0 0007	0 499	0 2493	1108 0	120 0	74 5	125 80	45 5	3 35	
3	Sink	0 0006	0 749	0 2494	1094 0	101 0	74 5	127 15	26 5	3 35	
4	Compound	0 0005	0 498	0 2495	1098 0	121 5	74 5	123 75	47 0	3 35	
1	16 No	0 0036	1 110	0 2464	1097 5	114 0	74 5	125 60	39 5	4 6	
2	Heat	0 0034	0 747	0 2466	1102 5	113 0	74 5	125 50	38 5	4 6	
3	Sink	0 0035	1 110	0 2465	1098 5	117 0	74 5	125 90	42 5	4 6	
4	Compound	0 0036	0 749	0 2464	1100 5	117 0	74 5	127 35	42 5	4 6	
1	17 Heat	0 0036	0 497	0 2464	1099 0	106 0	75 0	125 30	31 0	4 6	
2	Sink	0 0006	0 748	0 2494	1100 0	117 0	75 0	125 05	42 0	4 6	Leg broken
3	Compound	0 0035	0 497	0 2465	1100 5	103 0	75 0	125 55	28 0	4 6	
4	Used	0 0005	0 748	0 2495	1099 0	110 5	75 0	126 60	35 5	4 6	
1	18 No	0 0006	0 749	0 2494	1102 0	102 0	75 5	128 10	26 5	4 45	
2	Heat	0 0016	1 110	0 2484	1104 0	145 0	75 5	128 20	69 5	4 45	Leg broken
3	Sink	0 0005	0 748	0 2495	1103 0	114 0	75 5	128 40	38 5	4 45	
4	Compound	0 0015	1 110	0 2485	1094 0	112 0	75 5	128 15	36 5	4 45	
1	19 Heat	0 0034	0 747	0 2466	1089 0	100 0	74 5	125 20	25 5	4 45	
2	Sink	0 0016	0 748	0 2484	1099 0	100 0	74 5	127 65	25 5	4 45	
3	Compound	0 0036	0 749	0 2464	1100 0	100 0	74 5	127 75	25 5	4 45	
4	Used	0 0016	0 747	0 2484	1100 0	128 0	74 5	126 35	53 5	4 45	
1	20 No	0 0006	0 498	0 2494	1101 0	102 0	74 5	127 15	27 5	4 10	Possible Extraneous Generation
2	Heat	0 0016	0 747	0 2484	1101 0	108 0	74 5	126 90	33 5	4 10	
3	Sink	0 0007	0 499	0 2493	1100 0	118 0	74 5	126 85	43 5	4 10	
4	Compound	0 0016	0 748	0 2484	1100 5	103 0	74 5	126 40	28 5	4 10	Leg broken
1	21 Heat	0 0015	0 498	0 2485	1099 5	110 0	74 5	128 40	35 5	4 10	
2	Sink	0 0036	0 497	0 2464	1100 0	110 0	74 5	126 40	35 5	4 10	
3	Compound	0 0016	0 498	0 2484	1100 0	103 0	74 5	127 60	28 5	4 10	
4	Used	0 0035	0 497	0 2465	1094 0	103 0	74 5	125 80	28 5	4 10	
1	23 Heat	0 0036	1 110	0 2964	1092 0	90 0	74 5	126 70	15 5	4 10	
2	Sink	0 0005	1 112	0 2495	1102 0	86 0	74 5	126 40	11 5	4 10	
3	Compound	0 0036	1 110	0 2464	1103 0	96 0	74 5	127 20	21 5	4 10	
4	Used	0 0007	1 110	0 2493	1098 0	84 0	74 5	127 40	9 5	4 10	
1	24 Vacuum	0 0036	1 110	0 2464	1097 0	92 0	74 5	126 70	17 5	3 30	
2	Grease	0 0005	1 112	0 2495	1101 0	85 0	74 5	127 00	10 5	3 30	
3	Used	0 0036	1 110	0 2464	1100 0	97 0	74 5	127 60	22 5	3 30	
		0 0007	1 110	0 2493	1101 0	85 0	74 5	126 00	10 5	3 30	

Table 2-12. Cold End Heat Transfer Indium Test Data Summary

Leg No.	Test Description and Number	Follower to Hole Clearance (diam. - inch)	Follower Spherical Radius, in.	Follower Spherical Surface Finish μ in.	Cold Cap Spherical Radius, in.	Cold Cap Spherical Radius with Indium	Hot Button Temp. (T_h) °F	Cold Cap Temp. (T_c) °F	Follower Temp. (T_f) °F	Ave. Cold Frame Temp. T_{cf} (°F)	Seebeck Voltage (mv)	$T_c - T_f$ °F	$T_c - T_{cf}$ °F	$T_c - T_{cf}$ °F	Comments
1	Test #22	0.0013	0.1264	-	-	0.130	1102.0	100.0	87.0	75.0	129.00	13.0	12.0	25.0	NHC
2	Indium Plating	0.0010	0.1271	-	0.125	0.132	1101.0	92.0	84.0	75.0	128.70	8.0	9.0	17.0	HC
3	on all Cold Caps	0.0008	0.1264	-	0.125	0.134	1100.0	89.0	86.0	75.0	127.30	3.0	11.0	14.0	NHC
4		0.0012	0.1261	-	0.125	0.130	1102.0	92.5	83.0	75.0	127.30	9.0	8.0	17.5	HC

NHC – No Hard Coat in Follower Socket

HC – Hard Coat in Follower Socket

2.3.6.3 Leg Inspection Development Testing

During this report period development effort was continued to improve the testing methods used to evaluate the electrical resistance of thermoelectric segments, segmented legs and couples. This effort consisted of:

- Evaluating the end effect of current distribution on thermoelectric materials by development of correction factors.
- Development of apparatus to evaluate the resistivity of individual segments, segmented legs and couples.
- Statistical application of data generated from direct resistivity evaluation of segmented legs and couples.
- Further development and application extended to couples.
- Future development and applications of Seebeck testing.

When using the normal resistivity formula, $\rho = \frac{EA}{Il}$, for the evaluation of the resistivity of a conductive material, a measurement error is introduced by the distribution of the current through the element since it acts as an electrical conductor. The measurement of resistivity is effected because the current value is changed due to the length and diameter of the segment. Theoretically, current flow should be parallel to the longitudinal axis of the conductor in any increment of an infinitely long conductor. However, in a conductor of finite length, the current distribution is in effect constricted at the ends of the conductor. Thus, for a true resistivity measurement, it was necessary to establish a correction factor for each geometric configuration. This was done by measuring the resistivity of a standard material with the same diameter of the thermoelectric material in question. The standard material with a published true resistivity was machined accurately to a variety of lengths, including those of the thermoelectric material being evaluated. These samples were evaluated on the direct resistance equipment at a constant current and the results were plotted in ohm-inches with respect to length. Using this technique, the correction factors for SNAP-21 elements were developed. With the correction factors, the direct resistance measurements can be converted to resistivity.

The direct resistance measuring apparatus was modified to accept all segments and segmented leg sizes used in the SNAP-21 Program. By the application of correction factors, it was possible to directly obtain the resistivity of all segments and also evaluate the segment bond resistance by subtracting the total of the individual leg resistivities from the corrected total resistivity of the segmented leg. An additional modification has been completed which adapts this measuring apparatus to accept SNAP-21 couples for contact (cap to segment) resistance.

The degree of accuracy acquired with this new equipment is such that a change in acceptance criteria will be made. The data generated from the testing of each material configuration was statistically evaluated to predict new acceptance limits.

Extensive couple testing was done, resulting in establishing maximum acceptance limits for N- and P-legs used on SNAP-21. Maximum acceptance limits for couples for the SNAP-21 program were also established. The jumper wire and bond resistance was established at 200 microhms by subtracting the known resistance of the N- and P-leg segments and the total resistance of the couple. The total resistance of couples used on SNAP-21 has been tentatively set at 11 milliohms, maximum. It is assumed that total resistance in excess of this limit on this configuration is a result of increased or excessive bonding resistance.

Complete evaluation and firm acceptance limits will be forthcoming in the near future.

The test fixture has been adapted to accommodate all types of legs and couples for all programs now in progress. Tests have been made and the results are being evaluated and new limits will be established.

The DC testing of couples containing heat pump materials resulted in errors. The total resistance of couples of this type were successfully tested using AC current. The existing AC current supplies used for R vs L can be used for this test. The Dana Amplifiers presently used can also be used where higher sensitivity requirements dictate. Various AC voltmeters were evaluated for the readout on this system, and a purchase order was placed for a Dana Model 5500. Delivery is expected in 10 weeks.

During the next period, the fixture will be refined for direct resistance testing to better adapt it to a rapid, continuous production type of testing. Some effort will also be expended to improve the current control on the present current sources. Assembly and testing of the new Seebeck fixtures will be initiated during this next period. This new fixture uses a temperature regulated cold block. Placing a thermoelectric element in this fixture will establish a Δ T across the element immediately. This results in a thermal shock to the element. All aspects of this will be investigated.

2.3.6.4 Generator Development Testing

The family of four SNAP-21 development generators will go on test as soon as they are assembled. The necessary facilities for testing are available and the test plan has been written and is being reviewed. A complete description of the configuration of each generator, the test cycle each will undergo, and the ultimate disposition of each is given in the test plan.

2.3.6.5 Phase I Continuation Testing

Long term testing of thermoelectric devices which was initiated during Phase I continued during this report period.

The units on test are:

a) Three 6-couple test modules: A_1, A_3, and A_7

b) Four prototype generators: P_3, P_5, P_6, and P_7

Performance data of these units are shown in Figures 2-45 through 2-48 and Tables 2-13 and 2-14.

All 6-couple modules are continuing on test with no significant change in performance.

In April, 1967, Prototype P_5 underwent an input power reduction of approximately 5 to 6 watts. This is to simulate the decay of the isotope in a fueled system. The module has now accrued 18,641 hours of continuous testing and is performing with no significant change in performance over that time period.

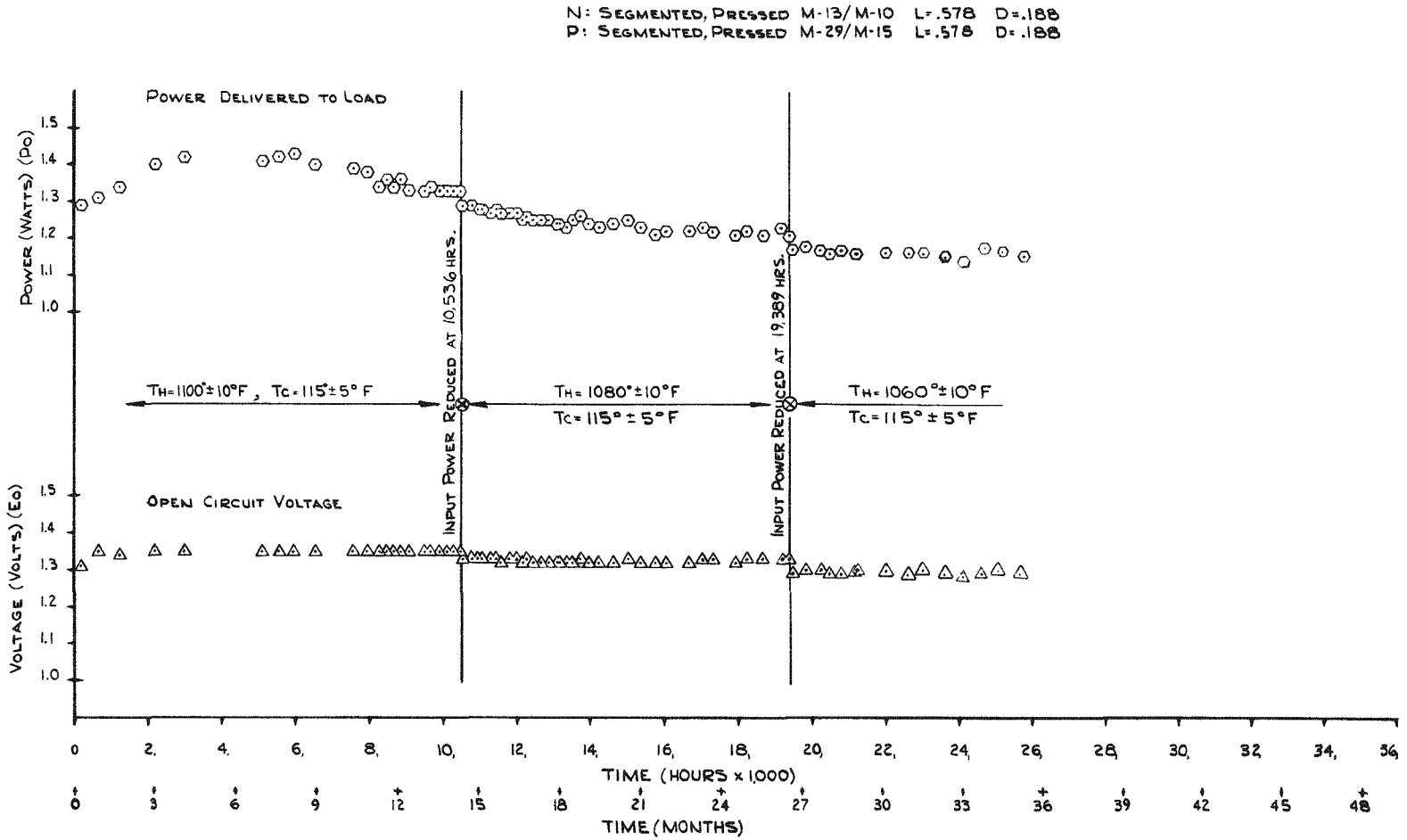

Figure 2-45. Performance Data, SNAP-21 6-Couple Module A1

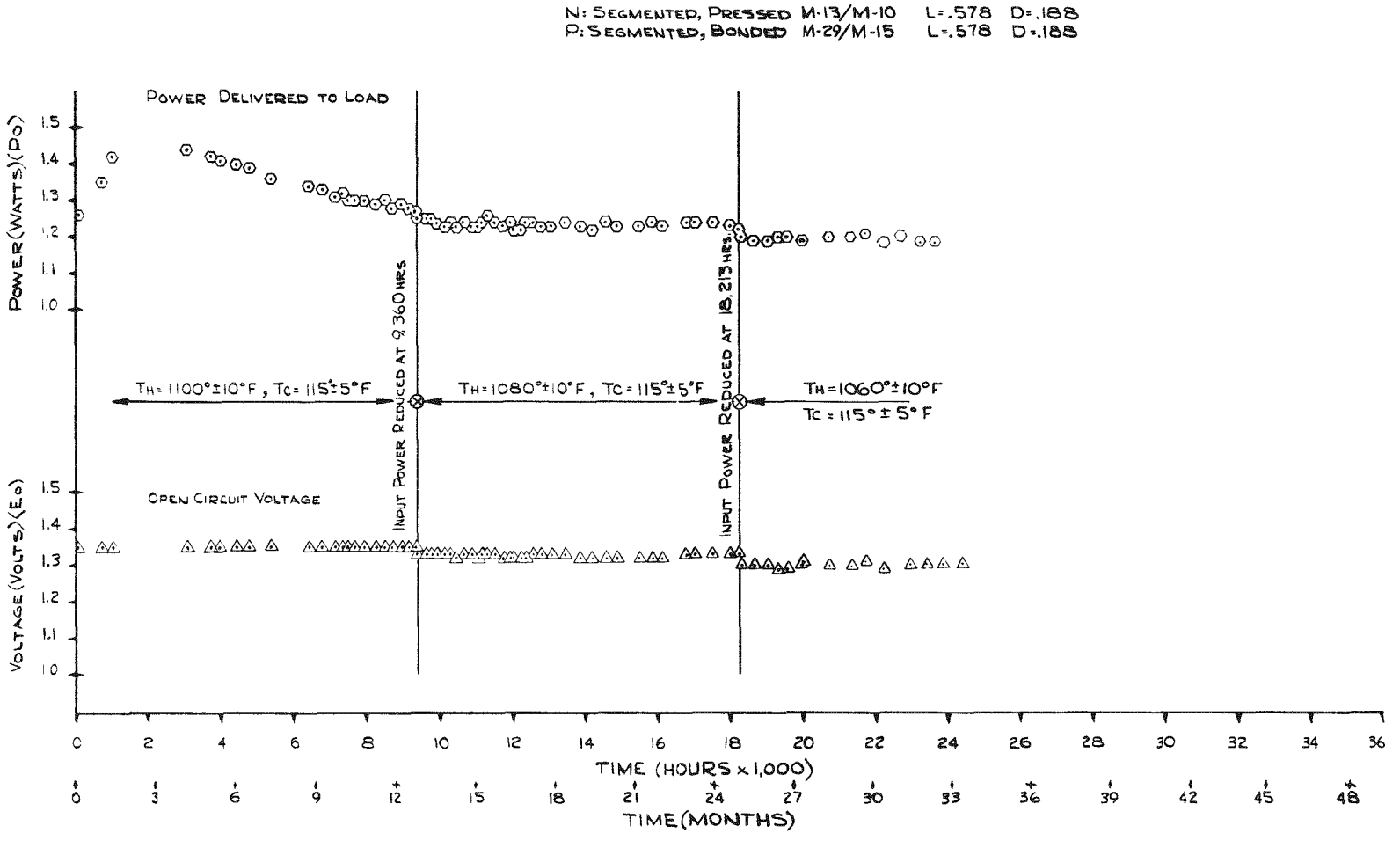

Figure 2-46. Performance Data, SNAP-21 6-Couple Module A3

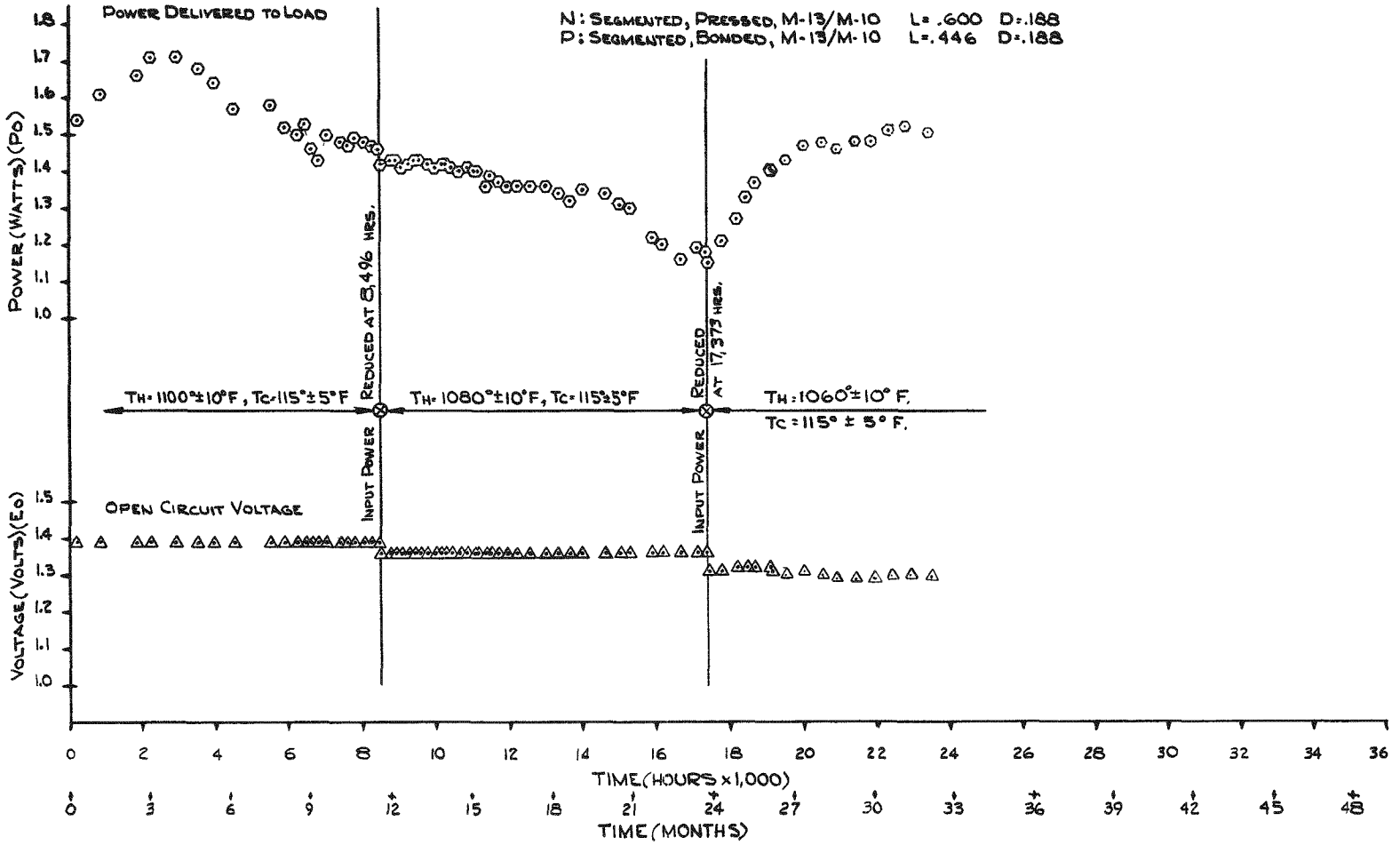

Figure 2-47. Performance Data, SNAP-21 6-Couple Module A4

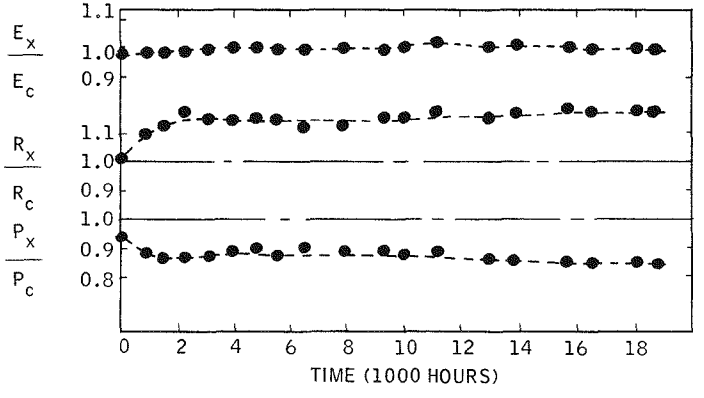

Prototype 3M-37-P3

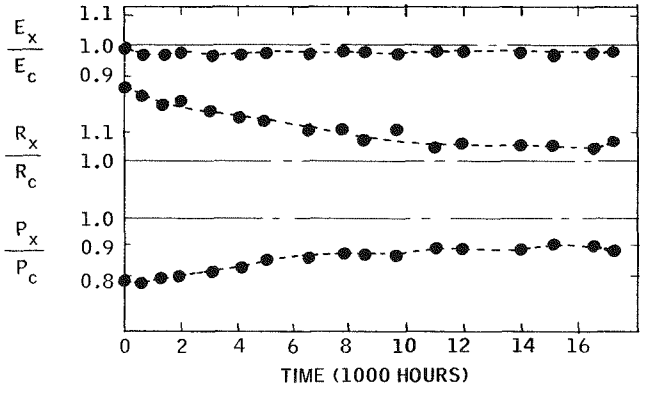

Prototype 3M-37-P5

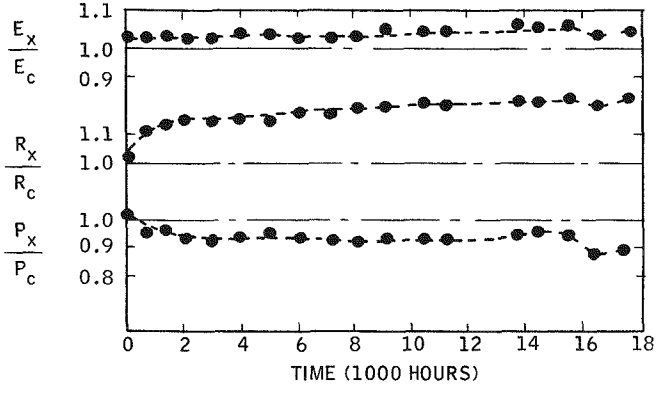

Prototype 3M-37-P6

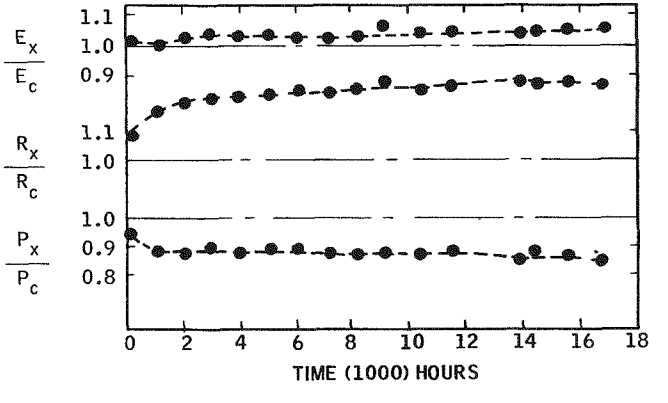

Prototype 3M-37-P7

Figure 2-48. Performance of Prototype 48-Couple Generator 3M-37-P3, P5, P6, P7 (E = voltage, R = resistance, P = power, x - experimental, C = computer)

Table 2-13. 6-Couple Module Performance Test Data

Module	Date	T-Hot (est)	T-Cold	E_o (volt)	E_L (volt)	I_L (amp)	P_o (watt)	R (M-ohm)	P_I (watt)	Hours
A-1	4-1-67	1060	113	1.29	0.63	1.82	1.15	361	34	23, 569
	4-11-67	1060	113	1.29	0.63	1.83	1.16	359	34	23, 809
	4-22-67	1060	115	1.28	0.63	1.80	1.13	361	34	24.073
	5-13-67	1060	115	1.29	0.64	1.84	1.17	355	34	24, 577
	5-27-67	1060	115	1.30	0.64	1.83	1.16	363	34	24, 933
	6-16-67	1060	113	1.30	0.63	1.84	1.16	363	34	25, 413
	6-23-67	1060	115	1.29	0.63	1.83	1.15	361	34	25, 581
A-3	4-1-67	1060	117	1.29	0.65	1.83	1.19	350	47	22, 233
	4-11-67	1060	118	1.30	0.65	1.83	1.19	354	47	22, 473
	4-22-67	1060	119	1.30	0.65	1.83	1.19	355	47	22, 737
	5-13-67	1060	119	1.30	0.65	1.84	1.20	356	47	23, 241
	5-27-67	1060	120	1.30	0.65	1.83	1.18	357	47	23, 577
	6-16-67	1060	119	1.30	0.65	1.83	1.18	357	47	24, 057
	6-23-67	1060	118	1.30	0.65	1.83	1.19	356	47	24, 225
A-4	4-1-67	1060	117	1.29	0.65	2.28	1.48	281	40	21, 393
	4-11-67	1060	117	1.30	0.66	2.30	1.51	280	40	21, 633
	4-22-67	1060	119	1.29	0.65	2.28	1.49	280	40	21, 897
	5-13-67	1060	118	1.30	0.66	2.31	1.53	277	40	22, 401
	5-27-67	1060	116	1.30	0.66	2.33	1.54	274	40	22, 737
	6-16-67	1060	116	1.29	0.66	2.30	1.51	275	40	23, 217
	6-23-67	1060	117	1.29	0.66	2.30	1.52	274	40	23, 385

Table 2-14. Prototype 48-Couple Generator Performance Test Data

Module	Date	T-Hot (est)	T-Cold	E_o (volt)	E_L (volt)	I_L (amp)	P_o (watt)	R (M-ohm)	P_I (watt)	Hours
P3	4-1-67	1088	158	10.60	5.30	2.01	10.63	2.64	193	18,167
	4-8-67	1085	158	10.52	5.16	2.01	10.57	2.62	193	18,335
	4-12-67	1077	159	10.50	5.25	2.02	10.58	2.60	193	18,431
	This Test Was Turned Off for Post-Test Analysis									
P5	4-1-67	1074	148	10.20	5.10	2.24	11.42	2.28	175	16,649
	4-8-67	1069	151	10.16	5.08	2.23	11.33	2.28	178	16,817
	5-13-67	1069	151	10.16	5.08	2.22	11.28	2.29	177	17,657
	5-24-67	1076	150	10.28	5.14	2.20	11.31	2.34	179	17,921
	5-24-67	Input Power Was Reduced							171	
	5-27-67	1062	154	10.02	5.01	2.23	11.17	2.25	171	17,993
	6-16-67	1065	155	10.08	5.04	2.20	11.09	2.29	172	18,473
	6-23-67	1064	154	10.08	5.04	2.16	11.89	2.33	173	18,641
P6	4-1-67	1075	168	10.32	5.16	2.05	10.60	2.51	190	16,020
	4-8-67	1075	171	10.52	5.26	2.09	10.99	2.52	194	16,188
	4-22-67	1075	168	10.38	5.19	2.07	10.72	2.51	194	16,524
	5-13-67	1075	167	10.40	5,20	2.07	10.76	2.51	194	17,028
	5-31-67	1075	172	10.34	5.17	2.06	10.65	2.51	194	17,460
	6-16-67	1075	176	10.58	5.29	2.05	10.84	2.58	194	17,844
	6-22-67	1075	177	10.34	5.17	2.05	10.60	2.52	194	17,988
	6-22-67	Power Input Reduced							186	
	6-23-67	1055	173	10.12	5.06	2.05	10.35	2.47	186	18,012

Table 2-14. Prototype 48-Couple Generator Performance Test Data (Continued)

Module	Date	T-Hot (est)	T-Cold	E_o (volt)	E_L (volt)	I_L (amp)	P_o (watt)	R (M-ohm)	P_I (watt)	Hours
P7	4-1-67	1075	183	10.60	5.30	1.93	10.20	2.75	186	16,016
	4-8-67	1075	188	10.70	5.35	.192	10.27	2.79	186	16,184
	4-22-67	1075	189	10.70	5.35	1.88	10.08	2.84	186	16,520
	5-13-67	1075	175	10.61	5.30	1.91	10.11	2.78	186	17,024
	5-27-67	1075	178	10.56	5.28	192	10.16	2.74	186	17,360
	6-16-67	1075	170	10.78	5.39	1.94	10.46	2.78	186	17,840
	6-22-67	1075	180	10.60	5.30	1.93	10.23	2.75	186	17,984
	6-22-67	Input Power Was Reduced							180	
	6-23-67	1055	171	10.30	5.15	1.91	9.84	2.70	180	18,008

In June, 1967, Prototype 6 and Prototype 7 were reduced in input power approximately 6 to 8 watts. Again, this was done to simulate the yearly decay rate of the isotope within a fueled system. Module P_7 has accrued 18,008 hours of continuous operation; Module P_6 has accrued 17,988 hours of continuous operation.

Prototypes P_6 and P_7 are continuing on test with no gross deviations in performance.

2.3.6.5.1 Post-Test Investigation, Prototype Unit P3

Prototype unit P3 was removed from continuation testing on 12 April 1967. The unit has now been completely dismantled and a detailed analysis of individual components is in process to determine the effects of long term operation at temperature. The study is being conducted according to Post-Test Investigation Plan, Prototype P3, MMM 36 1-15, dated 22 February 1967. The areas of the analysis which have been completed to date are reported in the following paragraphs.

a) Gas Analysis

The backfill gas of P3 was analyzed for the gases listed below. Concentrations are expressed in ppm except for that of xenon which is given in mole percent:

Xe – 96.1%	H_2O – 40
CH_4 – 14,000	CO – 0
N_2 – 4,500	CO_2 – 0
H_2 – 1,750	CS_2 – *
O_2 – 75	He – 0
Ar – 55	H_2S – 0
	SO_2 – 0

The detection of CS_2 was obscured by interference from other peaks. If present at all, it would be in small concentrations only (0-100 ppm).

b) Seebeck Analysis

Ten P-and N-legs were devided into five segments each and the Seebeck coefficient-temperature profile for each segment determined. The segments are identified in the sketch below.

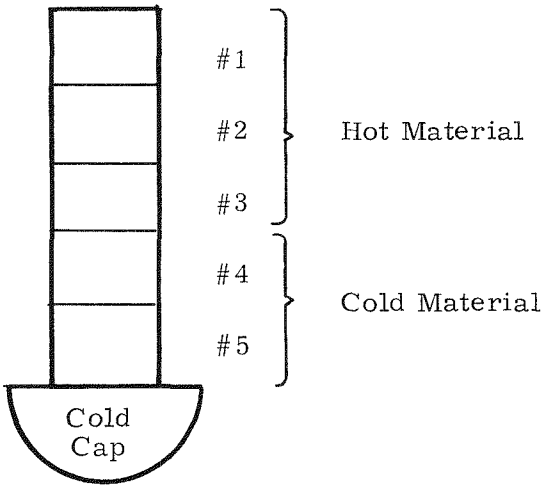

Segments 1, 2, and 3 comprise the hot end material, pbTe (p = 120 μΩ-in) or pb(Sn)Te for the N-and P-type materials, respectively. Segments 4 and 5 comprise the cold end material, pbTe (p = 400 μΩ-in) or Bi(Sb)Te for the N-and P-type materials, respectively.

To identify the N- and P-legs from the prototype, all of the hot button shoes are numbered, as illustrated in Figure 2-49. The N- and P-legs chosen for Seebeck analysis are bracketed in Figure 2-49. The legs are identified by type and hot shoe number. For example, a P-leg from hot shoe number 40 is called P-40, the N-leg from that shoe would be N-40.

Four N-legs and four P-legs from the same lot and batch used in prototype P3 were also divided into five segments each. A seebeck coefficient-temperature profile is being conducted on all eight legs. These eight legs are intended to be used as a standard of reference for the ten couples analyzed from the prototypes. However, there are two problems which arise when using these eight thermoelectric legs as a standard. The problems are:

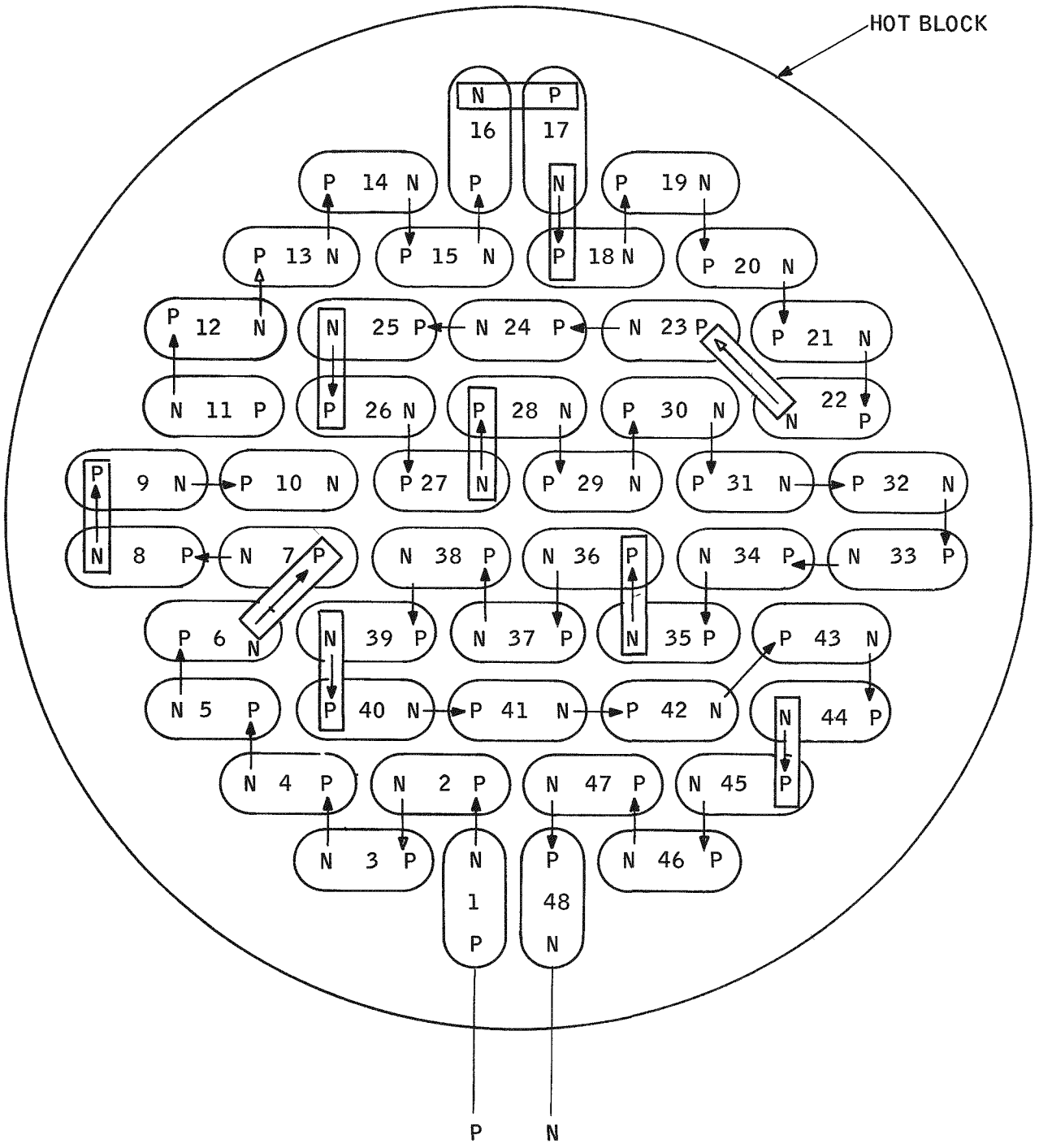

Figure 2-49. Arrangement of Couples in Prototype P3

(1) The leg standards do not have bonded cold caps. During the cold end binding process, the thermoelectric legs are annealed, resulting in a possible change in thermelectric property characteristics.

(2) The thermoelectric leg standards are over 2 years old, and they were not stored in an inert atmosphere. It is possible that the thermoelectric characteristics of the leg standards have changed during the period of storage.

Further studies are necessary to either validate or invalidate the leg standards. The N-leg standards were taken from Lot 22, Batch 1, manufactured on November 30, 1964. The P-legs standards were taken from Lot 27, Batch 1, manufactured on January 8, 1965. Each of the legs are identified by a leg number, directly traceable to the original resistivity curves. A summary of the Seebeck data is given in Table 2-15.

c) Resistivity (R vs L) Analysis

Room temperature resistivity measurements are not considered to be an accurate method of evaluating the resistance of the thermoelectric material while in a thermal gradient environment. This is due primarily to difficulty in accurately measuring and interpreting room temperature resistance. However, resistivity (R vs L) analysis is effective in detecting cracks and breaks within a thermoelectric material. No cracks or breaks have been detected in any of the P3 prototype couples tested with the R vs L equipment.

d) Chemical Analysis of Couples

Thermoelectric couples are being analyzed both with the emission spectrograph and with the microprobe. The results of these analyses will be included in a later quarterly.

e) Cold End Heat Transfer

Cold end heat transfer tests are being planned and developed to determine the cause of the cold cap temperature rise during the operation of the prototype. No test results have been obtained at this time.

Table 2-15. Seebeck Voltage of Leg Segments in Prototype P3
T_C = 75°F, T_H = 675°F - results in mv

	Leg Identification	Segment #1	Segment #2	Segment #3	Segment #4	Segment #5
P- and N-leg Standards	P leg #25; L27B1	34	33	33	46	46
	P leg #81; L27B1	34	33	32	39	46
	P leg #64; L27B1	32	32	34	37	46
	P leg #103; L27B1	34	33	32	39	48
	N leg #97; L22B1	58	58	57	75	84
	N leg #186; L22B1	56	56	55	85	82
	N leg #198; L22B1	55	55	56	74	84
	N leg #218; L22B1	54	56	55	73	
Prototype P-Legs	P-7	37	36	36	52	53
	P-9	36	37	33	46	48
	P-17	35	35	37	49	46
	P-18	34	35	34	47	48
	P-23	31	34	34	49	47
	P-26	35	36	38	44	49
	P-28	32	32	34	48	45
	P-36	34	35	33	51	49
	P-40	33	36	34	50	50
	P-45	34	36	36	52	51
Prototype N-Legs	N-6	58	60	57	81	83
	N-8	59	59	57	84	83
	N-16	60	58	62	82	80
	N-17	63	57	64	82	79
	N-22	45	56	57	79	81
	N-25	62	59	66	86	84
	N-27	60	59	65	87	82
	N-25	62	64	64	85	82
	N-39	64	57	66	85	82
	N-44	61	59	58	82	84

f) General Comments

Definite conclusions at this time on the post-test investigation would be premature. However, evidence from Table 2-15 suggests that the hot and cold segments of the N- and P-leg materials have remained homogeneous.

2.3.7 POWER CONDITIONER

The automatic selector switch and power conditioners A and D were shut down this month to permit testing of some parameters of power conditioner D. The long term testing is expected to resume during the next report period.

The tests performed on power conditioner D concerned the relationship between degradation in the resistance of the bias section of the thermopile and the starting characteristics of the power conditioner. The results of these preliminary tests indicate that if the power conditioner is operating into its rated load, a degradation of 2:1 in thermopile bias section resistance will not inhibit starting under normal operating conditions.

With a variable load resistance which is gradually increased from near short circuit to rated load, the present power conditioner may fail to start if the resistance of the bias section of the thermopile has degraded by only 10 percent. It is important that no transients be generated since the power conditioner will begin to operate upon the occurrence of the first transient.

This starting problem is not expected to occur during the normal operation of the power conditioner; however, the elimination of this problem is considered to be good design practice and will contribute to the overall reliability of the system.

Although these preliminary tests have shown that additional effort is necessary, it is not possible to determine the extent of the effort required. Power conditioner B (breadboard) will be used to test the several design approaches which will give a better safety margin. The best design approach will be chosen and incorporated into the final power conditioner design.

Power converter MP-B was removed from long term test on June 7, 1967 and preliminary test effort was started to ensure high reliability and performance of the end item.

Testing and the subsequent analysis of this test effort will be reported in a later report.

The remaining life testing efforts on the Phase I electronic components, (power conditioner, regulators and automatic selector switch) are continuing. Test data shows no significant change in performance. Test duration of these components range from 13,000 to 15,000 hours.

2.3.8 ELECTRICAL RECEPTACLE

No effort was expended in this area during the past report period.

2.4 SYSTEM FABRICATION, ASSEMBLY AND TESTING

2.4.1 PHASE I CONTINUATION TESTING

SNAP-21B-1, in May 1967, underwent an input power reduction of approximately 5 to 6 watts to simulate a yearly isotope fuel decay. The system is continuing on test and is performing with no significant change. The unit has accrued a total of 18,891 hours as of this report period.

2.4.2 PHASE II SYSTEM

Late in the report period, the Linde Phase I HTVIS system was assembled into the Phase I residual pressure vessel in preparation for thermal testing of the partial system. A pre-test analysis concluded that the U-8 Moly bolts that join the inner liner to the biological shield would creep excessively at system operating temperature. The entire system was therefore rotated 180°. This action will remove the tension from the bolts and eliminate the creep in the bolts at system operating temperatures, eliminating a possible failure mode. The rotation puts the neck tube in compression so that it will support the weight of the shield during elevated temperature testing.

A detailed description of the proposed thermal (vacuum) monitoring is as follows:

The system temperature will be stabilized at 1285°F. This temperature value is a mean temperature evolved from earlier test data, and is indicative of temperatures adjacent to the area of the SNAP-21 thermopile. Figure 2-50 is a schematic of the electrically heated hot block and the location of chromel-alumel thermocouples.

Thermocouple No. 2 is the control thermocouple for final system operating temperature. All remaining thermocouples are monitored but are classed as reference only.

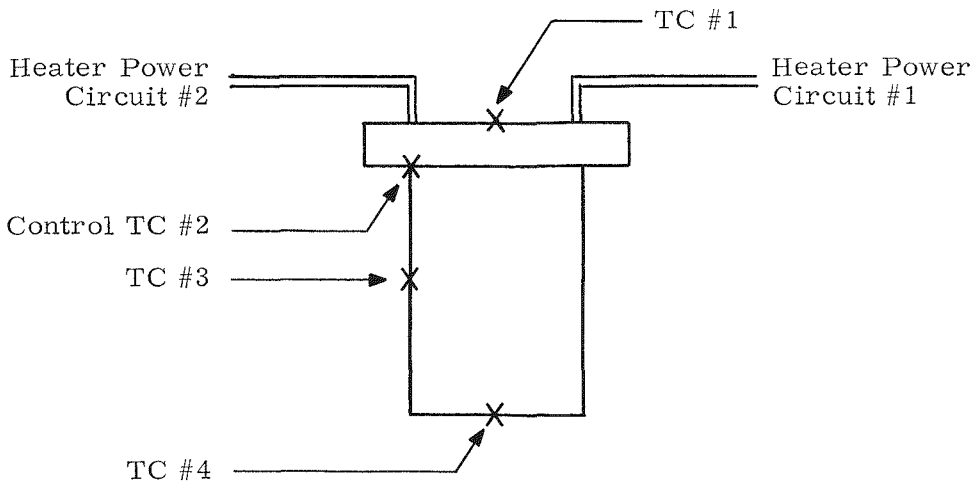

Figure 2-50. Schematic of Electrically Heated Hot Block and Location of Thermocouples

Four 500-watt 115 VAC cartridge heaters supply heat to the heater block and hence to the system. Two variac controlled circuits of two heaters each, wired in parallel, constitute the wiring to the system.

Each circuit contains an isolation transformer to preclude any system damage due to cartridge heater malfunction.

Each circuit contains a voltmeter and wattmeter and monitors input power to the system.

The sequence of the test effort is as follows:

1) Instrument heater block with chromel-alumel thermocouples by T. I. G. welding process.

2) Insert heater block into system.

3) Align bolt holes and insert stainless steel cap screws that have been previously treated and an anti-seize and/or high temperature anti-galling compound.

4) Torque bolts to minimum value.

5) Wire two heaters in parallel for one circuit. Wire remaining two heaters for remaining circuit in a similar manner.

6) Carefully insert block MIN-K 1301 as heat loss material into neck tube area.

7) Assemble MIN-K retainer plate.

8) Check all wiring for shorts, opens and continuity.

9) Assemble pressure vessel dome to system and torque bolts.

10) Apply 25 watts of power to each circuit or a total of 50 watts power to entire system. Hold this input power for 24 hours.

11) Monitor and record all temperatures each 1 hour time period.

12) Increase input power to each circuit by 10 watts, 35 watts input power per circuit, such that total input power to system is 70 watts.

13) Hold above conditions until temperature approaches 1285°F (within 15 degrees), recording each 1 hour time period.

14) As the temperature of the control thermocouple, thermocouple #2, attains the 1285°F value, input power will have to be decreased from 70 watts (35 watts each circuit) to approximately 45 watts (22-1/2 watts each circuit). This input power level will theoretically result in a stable operating temperature of 1285°F.

15) Minor power adjustment (plus or minus) may be required to stabilize the system operational temperature of 1285°F.

The following equipment is used in monitoring the Linde (HTVIS) System and residual pressure vessel test.

Quantity	Item
2	Simpson Wattmeters 0-75 Watts
2	Stancor Isolation X' Formers 15150 - 150VA, Sec. 115V
2	Adjustavolt Variac - Output Voltage 0-135 VAC, 7.5 Amp
1	Simpson AC Voltmeter 0-50 VAC
1	Howell Autotemp Type K Temperature Meter 3M03733
1	Leeds Northrup Rotary Thermocouple Switch
1	Hastings Vacuum Gauge #902
4	115 VAC - 500 Watt Rama Corp. Cartridge Heaters

The test started on June 23, 1967. Preliminary results will be reported in the next Quarterly Report.

2.5 SAFETY ANALYSIS AND TESTING

2.5.1 OCEAN EXPOSURE STUDIES OF RADIOISOTOPE FUEL CAPSULE

Comments pertaining to the basic test plan for ocean exposure studies of the radioisotope fuel capsule were submitted to the Naval Radiological Defense Laboratory (NRDL). As a result, the design of the exposure shield chamber has been revised to reflect the comments as follows:

- Two separate chambers suspended by one buoy will be used to accommodate the two fueled capsules.
- A more indirect water circulation system will be used to avoid possible radiation streaming.
- To eliminate the possibility of problems during transportation and handling, the exposure shield chamber will act as the shipping container for the fueled capsules from Battelle Northwest Laboratories to NRDL. The exposure shield chamber will be shipped without water to prevent boiling problems.
- The shipping chamber will have a different top from the exposure chamber; at San Clemente Island NRDL's Health and Safety Department will replace the top with one which provides instrumentation and water circulation. The capsule will not be handled by NRDL personnel.

The revised test plan for the ocean exposure of the fueled capsules is to be provided to 3M soon. The detailed prints of the exposure shield chamber should be submitted to 3M by the end of July. NRDL is now evaluating the extra cost of accommodating two fueled capsules.

2.5.2 LABORATORY CORROSION TESTING OF SNAP-21 MATERIAL

Laboratory corrosion testing of SNAP-21 materials is awaiting Hastelloy-X material samples. The samples consist of sheet and bar stock. Hastelloy-X sheet and bar samples are being provided to 3M by Union Carbide.

2.5.3 OCEAN EXPOSURE STUDIES OF ELECTRICALLY HEATED FUEL CAPSULE TEST SYSTEMS

The prints for the electrically heated fuel capsule mockup were submitted to 3M. After reviewing the prints, 3M suggested using electron-beam welding for the enclosure weld of the electrically heated Hastelloy-C fuel capsule. The desired tolerances between the electron beam welded parts were provided to NRDL. They will incorporate the changes to the system and forward the prints to 3M by the end of June.

The prints of the marine fouling systems mockup have been sent to 3M. These prints are now being reviewed. Comments will be provided to NRDL as soon as possible. Also, the Ti-621 flange which is part of the marine fouling system enclosure is being procured.

Prints for the galvanic coupling systems mockup are expected by 3M very soon.

2.5.4 OCEAN FUEL RELEASE STUDIES

Very little work has been devoted to planning ocean fuel release studies.

2.5.5 RADIATION TESTING AND ANALYSIS

Measurements of the external radiation levels for a fueled SNAP-21 system were performed at Oak Ridge National Laboratory. A system mockup was assembled from residual Phase I parts consisting of: a Linde high vacuum thermal insulation system including a uranium radiation shield, a titanium pressure vessel, a simulated thermoelectric generator (cold frame, hot frame and outer case), and a segmented centering and mounting ring. The mockup system was assembled in and supported by an aluminum cradle. A wooden stand was used to support the cradled system at the proper height in the hot cell for the fueling operation. The system was fueled with a 200-watt SrO source. Since its physical size was considerably smaller than the shield cavity, no special provision for inserting the capsule was necessary to prevent interference from thermal expansion.

After the fuel capsule was inserted and the radiation shield plug installed, a general area survey was made to determine whether radiation levels were low

enough to allow personnel access. The radiation levels were found to be low and the unit was removed to the test area. Radiation test measurements were taken using a Cutie Pie survey instrument (Figure 2-51) and Landsverk L-64 roentgen meter dosimeters. The initial radiation levels as indicated by the survey instrument agreed quite well with calculated values. Upon review of instrument calibration the values recorded by the dosimeters were discredited. It was decided that the test should be rerun using newly calibrated instruments. The system had already been defueled at this time and it was necessary to repeat the fueling sequence. Radiation measurements were taken using two Cutie Pie instruments, direct reading dosimeters and personnel type film packs.

Radiation survey data is presented in Table 2-16. The positions at which the measurements were taken and average values obtained from all types of dosimetry are shown in Figure 2-52.

The film badge dosimetry is given in Table 2-17. The "window" reading is through 80-mg/cm^2 paper and the "plastic" through 300-mg/cm^2 plastic. The "aluminum" is used to filter out low-energy photons and to distinguish between X and gamma radiation. The reading through cadmium is a hard dose and is considered the dose to critical organs. The skin dose is calculated as shown by the formula:

$$\text{Skin Dose} \quad D_s = (D_{window} - D_{plastic})\, 2.5 + D_{cadmium}$$

The small differences between the absorption values indicate relatively hard radiation which is what might be expected with a thick shield.

Radial measurements were taken to verify axial position of fuel capsule.

The dose rate determined from the film as dose point 8(0°) is not reliable since these films cannot be accurately read below a total dose of 50 mr. The dosimeter reading at this point will probably be the most accurate.

The radiation levels measured at positions 12 and 13 were approximately 50 percent higher than estimated. The higher dose rate at position 13 is explained by the removal of material in reworking the shield (Figure 2-53). The simulated generator had a copper cold frame over an inch thinner than will be used in the generator and it is expected that the intensity at this point would be less than 100 mr/hr.

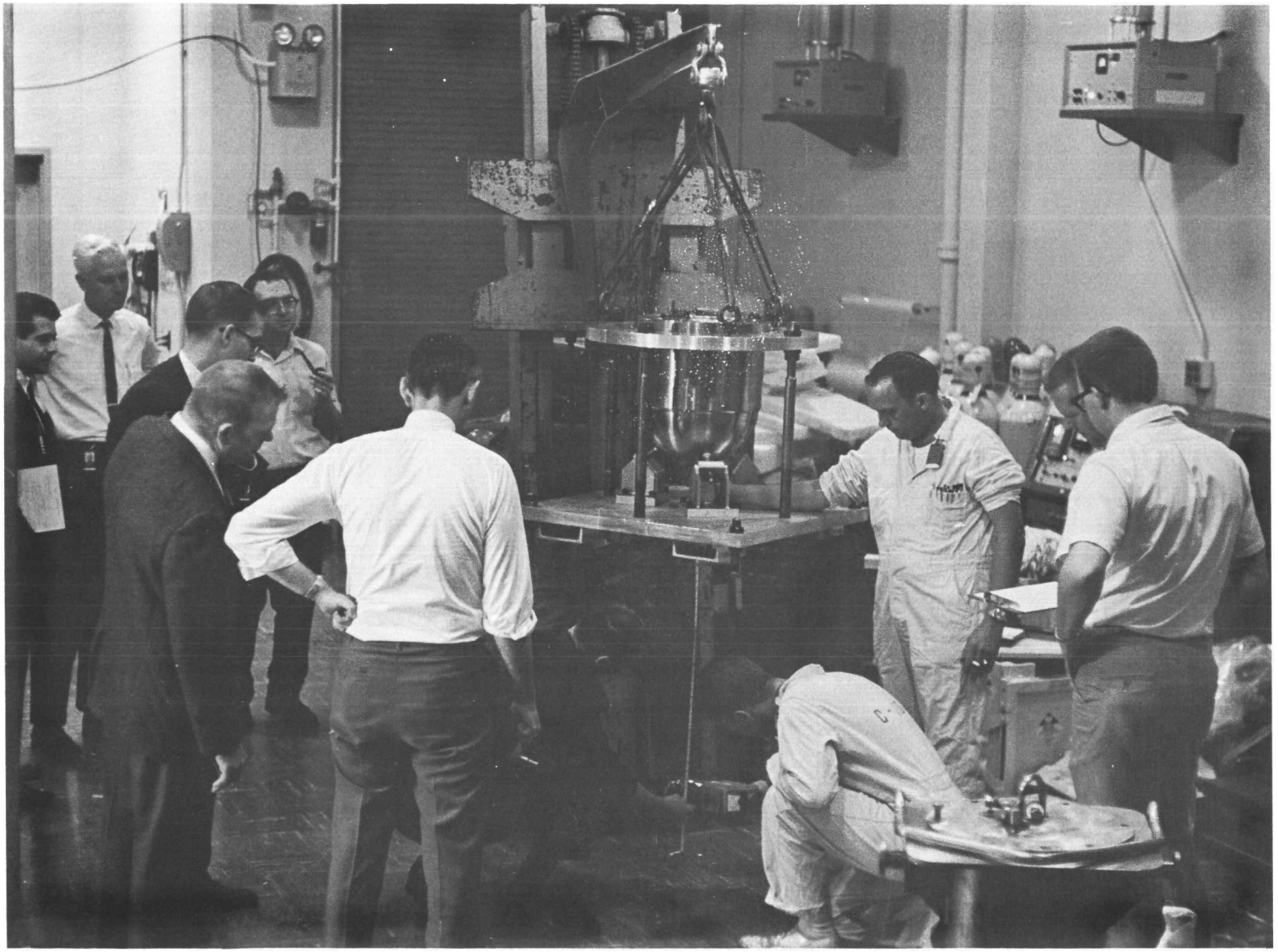

Figure 2-51. Taking Radiation Measurements in Test Area

Table 2-16. Radiation Survey

Dose Points	Cutie Pie 1, mr/hr	Cutie Pie 2, mr/hr	Dosimeter, mr/hr	Film, mr/hr
1	44	46		
2 (90°)	46	58	50	80
(270°)			73	
3 (0°)	260	280	327	240
check at 0°	260	260		
90°	250	260	222	
180°	260	250		
270°	280	280	249	
4 (0°)	200	200	218	191
check at 0°	200	180		
90°	200	190		
180°	180	180		
270°	200	200		
5	280	320	261	334
6	10	10		
7 (0°)	8	10		
8 (0°)	9	7	15	29
9 (0°)	10	9		
10 (90°)	5	3		
11	8	6		
12	720	720		
13	160	160	166	216

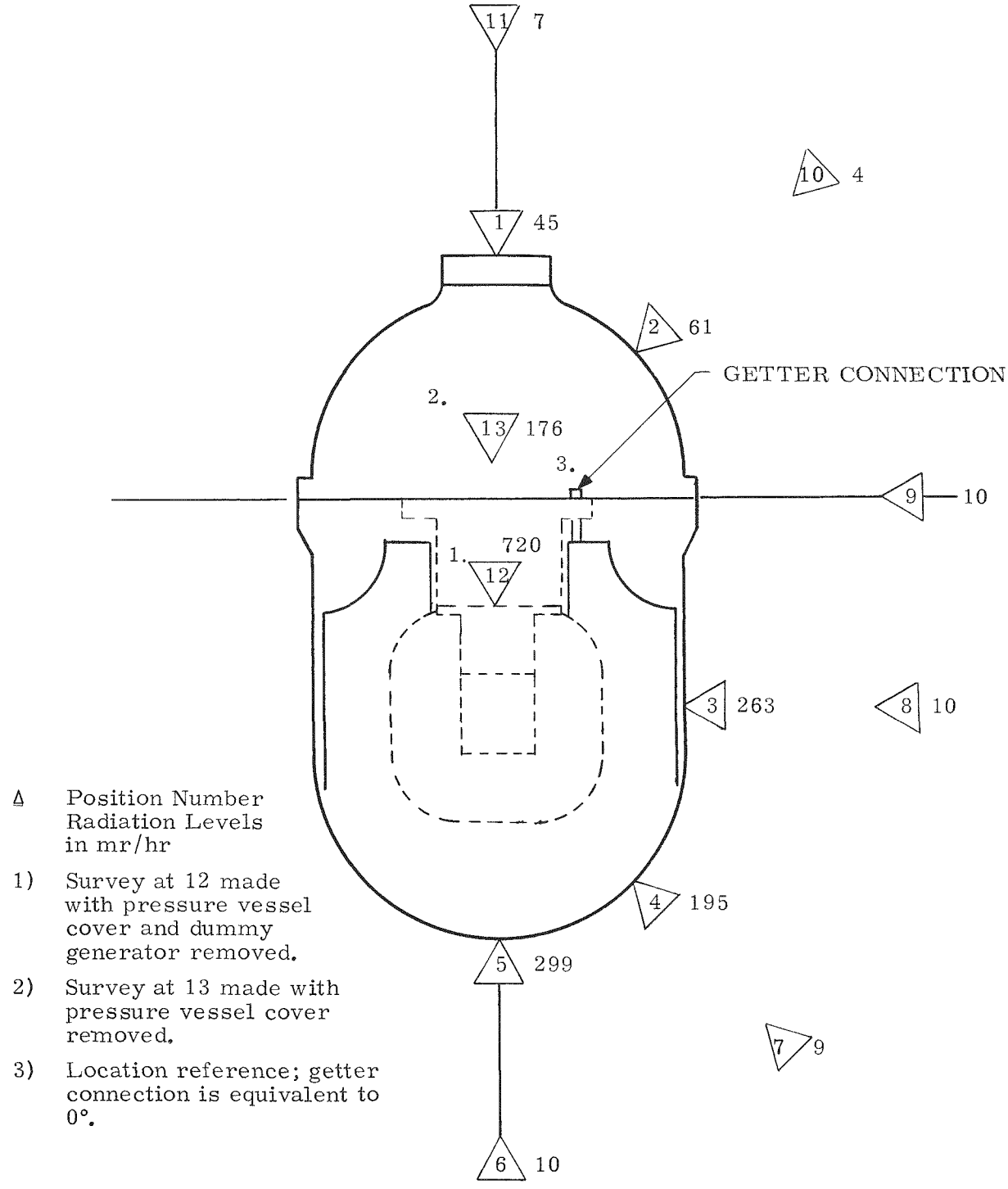

Figure 2-52. Radiation Measurement Points on Mock-Up System

Table 2-17. Film Badge Dosimetry

Dose Point		Window	Dose Rate, Mr/Hr		Cadmium	Time, hr	Ds Skin dose, mr/hr
			Plastic	Aluminum			
2 (90°)	F-104	70	70	70	80	1.00	80
3 (0°)	F-103	254	268	296	275	1.4167	240
4 (0°)	F-102	247	261	247	226	1.4167	191
5	F-101	480	544	551	494	1.4167	334
8 (0°)	F-106	39	39	39	29	1.0333	29
13	F-105	226	226	236	216	1.0167	216

Since the shield plug was not encapsulated, care was taken to insure that the temperature of the unit did not exceed 500°F where oxidation might become a problem. A chrome-alumel thermocouple was attached to the top of the radiation plug and the temperature rise recorded during the test (Table 2-18) no damage to the shield plug was incurred.

While radiation levels at one meter from the systems surface appear within the 10 mr/hr limit, surface values in several locations exceeded the permissible 200 mr/hr limitation.

Careful analysis of the actual configuration tested revealed a number of differences which account for the higher dose rates. For example, the original shield dimensions were based upon a 187-watt $SrTiO_3$ source. SrO fuel has a radiation intensity 13.6 percent higher than from $SrTiO_3$; therefore, the radiation from the 200-watt source used for the test corresponded to about 227 watts of $SrTiO_3$. Furthermore, the fuel capsule used had a wall thickness of 0.090 inch compared to 0.250 inch for the SNAP-21 design.

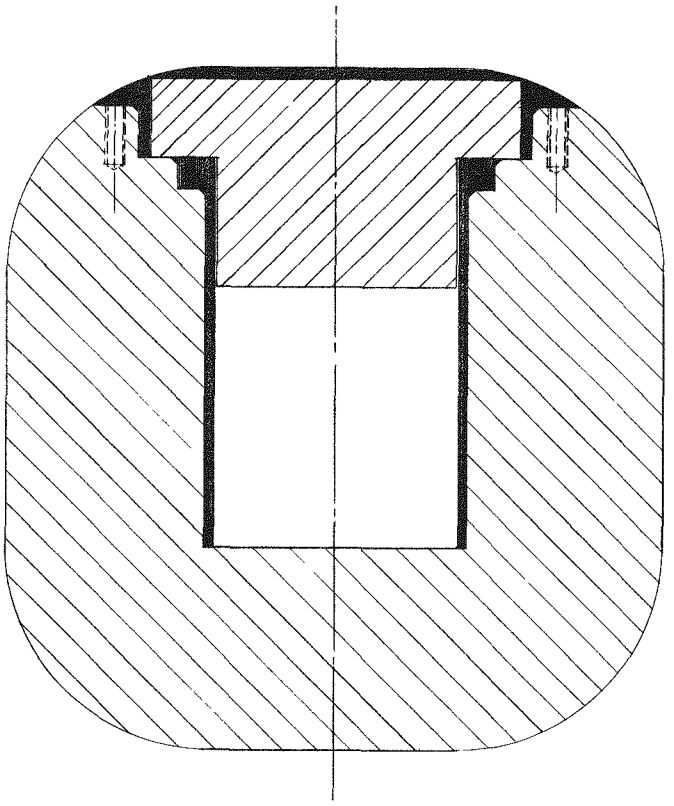

Figure 2-53. Reworked Biological Radiation Shield Showing Material Removed

In reworking the Phase I shield for use in the insulation system the cavity was bored out 0.200 inch to accommodate the inner liner. The shield wall thickness was therefore less than originally specified (2.559 vs 2.695 inches). The bottom thickness was 2.658 inches. Using the attenuation curves of Arnold, the additional shielding required to reduce the radiation to 200 mr/hr at the surface was determined (Table 2-19).

The spatial relationship and dimensions of these designs are shown in cross section in Figure 2-54.

Table 2-18. Temperature Measurements During Radiation Tests

Run No. 1		Run No. 2	
Time, min	Temperature, °F	Time, min	Temperature, °F
0	~80.0	0	--
35	217.0	20	155
45	225.5	30	194
55	235.5	40	226
65	248.1	50	248
75	260.0	60	268
85	271.5	70	282
98	285.5	80	296
105	292.5	90	307
115	302.3	100	326
125	321.0	115	345
135	325.0	122	352
145	328.5	130	361
155	338.5	150	380
165	345.0	157	406

NOTE: Run No. 1 was started with shield plug approximately room temperature; Run No. 2 was started with shield plug at a higher temperature due to heatup from Run No. 1.

Table 2-19. Shield Thickness Required to Achieve 200 mr/hr Maximum System Surface Radiation

Shield Design	Fuel Loading	Shield Thickness (inches)	
		Side	Bottom
Phase I	187 W_{th} $SrTiO_3$	2.695	2.658
Test Unit Δ	227 W_{th} $SrTiO_3$	2.559 Actual Dimensions	2.658
		2.679 Indicated Thickness Required From Test Date	2.818
Present Design	216 W $SrTiO_3$	2.659	2.798

Δ Radiation level outside = 263 mr/hr
Out bottom = 299 mr/hr
Equivalent to 200W SrO source actually used

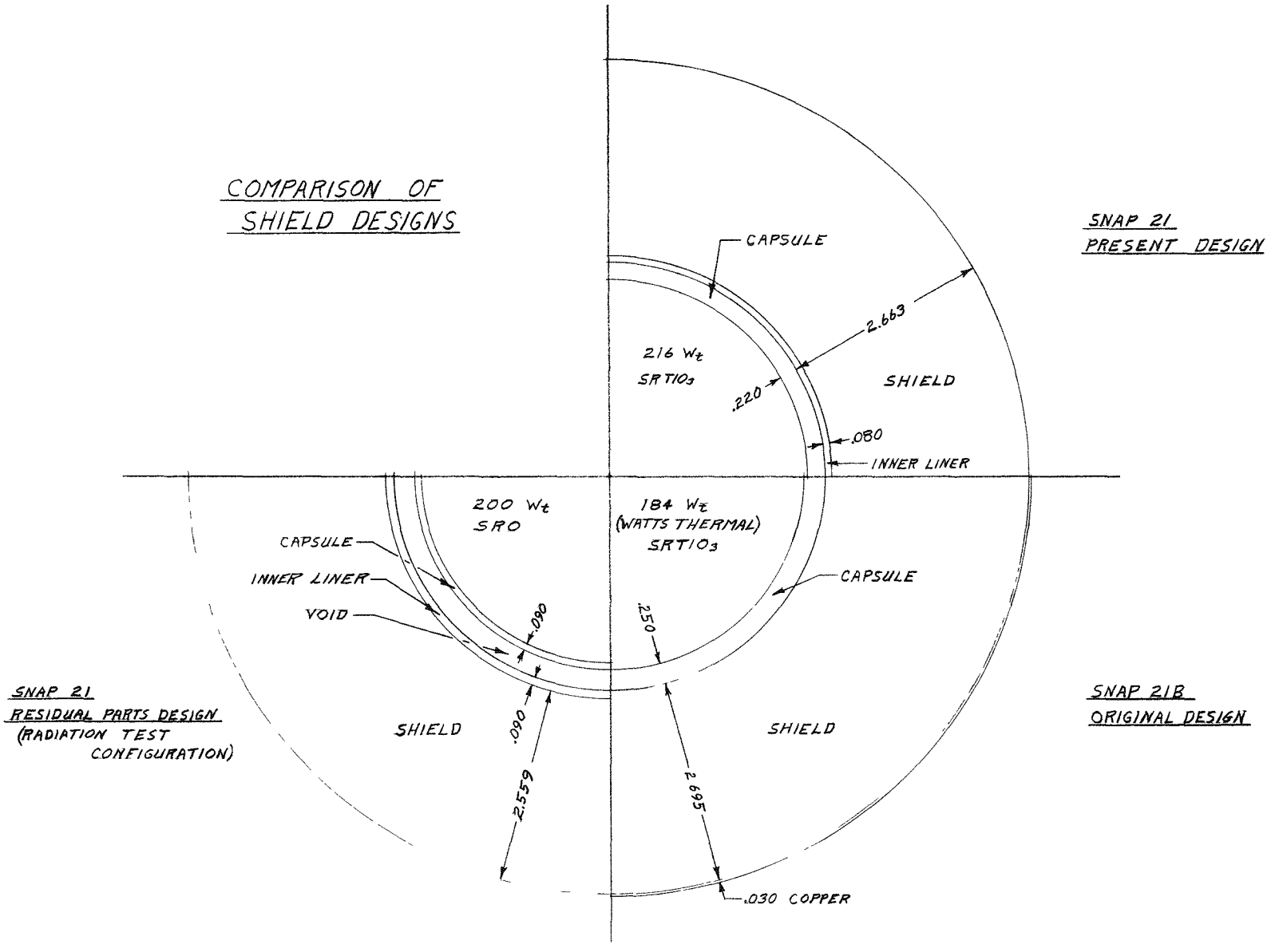

Figure 2-54. Spatial Relationship of Shield Designs

3.0 TASK IIA – 20-WATT SYSTEM

3.0 TASK IIA–20-WATT SYSTEM

3.1 CONCEPTUAL DESIGN

Efforts were concerned primarily with producing a conceptual drawing of the 20-watt system which would be suitable for use in planning the 20-watt development program. An updated design envelope for the 20-watt high vacuum thermal insulation system (HVTIS) was also prepared. Together these drawings provide a starting point for evaluating system components and their relationship to each other.

The thermoelectric generator was the first system component evaluated. To establish the size of the generator it was necessary to determine the thermoelectric leg geometry. For this initial conceptual effort, the segmented legs of the 10-watt system was selected, doubling the number used in the 10-watt system to obtain the 20-watt output. The alternative method of increasing power output by reducing the length to area (L/A) ratio of the legs has been found to be less efficient, requiring more heat per output watt. Doubling the power output by this method would require reducing the L/A ratio to less than half the original (10-watt system legs) to compensate for wire losses. Wire losses are part of the total internal resistance of the thermopile and cannot be halved.

The internal resistance of the thermopile consists of the sum of the wire, thermoelectric material and contact resistances. The latter two factors are difficult to separate and evaluate, and, to get a somewhat better evaluation of internal resistance with respect to time, test data from the Phase I 10-watt prototype units P3 and P5 was reviewed. The test data consisted of measured leg resistance, which includes the resistances of the cold cap, thermoelectric material, hot junction button material and the hot end, cold end and segmented joint contacts. The extraneous resistance is obtained by subtracting the thermoelectric material book value resistance from the measured value.

The test data showed that, after a short period of stabilization, the extraneous resistance increased slightly with respect to time. The increase was due primarily to an increase in contact resistance at the hot end. It is possible that the resistance of the thermoelectric material at the hot end itself is changing with time.

The test data covered a period of somewhat greater than two years for Prototype P3 and slightly less than two years for Prototype P5. Because of the changing resistances, a 5-year projection was not made.

Tests indicate that a 3M proprietary P-leg contacting technique will greatly reduce the P-leg contact resistance. However, this technique was not available when the units were built and therefore its effectiveness with respect to time is not known. If a decrease in resistance can be realized, either a reduction in operating temperatures or reduction in generator size is possible.

A system heat analysis was made to determine the problem areas in dissipating the heat from the thermoelectric generator to the surrounding environment.

Preliminary calculations indicate that the thermal resistance of titanium is too great to consider it as a pressure vessel for this design. An alternative being considered is a BeCu alloy that has structural and corrosive properties similar to that of titanium, but has 15 times the heat dissipating ability. This material makes the design practical by allowing the generator to operate near design conditions. Further analysis may indicate that design changes are required to increase the thermal safety margin of operation for the generator. The present analysis used a mean thermal path through components and did not consider the interfaces between components. Comparing the results using this technique on 10-watt components to the data from the test system the accuracy is within 5%.

The high vacuum insulation system required a structural loading on the outer shell and neck tube of the inner liner. The static weight of the biological shield and other 3M supplied components is 350 pounds. This weight, plus that of the insulation system and loads imposed during handling, require that the shell support approximately 5000 pounds. The design concept will be determined on the basis of results obtained from the nearly completed 10-watt design.

4.0 EFFORT PLANNED NEXT QUARTER

4.0 EFFORT PLANNED NEXT QUARTER

The following items are planned for the next quarter:

- Begin compatibility testing
- Complete test plans for fuel release (ocean environment) studies
- Fabricate and performance test the remaining three development generators
- Complete the design of the in-line concept generator
- Assemble the SNAP-21 residual Phase I system
- Complete design and select vendors for the electrical receptacle and strain relief plug
- Complete the design of the segmented retaining ring
- Complete the tension tie-rod development
- Complete the design of the tension tie-rod connectors
- Begin assembly of Insulation System Development Unit No. 1
- Complete design of insulation system shipping container
- Complete any necessary circuit design modifications in the power conditioner and hold design review for final release of the circuit
- Complete the design analysis for final release of the power conditioner enclosure and seal-off device

- Establish welding specifications, design necessary fabrication tooling, and select vendors for the power conditioner
- Assemble and test new devices for determining Seebeck coefficients
- Thermoelectric leg inspection techniques will be refined for production type testing.
- Design of the biological shield will be completed and released.
- Fuel capsule weld method will be selected.

APPENDIX A

SNAP-21 PROTOTYPE UNIT THERMAL PERFORMANCE TEST– CALCULATION OF UNIT HEAT LOSS

APPENDIX A

SNAP-21 PROTOTYPE UNIT THERMAL PERFORMANCE TEST— CALCULATION OF UNIT HEAT LOSS

Measured Test Data: Data Book 1291B, pp. 64-66

Hot end neck tube temperature	1285°F
Cold end neck tube temperature	135°F
Steady-state power input (W)	43.42 watts avg.
Steady-state voltage (E)	29.22 volts avg.
Steady-state current (I)	1.50 amps

Instrumentation Constants

Resistance of voltmeter (R_V)	3000 Ω
Resistance of wattmeter (R_W)	409.5 Ω/volt
Resistance of power lead to heaters (R_L)	0.081 Ω

$$\text{Corrected input power} = W - \left[\frac{E^2}{R_W} + \frac{E^2}{R_V}\right] - I^2R_L$$

$$= 43.42 - \left[\frac{853.8}{11966} + \frac{853.8}{3000}\right] - 2.25\,(0.081$$

$$= 42.88 \text{ watts}$$

To determine the heat loss of the unit, which includes the neck tube loss and insulation loss, the calculated loss through the following components must be subtracted from the corrected input power.

1. Neck tube insulation loss
2. Heater wire and insulation loss
3. Thermocouple wire and insulation loss

1. Neck Tube Insulation Loss

The neck tube was filled with block MIN-K 2000 insulation. Powdered MIN-K 2000 insulation was used to fill around the circumference of the neck tube and two 5/8-inch diameter holes in the block insulation for the passage of the heater and thermocouple wires.

Insulation thickness	2.65 inches
Insulation diameter	4.900 inches
Insulation area	18.75 sq. in.

Area of 2-5/8 in. diameter holes = 0.59 sq. in.

Area of circumference gap 1/16 in. wide = 0.96 sq. in.

Area of block insulation = 18.75 - 0.59 - 0.96 = 17.20 sq. in.

Area of powdered insulation = 1.55 sq. in.

$$\text{Mean temperature} = \frac{1285 + 135}{2} = 710°F$$

$$\Delta T = 1285 - 135 = 1150°F$$

$$\text{Conductivity of block insulation} = 0.26 \frac{\text{Btu-in}}{\text{Hr-ft}^2 - °F}$$

$$\text{Conductivity of powdered insulation} = 0.51 \frac{\text{Btu-in}}{\text{Hr-ft}^2 - °F}$$

$$\text{Heat loss} = \frac{\text{Block } KA\,\Delta T}{L} + \frac{\text{Powder } KA\,\Delta T}{L}$$

$$= 0.26 \frac{\text{Btu-in}}{\text{Hr-ft}^2 - °F} \times \frac{17.20 \text{ in}^2 (\text{ft}^2)}{144 \text{ in}^2} \times \frac{1150°F}{2.65 \text{ in}}$$

$$+ 0.51 \frac{\text{Btu-in}}{\text{Hr-ft}^2 - °F} \times \frac{1.55 \text{ in}^2 (\text{ft}^2)}{144 \text{ in}^2} \times \frac{1150°F}{2.65 \text{ in}}$$

$$= 13.49 \text{ Btu/hr} + 2.38 \text{ Btu/hr} = 15.87 \text{ Btu/hr}$$

$$= \frac{15.87 \text{ Btu}}{3.41 \text{ Hr}}$$

Neck tube ins. loss = 4.66 watts

2. Heater Wire and Insulation Loss

Eight heater wires penetrated the neck tube insulation. Four wires had 42 strands and four wires had 7 strands each. Consider first the heat loss through the 42 strand wires.

Heater wires – 42 strands of 201 nickel – 30 ga. – 0.010 in. dia. Covering the stranded wires was asbestos with an outside diameter of 0.140 in.

Stranded wire length = 2.31 in. as the stainless steel wire connector extended 0.34 in. above the heater block.

This connector was 0.156 in. O.D. and 0.090 in I.D.

$$\text{Area of one stranded wire} = \frac{\pi}{4} (0.010 \text{ in.})^2 (42) = 0.0033 \text{ in.}^2$$

$$\text{Area of asbestos} = \frac{\pi}{4} (0.140 \text{ in.})^2 - 0.0033 \text{ in.}^2 = 0.121 \text{ in.}^2$$

$$\text{Area of solid heater wire} = \frac{\pi}{4} (0.090 \text{ in.})^2 = 0.00631 \text{ in.}^2$$

$$\text{Area of stainless connector} = \frac{\pi}{4} (0.156 \text{ in.})^2 - 0.00631 = 0.0119 \text{ in.}^2$$

$$\text{Conductivity of 201 nickel (135°F - 1285°F)} = 432 \frac{\text{Btu-in}}{\text{Hr-ft}^2 - °\text{F}}$$

$$\text{Conductivity of 201 nickel at 1285} = 428 \frac{\text{Btu-in}}{\text{Hr-ft}^2 - °\text{F}}$$

$$\text{Conductivity of asbestos} = 0.12 \frac{\text{Btu}}{\text{Hr-ft - °F}}$$

$$\text{Conductivity of stainless} = 10 \frac{\text{Btu}}{\text{Hr-ft - °F}}$$

First determine the temperature at the end of the stainless connector. The heat loss through the stranded wire and insulation is equal to the heat loss through the connector and heater pin wire.

$$\underset{\text{Wire}}{\text{Stranded}} \quad \underset{}{\text{Asbestos}} \qquad \underset{\text{Wire}}{\text{Pin}} \quad \underset{}{\text{Connector}}$$

$$\left(\frac{KA}{L} + \frac{KA}{L} \right) \Delta T_1 = \left(\frac{KA}{L} + \frac{KA}{L} \right) \Delta T_2$$

$$\left[432 \frac{\text{Btu-in}}{\text{Hr-ft}^2\text{ - °F}} \times \frac{0.0033 \text{ in.}^2 (\text{ft}^2)}{144 \text{ in}^2 (2.31 \text{ in.})} + 0.12 \frac{\text{Btu}}{\text{Hr-ft}^2\text{ - °F}} \times \frac{0.0121 \text{ in.}^2 (\text{ft})^2}{144 \text{ in.}^2} \times \frac{12 \text{ in.}}{2.31 \text{ in. (ft)}} \right] \Delta T_1 = \left[\frac{428 \text{ Btu-in}}{\text{Hr-ft}^2\text{ - °F}} \times \frac{0.00631 \text{ in.}^2 (\text{ft})^2}{144 \text{ in}^2 (0.34 \text{ in.})} + \frac{10 \text{ Btu}}{\text{Hr-ft-°F}} \times \frac{0.0119 \text{ in.}^2 (\text{ft}^2)}{144 \text{ in.}^2} \times \frac{12 \text{ in.}}{0.344 \text{ in. (ft)}} \right] \Delta T_2$$

$$(0.00428 + 0.0000525) \Delta T_1 = (0.0545 + 0.0288) \Delta T_2$$

$$0.00433 \Delta T_1 = 0.0833 \Delta T_2$$

$$\Delta T_1 = 19.3 \Delta T_2$$

$$\Delta T_1 + \Delta T_2 = 1150°F \text{ (test data)}$$

$$1150 - \Delta T_2 = 19.3\ \Delta T_2$$

$$\Delta T_2 = 56.7°F$$

$$\Delta T_1 = 1093.3°F$$

The heat loss for one heater wire is:

$$0.00433 \times 1093.3 = 4.73 \text{ Btu/hr.}$$

The heat loss for four 42-strand wires is:

$$\frac{4.73 \times 4}{3.41} = 5.55 \text{ watts}$$

Next consider the heat loss through the four 7-strand wires.

Heater wires – 7 strands of 201 nickel – 30 ga. – 0.010 in. dia. Covering the stranded wire was asbestos with an outside diameter of 0.0937 in. stranded wire. Length was 2.65 inches.

$$\text{Area of one stranded wire} = \frac{\pi}{4} (0.010 \text{ in.})^2 (7) = 0.00055 \text{ in.}^2$$

$$\text{Area of asbestos} = \frac{\pi}{4} (0.0937 \text{ in.})^2 - 0.00055 \text{ in.}^2 = 0.00603 \text{ in.}^2$$

$$\text{Heat loss one wire} = \left(\frac{KA}{L}_{\text{Stranded Wire}} + \frac{KA}{L}_{\text{Asbestos}} \right) \Delta T$$

$$= \left(\frac{432}{2.65} \times \frac{0.00055}{144} + \frac{0.12}{2.65} \times \frac{0.00603}{144} \times 12 \right) 1150$$

$$= (0.000623 + 0.0000228)\ 1150$$

$$= 0.744 \text{ Btu/hr.}$$

$$\text{Heat loss}_{\text{4 wires}} = \frac{0.744 \times 4}{3.41} = 0.87 \text{ watt}$$

Total heat loss for the eight heater wires used is 5.55 watts + 0.87 watt = 6.42 watts.

3. Thermocouple Wire and Insulation Loss

Two Chromel-Alumel thermocouples were used to measure the hot end neck tube temperature. The wires were each 20 ga. – 0.032 in. dia. and had a thermal length of 2.65 in. Each wire was insulated with ceramic beads 0.108 in. O.D. x 0.055 in. I.D.

$$\text{Area of thermocouple wire} = \frac{\pi}{4} (0.032 \text{ in.})^2 = 0.000804 \text{ in.}^2$$

$$\text{Area of bead insulation} = \frac{\pi}{4} [(0.108 \text{ in.})^2 - (0.055 \text{ in.})^2] = 0.00677 \text{ in.}^2$$

Conductivity of Chromel = 15.2 Btu/hr-ft-°F

Conductivity of Alumel = 19.8 Btu/hr-ft-°F

Conductivity of ceramic = 1.02 Btu/hr-ft-°F

$$\text{Heat loss}_{\text{2 Chromel Wires}} = \frac{KA\,\Delta T}{L} = \frac{15.2 \text{ Btu}}{\text{Hr-ft-°F}} \times \frac{0.000804 \text{ in.}^2 (\text{ft}^2)}{144 \text{ in.}^2} \frac{1150°\text{F}}{2.65 \text{ in.}} \times \frac{12 \text{ in.}}{\text{ft.}}$$

$$= 0.884 \text{ Btu/hr.}$$

$$\text{Heat loss}_{\text{2 Alumel Wires}} = \frac{KA\,\Delta T}{L} = \frac{19.8 \text{ Btu}}{\text{Hr-ft-°F}} \times \frac{0.00804 \text{ in.}^2 (\text{ft}^2)}{144 \text{ in.}^2} \times \frac{1150°\text{F}}{2.65 \text{ in.}} \times \frac{12 \text{ in.}}{\text{ft.}}$$

$$= 1.052 \text{ Btu/hr.}$$

For the ceramic bead heat loss, the conductivity of the ceramic was divided by 2 because of the surface contact resistance.

$$\text{Heat loss 4 ceramic Beads} = \frac{KA\,\Delta T}{L} = \frac{0.60\ \text{Btu}}{\text{Hr-ft-°F}} \times \frac{0.00677\ \text{in.}^2\ (\text{ft}^2)}{144\ \text{in.}} \times \frac{1150°\text{F}}{2.65\ \text{in.}} \times \frac{12\ \text{in.}}{\text{ft}} \times 4$$

$$= 0.59\ \text{Btu/hr.}$$

Total heat loss through thermocouples is:

$$\frac{0.844 + 1.052 + 0.59}{3.41} = 0.74\ \text{watt}$$

The unit heat loss is therefore equal to corrected power input — calculated losses: 42.88 watts - 4.66 watts - 6.42 watts - 0.74 watt.

Unit heat loss is therefore 31.06 watts.

BLANK

APPENDIX B

CALCULATION OF ALLOWABLE PROTOTYPE UNIT PRESSURE RISE FOR A ONE-YEAR LIFE

APPENDIX B
CALCULATION OF ALLOWABLE PROTOTYPE UNIT PRESSURE RISE FOR A ONE-YEAR LIFE

The allowable unit pressure rise rate prior to actuation of the getter can be used to calculate the unit offgassing plus leak rate by the following expression

$$\text{Offgassing Rate} = \text{Unit volume x pressure rise rate}$$

$$= \text{Liters} \times \frac{\text{mixron}}{\text{sec.}}$$

$$= \frac{\text{Micron-liters}}{\text{sec.}}$$

The allowable pressure rise rate is determined by the pumping speed of the getter and/or the capacity of the getter.

ALLOWABLE PRESSURE RISE RATE AS DETERMINED BY GETTER PUMPING SPEED CALCULATION

The effective pumping speed on the insulation system is related to the pumping speed of the getter and the vacuum conductance of system components between the getter and the insulation system and is related by the following equation

$$\frac{1}{S_e} = \frac{1}{S_G} + \frac{1}{C}$$

where S_e is effective pumping speed, S_G = getter pumping speed, C = vacuum conductance of system components between getter and insulation space.

Calculation of Vacuum Conductance

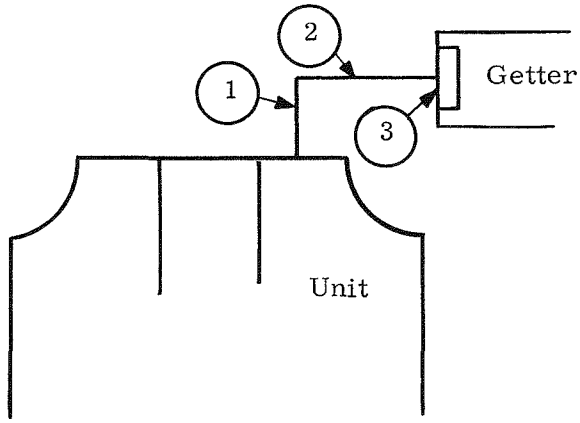

1. Unit Tube

2.37 in. long x 3/8 in. O.D. x 0.049 in. wall

$C_1 = 6.5\ D^3/L$ where C = ℓ/sec, D = inch, L = ft.

$$= 6.5 \frac{(0.277 \text{ in.})^3}{2.37 \text{ in.}} \quad \frac{12 \text{ in.}}{\text{ft.}}$$

$C_1 = 0.69$ ℓ/sec.

2. Tube Connection

2.12 in. long x 3/8 in. O.D. x 0.049 in. wall

$$C_2 = 0.69 \text{ ℓ/sec.} \times \frac{2.37}{2.12}$$

$C_2 = 0.77$ ℓ/sec.

3. Getter Retainer

Measured conductance for the material used was 35 ℓ/sec-ft^2. The retainer was 5/8 in. dia.

$$\text{Area of retainer} = \frac{\pi}{4}\left(\frac{25}{64}\,\frac{\text{in}^2}{144\ \text{in.}}\,\text{ft}^2\right)^2 = 0.00212\ \text{ft}^2$$

$$C_3 = \frac{35\ \ell}{\text{sec-ft}^2} \times 0.00212\ \text{ft}^2 = 0.0745\ \ell/\text{sec.}$$

$$\frac{1}{C_{Tot}} = \frac{1}{C_1} + \frac{1}{C_2} + \frac{1}{C_3}$$

$$= \frac{1}{0.69} + \frac{1}{0.77} + \frac{1}{0.0745}$$

$$= 1.45 + 1.30 + 13.4$$

$$= 16.15$$

$$C_{Tot} = 0.062\ \ell/\text{sec.}$$

$$S_G = 0.166\ \ell/\text{sec. (minimum)}$$

The effective pumping speed is:

$$\frac{1}{S_e} = \frac{1}{0.166} + \frac{1}{0.062}$$

$$= 6.05 + 16.15$$

$$= 22.2$$

$$S_e = 0.045\ \ell/\text{sec.}$$

At one micron pressure the throughput would be:

$$\text{Throughput} = 0.045 \frac{\text{micron-liter}}{\text{sec.}}$$

With this throughput and a 15.6 liter unit volume, the allowable pressure rise rate based on pumping speed would be:

$$\text{Allowable Pressure Rise Rate} = \frac{0.045}{15.6\ \ell} \frac{\mu\text{-}1}{\text{sec}}$$

$$= 0.00288\ \mu/\text{sec.}$$

$$= 10.4\ \mu/\text{hr.}$$

CALCULATION OF ALLOWABLE PRESSURE RISE RATE BASED ON GETTER CAPACITY

A total of 9.3 grams of getter was used in the prototype unit. This getter has an effective capacity of 80,000 μ-1/gm. The total capacity of the getter is therefore:

$$\text{Capacity} = 80{,}000 \frac{\mu\text{-}1}{\text{gm.}} \times 9.3\ \text{gm.}$$

$$= 744{,}000\ \mu\text{-}1$$

For a one-year unit life (8760 hr.) and a unit volume of 15.6 liters, the allowable pressure rise rate based on capacity is:

$$\text{Allowable Pressure Rise Rate} = \frac{744{,}000\ \mu\text{-}1}{15.6\ \ell \times 8760\ \text{hr.}}$$

$$\text{Allowable Pressure Rise Rate} = 5.44 \frac{\text{microns}}{\text{hr.}}$$

In summary, it can be seen that the quantity of getter used (grams) governs the maximum allowable pressure rise rate (5.44 μ/hr). If the getter was required to perform at maximum pumping speed (10.4 μ/hr), the unit life based on getter capacity would be 5.44/10.4 x 1 year = 0.52 year.

BLANK